2005

Water vapor diffusion through glass fiber reinforced polymer nanocomposites

Mohit Bhardwaj
West Virginia University

WATER VAPOR DIFFUSION THROUGH GLASS FIBER REINFORCED POLYMER NANOCOMPOSITES

Mohit Bhardwaj

Thesis Submitted to the
College of Engineering and Mineral Resources
at West Virginia University
in partial fulfillment of the requirements
for the degree of

Master of Science
in
Chemical Engineering

Dr. Rakesh Gupta, Committee Chair
Dr. Gangarao V. Hota
Dr. Joseph A Shaeiwitz

Department of Chemical Engineering

Morgantown, West Virginia
2005

Keywords: Moisture Diffusion, Barrier Properties, Polymer Nanocomposites, Nanoclay, and Carbon Nanofibers

Abstract

WATER VAPOR DIFFUSION THROUGH GLASS FIBER REINFORCED POLYMER NANOCOMPOSITES

Mohit Bhardwaj

Fiber reinforced plastics (FRPs) are used to make aircraft structures, highway bridges, automobile components, storage tanks, boat hulls, truck beds, and so on. When these FRPs are exposed to the atmosphere, environmental humidity can weaken the structural integrity and cause fiber delamination. The use of glass-fiber-reinforced nanocomposites made by addition of nanoclay, reduces the fiber damage and delamination because of its ability to enhance the barrier property of the matrix material. Clay not only acts as a barrier toward moisture diffusion, it also sequesters the moisture and protects the glass surface. During the course of this study the role of nano and micro fillers such as Montmorillonite clay, carbon nanotubes and Kevlar™ pulp in decreasing the diffusion coefficient for steady-state moisture transport through vinyl ester-based composites was quantified. Effects of temperature, concentration gradient, filler-type, filler content, extent of filler dispersion, filler orientation, and moisture adsorption on the filler surface were studied. It was found that nano and micro fillers bring about a decrease in diffusivity of vinyl ester composites, but the decrease is not as substantial as predicted by available equations in literature. An attempt was also made to evaluate the applicability of existing models in quantifying the decrease of diffusion coefficient for nanocomposites. It was found that the models developed during the course of this work were more effective in predicting the experimental results then the existing models.

ACKNOWLEDGEMENTS

I would like to thank first of all, my parents and family for their support and blessing throughout my education. I also express my sincere gratitude to David Statler and Preetanshu Pandey for their help during my stay in Morgantown.

I'm greatly indebted to my advisor Dr. Rakesh Gupta, for giving me the opportunity to work under him and for all his invaluable guidance and advice, not only in my research, but also my entire graduate education. I am also grateful to Dr. Hota GangaRao and Dr. Joseph Shaeiwitz for their valuable suggestions, recommendations, and comments that have gone towards shaping my research. All the advice and suggestions were very much appreciated.

I would like to express my special gratitude to Dr. Lakshmi Sridhar, Professor, University of Puerto Rico, for sharing his valuable insights and experience in nanoclay technology with me, and helping me out in my research. I am also grateful to Dr Vinod Berry, for carrying out Transmission Electron Microscopy on my nano-composite samples. I am thankful to Dr. Sushant Agarwal for guiding me in performing my tests and in analyzing the data. My heart felt thanks to James Hall, in helping me design some of my experiments and also rectifying some of the problems during the course of my work in spite of his other commitments.

TABLE OF CONTENTS

LIST OF FIGURES

LIST OF TABLES

LIST OF SYMBOLS

D_0: Diffusivity of water vapor through neat resin

l: Thickness of the film sample

Δp: Partial pressure difference of the diffusing solute across a film

J: Flux of the diffusing solute

S: Solubility of the diffusing solute in a particular solute or Henry's Law constant

c: Concentration of the diffusing solute at a particular position in the film

P: Permeability

M_t: Total amount of diffusant in the sample at time, t, during a sorption experiment

M_∞: Total amount of diffusant in the sample after infinite time during a sorption experiment

Q_t: Amount of diffusing substance that has passed through per unit area of the membrane

η: Lag time

ν_a: Volume fraction of the amorphous phase in a semi-crystalline polymer film

κ: Structure factor, which is a function of volume fraction of the amorphous phase in a semi-crystalline polymer film

τ: Tortuosity of penetrant path

B_1: Blocking factor

ϕ: Volume fraction or the 'loading' of the fillers in a polymer barrier film

a_1: Radius of the smaller spheres in Maxwell's resistance model

k_1: The electrical resistance of the smaller spheres in Maxwell's model

a_2: Radius of the larger sphere in Maxwell's model which encompasses the other spheres

k_2: The electrical resistance of the larger sphere

K: Cumulative resistance of Maxwell's system of n spheres

L: Length of a face of the filler particle

W: Thickness of the filler particle

P_{FL}: Permeability through the filled particle

P_{PL}: Permeability through the bulk polymer

P_i: Permeability through the interface

P_F: Permeability through the filler particle

ϕ_{Li}: Volume fraction of diffusing liquid in the interface of a swelled polymer

ϕ_{LP}: Volume fraction of the liquid in the interface

s: Half the distance between Cussler's rectangular flakes in a polymer matrix

d: Half the width of the flakes in Cussler's rectangular geometry

b: The distance between two layers in Cussler's rectangular geometry

a: Thickness of the flakes

σ: Point aspect ratio (s/d)

α: Flakes aspect ratio (d/a)

N: Number of flake layers in the polymer sample

p_n: probability of a diffusing solute molecule hitting n flakes

λ: Mean free path used in the Monte Carlo simulations carried out by Cussler and co-workers

H: partition coefficient

K: Equilibrium constant

1.0 Introduction

Glass fiber reinforced composites (GFRP) employing thermosetting polymer matrices, such as epoxy, vinyl ester or unsaturated polyester are finding their use in construction and repair of bridges and other civil structures because of high strength-to-weight ratio and a high stiffness-to-weight ratio, as compared to conventional materials such as steel and aluminum.

Fiber reinforced polymer composites consist of fibers of high strength and modulus embedded in or bonded to a polymer matrix with distinct interfaces (boundary) between them. High strength and high modulus fibers bonded by a matrix carry the load while the matrix helps in maintaining the orientation of fibers and helps in distributing the stress across the fiber boundary. Both the fiber and the matrix retain their chemical and physical identities but produce a combination of properties that cannot be achieved with either constituent acting alone. Even though fibers in a composite transfer forces in different directions, the matrix performs several vital functions. The role of the matrix in the GFRPs can be summarized as (1) to transfer shear stress between the fibers, (2) to provide a barrier against adverse environment such as chemicals and water, and (3) to protect fibers against mechanical abrasion. The various polymeric matrix materials that have been used in FRPs are listed in Table 1.

Table 1: Polymeric matrix materials and their uses [1]

Thermosetting Polymers	
Polymer	**Application**
Epoxies	Aerospace and Aircraft applications.
Polyester and Vinyl Ester Resins	Automotive, marine, chemical and electrical applications
Phenolics	Bulk molding compounds
Polyimides, Polybenzimidazoles (PBI), Polyphenylquinoxaline (PPQ)	High temperature aerospace applications
Thermoplastic Polymers	
Nylons (Nylon 6, Nylon 6,6), Thermoplastic Polyesters (PET, PBT), Polycarbonate (PC)	Used in injection molded articles
Polyamide-Imide (PAI), polyether-ether ketone, polysulfone, polyphenyline sulfide (PPS), polyether Imide (PEI)	Suitable for moderately high temperature applications.

Among these polymeric matrix materials, thermosetting polymers such as epoxies, unsaturated polyesters, and vinyl esters are in great commercial use, mainly due to the ease of processing and composite manufacturing, higher thermal stability, and chemical resistance.

However their use has been restricted by a lack of long-term durability and performance data, because they are intended to function/perform safely for 50 or more years. Furthermore, it is found that atmospheric moisture can diffuse to the fiber matrix

interface and cause de-bonding of laminae and fiber weakening. Efforts have been made to reduce the moisture diffusion coefficient. The basis for these studies has come from Maxwell's [2] work, in which he calculated the diffusion coefficient, D, of a small solute through a continuum partially filled with a suspension of impermeable spheres.

$$\frac{D_0}{D} = \frac{1+\frac{\phi}{2}}{1-\phi} \qquad \ldots (1)$$

where, D_0, is the diffusion coefficient in the absence of spheres and ϕ is the 'loading', that is, the volume fraction of the spheres.

1.1 Objectives and Scope of Research

Any application of polymer composites in an outdoor environment involves exposure to moisture, either in the form of water vapor or rain. In addition to water, composite materials may also be exposed to other chemicals depending on the type of material being used. The durability or the effectiveness of the matrix material to act as a barrier to diffusion of such chemicals, thereby protecting the fibers, becomes important. A modified matrix material having an inorganic phase just might serve this purpose of enhancing the barrier property. The following objectives were achieved:

1. Permeability, diffusion coefficient, and mechanism of water diffusion through neat and fiber-reinforced vinyl ester samples were measured.
2. The effect of nano-filler 'loading' on diffusion properties of the matrix with and without glass fiber was studied.

3. The effectiveness of clay, carbon nanofibers and Kevlar fibers as a barrier material was investigated.
4. Techniques like Transmission Electron Microscopy (TEM)& Differential Scanning Calorimetry (DSC) were used to characterize the structure of nanocomposites.
5. The applicability of various models quantifying the decrease in diffusion coefficient was studied.

To summarize, water permeation experiments were carried out to test the effectiveness of nano-fillers in decreasing the permeability and diffusion coefficient through vinyl ester based glass fiber composites. TEM and DSC were used to characterize the structure change that is obtained with the formation of nano-composites.

2.0 Theory

To understand the transport properties of polymers, it is useful to group materials [3] into two different groups according to their structure:

(1) Amorphous vs crystalline on a super-segmental level

(2) Rubbery vs glassy in nature on a segmental level

Combinations of these two categories gives rise to four different subgroups:

(1) Amorphous rubbery

(2) Amorphous glassy

(3) Semi-crystalline rubbery

(4) Semi-crystalline glassy

The latter two categories indicate the degree of segmental motion in the non-crystalline regions of a semi crystalline sample. The crystalline regions are generally impermeable to all penetrants.

The characteristic physical properties of materials in these four subcategories affect the ability of small penetrants to diffuse in response to a chemical potential driving force. These characteristic differences between the subcategories reflect the morphological factors that are both segmental level and larger than segmental level. Imposed orientations at both segmental and super-segmental levels can cause further changes in the properties of chemically identical samples within these four subcategories. Efficient orientation of impermeable crystalline domains in a sample increases the effective diffusion path of a penetrant within the sample. The added path length effectively decreases the ability of penetrants to cross through a film composed of the material, making it a better barrier.

2.1 Process of diffusion

Diffusion of gases and vapors through solid, non-porous polymers is a three-step process. In the first step, the gas has to dissolve in the polymer at the high-pressure side. Then the gas has to diffuse as a solute to the low-pressure side. In the third step, the solute evaporates back to the gas phase. The steady state diffusion through a membrane of thickness (L) exposed to a partial pressure difference (Δp), the mass flux (J) [4] though the membrane is given by:

$$J = DS\left[\frac{-\Delta p}{L}\right] \quad \ldots (2.1)$$

where, D is diffusivity of the gas and S is solubility of the gas in the polymer at pressure (p).For such a case the concentration (c) of the gas in the polymer is given by:

$$c = Sp \quad \ldots (2.2)$$

For simple gases above their critical temperatures and dissolved in rubbery polymers, S is Henry's law constant, which is independent of p. However, for glassy polymers, the solubility may become more complex and at higher pressure can approach the Langmuir isotherm. In these cases Michaels et al. [5,6] have distinguished between true molecular solution and solution in preexisting cavities. It should be emphasized, that up to 1 atmosphere, this complex behavior is quite rare even with glassy polymers, and Henry's law is usually closely obeyed.

2.2 Measurement of diffusivity

2.2.1 Constant D

2.2.1.a) Time lag method

When diffusion occurs through a plane sheet or membrane of thickness (l) and diffusion coefficient (D), whose surfaces at x = 0 & x = l are maintained at constant concentrations, c_1, c_2, respectively, a steady state is reached in which the concentration remains constant at all points of the sheet. The steady state diffusion equation in one dimension is given as:

$$\frac{d^2c}{dx^2} = 0 \qquad \ldots (2.3)$$

provided the diffusion coefficient (D) is a constant. On integrating with respect to x we obtain:

$$\frac{dc}{dx} = \text{constant} \qquad \ldots (2.4)$$

On further integrating and applying the boundary conditions *at* $x = 0$ & $x = l$ we obtain:

$$\frac{c - c_1}{c_2 - c_1} = \frac{x}{l} \qquad \ldots (2.5)$$

The above equations show that the concentration changes linearly from c_1 to c_2 through the sheet. The flux of diffusing substance is same across all sections of the membrane and is given by

$$Flux = -D\frac{dc}{dx} = D\frac{c_1 - c_2}{l} \qquad \ldots (2.6)$$

D can be deduced using Equation (2.6), from an observed value of flux.

For permeation experiments, the surface concentrations, c_1 and c_2, are not known. However, the vapor pressures, p_1 and p_2, on the two sides of the membrane are available. For this case the rate of transfer in the steady state is written as:

$$Flux = P\frac{p_1 - p_2}{l} \quad \ldots (2.7)$$

and constant P is then referred as the permeability constant. Here P is expressed, for example, as cm^3 of gas at some standard temperature and pressure passing per second through 1 cm^2 of the surface of a membrane 1 cm thick when the pressure difference across the membrane is 1 cm of mercury. The permeability constant is not as standard a fundamental constant as the diffusion coefficient particularly as different investigators use different units and even different definitions of P.

If the diffusion coefficient is constant and the sorption isotherm is linear, i.e., there is a linear relationship between the external vapor pressure and the corresponding equilibrium concentration within the membrane, the linear isotherm may be written as:

$$c=Sp \quad \ldots (2.8)$$

where, c is the concentration within the material of the membrane in equilibrium with an external vapor pressure, p, and S is the solubility. Since c_1, p_1, c_2, and p_2, are correlated by the above equation, it follows that

$$P=DS \quad \ldots (2.9)$$

where P is the permeability, D is the diffusion coefficient and S is the solubility.

When one face of the membrane at x = 0 is at a constant concentration c_1 and the other at x= l is at c_2, while the membrane is initially at a uniform concentration c_0, there is a finite interval of time during which this concentration profile develops. During this time, the concentration [7] changes according to

$$c = c_1 + (c_2 - c_1)\frac{x}{l} + \frac{2}{\pi}\sum_{n=1}^{\infty}\frac{c_2\cos n\pi - c_1}{n}\sin\frac{n\pi x}{l}e^{-Dn^2\pi^2/l^2} + \frac{4c_0}{\pi}\sum_{m=0}^{\infty}\frac{1}{2m+1}\sin\frac{(2m+1)\pi x}{l}e^{-D(2m+1)^2\pi^2 t/l^2} \quad \ldots (2.10)$$

As time (t) approaches infinity, terms involving the exponentials become negligible and a linear distribution of concentration is obtained again as before. If M_t denotes the total amount of diffusing substance that enters the sheet during time (t) and M_∞ the corresponding amount during infinite time, then [9]

$$\frac{M_t}{M_\infty} = 1 - \frac{8}{\pi^2}\sum_{n=0}^{\infty}\frac{1}{2m+1}\sin\frac{(2m+1)\pi x}{l}e^{-D(2m+1)^2\pi^2 t/l^2} \quad \ldots (2.11)$$

In this case $M_\infty = l\left(\frac{c_1 + c_2}{2} - c_0\right)$ and the total content of the membrane at time (t) is given by $M_t + lc_0$. The expression is similar to and is readily evaluated from the zero fractional uptake curves.

The rate at which gas or other diffusing substance emerges from unit area of the face at x=0 of the membrane is given by $D\left(\frac{\partial C}{\partial x}\right)_{x=0}$. By integrating with respect to t, the total amount of diffusing substance (Q_t) passing through the membrane in time (t) is obtained, where [9]

$$Q_t = D(c_2 - c_1)\frac{t}{l} + \frac{2l}{\pi^2}\sum_{1}^{\infty}\frac{c_2\cos n\pi - c_1}{n^2}(1 - e^{-Dn^2\pi^2 t/l^2}) + \frac{4c_0 l}{\pi^2}\sum_{m=0}^{\infty}\frac{1}{(2m+1)^2}(1 - e^{-D(2m+1)2\pi^2 t/l^2}) \quad \ldots (2.12)$$

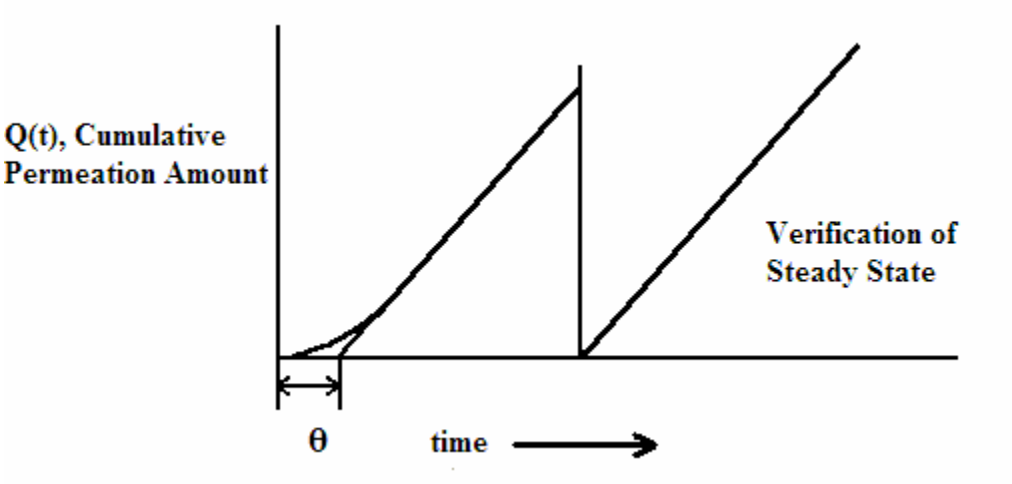

Figure 1: Time Lag method for calculating diffusion coefficient [3]

In the experiment for which the membrane is at zero concentration (c_0=0) and the concentration at the face through which the diffusing substance emerges is also maintained at zero, Equation 2.12 reduces to:

$$\frac{Q_t}{lc_2} = \frac{Dt}{l^2} - \frac{1}{6} - \frac{2}{\pi^2}\sum_{1}^{\infty}\frac{(-1)^n}{n^2}e^{-Dn^2\pi^2 t/l^2} \qquad \ldots (2.13)$$

which, as t→∞, approaches the line

$$Q_t = \frac{Dc_2}{l}\left(t - \frac{l^2}{6D}\right) \qquad \ldots (2.14)$$

This line has an intercept, η, on the time axis given by

$$\eta = \frac{l^2}{6D} \qquad \ldots (2.15)$$

This is used to calculate the diffusion coefficient.

2.2.1.b) Sorption method

For an experimental arrangement where the concentrations within the surfaces of a plane sheet of thickness (l) are maintained constant, the amount of diffusant, M_t, [9] taken up by the sheet in time (t) is given by

$$\frac{M_t}{M_\infty} = 4\left(\frac{D_t}{l^2}\right)^{1/2}\left(\frac{1}{\pi^{1/2}} + 2\sum(-1)^n ierfc\frac{nl}{2(Dt)^{1/2}}\right) \quad \ldots (2.16)$$

The uptake is considered to be a diffusion process controlled by a constant diffusion coefficient (D). M_∞ is the equilibrium sorption attained theoretically after infinite time. Equation 2.16 also describes desorption from the same sheet, initially conditioned to a uniform concentration, whose surface concentration is brought to zero at t = 0. The value of D can be deduced from an observation of an initial gradient of the graph of M_t/M_∞ as a function (t/l^2)

2.2.2 Variable D

Frisch et al. [8] obtained expressions for time lag in linear diffusion through a membrane with a concentration dependent diffusion coefficient without explicitly solving the diffusion equation. The relationship between the diffusion coefficient and concentration must be of a known form or be assumed to satisfy an arbitrary analytical expression containing unknown parameters. Frisch's method yields numerical values for the parameters, e.g., if the relationship is known to be of the form $D = D_0 e^{\beta C}$, where D_0 is the diffusivity and β is a constant, the values of D_0 and β are determined from a series of measurements of the time lag. For the conditions

$$c = c_0, x = 0, t \geq 0,$$
$$c = 0, x = l, t \geq 0, \quad \ldots (2.17)$$
$$c = 0, 0 < x < l, t = 0,$$

Frisch shows that the time lag (η) is given by

$$\eta = \frac{\int_0^l x c_{ls}(x) dx}{\int_0^l D(c) dc} \quad \ldots (2.18)$$

where c_{ls}(x) is the concentration distribution in the steady state and can be found from the equation

$$\int_{C_s}^{C_0} D(c) dc = \frac{x}{l} \int_0^{C_0} D(c) dc \quad \ldots (2.19)$$

There is one limitation in the method described above. The extraction of c as a function of x from Equation (2.19), in order that it can be used in Equation (2.18), is not easy and a series expansion becomes necessary. Clearly, if the diffusivity-concentration relationship contains two parameters, at least two measurements of η for different values of c_0 are needed for their determination.

2.3 Experimental determination of permeation rate

Both steady-state diffusion and the time lag technique for determining diffusion coefficient require measurement of the permeation rate of a diffusant through a film. These measurements are made under constant well-defined conditions of surface concentration. The surface concentration will remain constant if it is in equilibrium with a constant concentration source of the diffusant.

Membrane permeation

Polymer laminas for use in permeation experiments do not present a problem when these experiments are being used for the evaluation of existing films as diffusion barriers. The calculation of diffusion coefficients from experiments on such films may, however, lead to erroneous values due to inhomogeneities in the structure. Commercial cellulose film, for instance, may possess a skin that has a structure. The film may contain a non-volatile plasticizer and though it might be argued that the sole effect of this would be to give a coefficient for diffusion in plasticized polymer. This overlooks any migration of plasticizer that occurs to minimize the free energy of the three-component system in the presence of a gradient of diffusant concentration.

2.3.1 Partition cell methods

For accurate measurements, partition method is used. In this method, the vapor pressure is controlled on both sides of the membrane, and the permeation rate is measured independently.

An example of this assembly is that used by Barrer and Skirrow [10] for studying the diffusion of paraffin hydrocarbons and nitrogen in natural rubber. This is shown in Figure 2. All air is removed from the apparatus and one side of the membrane is maintained in a constant pressure atmosphere of the diffusant by the manual operation of a Toepler pump. Initially, the other side of the membrane is at zero pressure. As gas permeates through the membrane, the pressure builds up, and a sensitive Macleod gauge measures the built-up pressure. Using this equipment both the time lag (η) and the steady state flow rate can be measured. The increase in pressure measured by the gauge is so small that the outgoing side of the membrane can be considered to be effectively at zero pressure throughout.

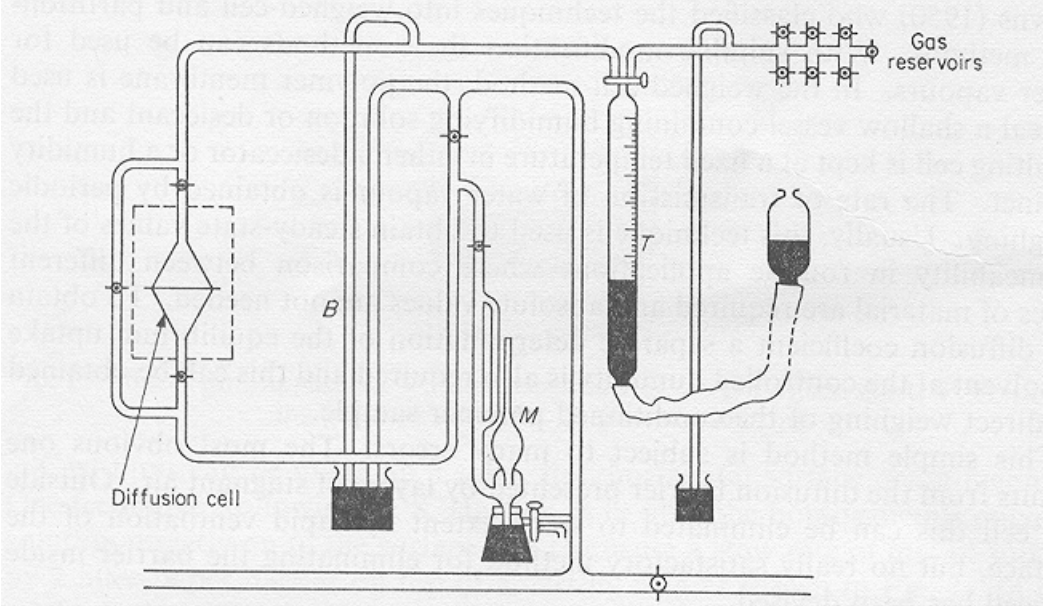

Figure 2: Partition cell method for determining permeability [9]

The continual operation of the Toepler pump for controlling the pressure on the ingoing side of the membrane can be dispensed with the use of a larger buffer volume. In the case of vapors, a liquid vapor source can be used and the pressure can be controlled by the adjustment of temperature. Vapor pressures lower than saturation can also be obtained by addition of a nonvolatile diluent to the liquid source or in the case of diffusion of water, by the use of hydrate mixtures.

2.4 Factors affecting permeability in polymers

Factors [9] influencing permeability through a polymeric film can be divided into:

a) External (temperature, pressure, concentration, humidity, etc)

b) Penetrant related (solubility, molecular weight, shape etc)

c) Related to matrix polymer

These effects are described below:

2.4.1. Dependence on relative pressure

For a number of systems, P is not a constant but depends on the relative pressure difference across the membrane. Steady state integration of Fick's first law gives

$$J = \frac{1}{l}\int_{C_2}^{C_1} Ddc \qquad \ldots (2.20)$$

where c_1 and c_2 are the concentrations at the ingoing (x = 0) and the outgoing (x = l) faces of the membrane. The permeability coefficient (P_{12}) can be written as:

$$P_{12} = \frac{Jl}{p_1 - p_2} \qquad \ldots (2.21)$$

and it follows that

$$P_{12} = \frac{1}{p_1 - p_2}(p_1 P_{10} - p_2 P_{20}), \qquad \ldots (2.22)$$

where P_{10} and P_{20} are the coefficients measured with pressures p_1 and p_2 at x = 0 and zero pressure at x = l, respectively. Only when the flux (J) varies linearly with ingoing pressure can the permeability coefficient be uniquely defined for the system such that $P_{12} = P_{20} = P_{10}$. If P_{10} is known as a function of p_1, then P_{12} can be evaluated for any difference of p_1 & p_2.

2.4.2. Dependence on thickness

If the diffusion is Fickian then it follows from Equation 2.21 that P is dependent on l. Structural effects, which are a function of the membrane thickness, may arise during the processing of films. The results of Taylor et al. [11] indicate that the dependence of P on l was only observed at high relative pressures. With the more hydrophilic polymers the ingoing side of the membrane is swollen relative to the outgoing side and, as a result, stresses are developed which may lead to a variation in P with l.

2.4.3. Dependence on temperature

Generally, the permeability coefficient increases with temperature. Barrer [12] pointed out that usually the least permeable membranes are more sensitive to changes in temperature. When Henry's law is obeyed and D is constant then P=Dσ, where σ is the Henry's constant. Over a considerable range of temperature, permeability varies exponentially as:

$$P = P_0 \exp(-E_P / RT) \quad \ldots (2.23)$$

$$E_P = \Delta H + E_D \quad \ldots (2.24)$$

When Henry's law is not obeyed these relations are valid only in the limit of zero concentration. [9]

$$\frac{\partial \ln P}{\partial 1/T} = -\frac{\partial(\ln p_1)}{\partial(1/T)} + \frac{\partial(\int_0^{C_1} Ddc)}{\partial(1/T)} \quad \ldots (2.25)$$

If the pressure (p_1) is held constant then the first term on the right becomes zero. The second term may be evaluated if the D versus c relation is known at several temperatures.

2.4.4. Dependence on the physical state of water

Since the chemical potential of the vapor at unit relative pressure is the same as the liquid, P may be expected to be independent of the physical state of the penetrant. Differences between vapor and liquid permeabilities have been observed (Yasuda and Stanett, [13]; Sivadijian and Ribiero, [14]). On the other hand, for several polymers, both permeabilities are identical since the permeability varies linearly with pressure. It would appear that differences between the liquid and vapor permeabilities are largely due to experimental difficulties in maintaining the vapor phase at unit relative pressure. Significant differences may arise if the soluble material is extracted from the membrane or if thermal equilibrium is not established throughout the system.

2.4.5. Dependence on the structure of the polymer

2.4.5 (a) Physical structure. The presence of crystallites in a polymer reduces the effective cross-sectional area for diffusion, increases the effective path length and may also result in restraints being imposed on the amorphous phase. For a simple model:

$$P=P_a v_a \kappa \qquad \ldots (2.26)$$

where, P_a is the permeability coefficient, and v_a is the volume fraction of the amorphous phase. The structure factor κ is a function of v_a. From Equation (2.26) and Equation (2.23) it follows that

$$E_P = E_{Pa} - R\frac{\partial \ln(v_a \kappa)}{\partial(1/T)} \qquad \ldots (2.27)$$

When the polymer is cooled, crystallization eventually sets in so that v_a and κ decrease as (1/T) increases. It has been inferred that local cooperative vibrations of only a few structural units were sufficient for the water molecule to diffuse. This case is not

pertinent to vinyl ester since a cross-linked polymer does not crystallize. It appears that somewhat unique behavior of water is attributed to its comparatively small size and to specific interactions with polar groups of polymer.

2.4.5 (b) Chemical structure: Polymers with low permeabilities have several features in common: skeletal chain is carbon with no hydrophilic substituents, substituents are relatively small, and there is a lateral symmetry on each carbon atom of the chain. Regularity of structure, which encourages crystallization or close packing, and the absence of highly polar groups appear to be necessary prerequisites for low water permeabilities. There are other cases where crystallization is not essential, for example, amorphous glass is an excellent water barrier. High permeabilities are generally encountered with polar polymers or where the segmental mobility is high as for polydimethylsiloxane.

It has been recognized that during permeation the structure of the polymer changes. In the presence of penetrant molecules a partial plasticization, i.e., an increase in chain mobility may take place, which in turn may lead to stress relaxation and shrinkage.

As discussed before, the simplest multiphase material is a semi-crystalline polymer. It has been shown that the sorption and diffusion coefficients in the crystalline phase are substantially smaller than in the glassy or rubbery phases. As a result, it is generally assumed that the crystalline phase does not sorb and hence does not allow any penetrant to pass through it. In this case, D depends on the volume fraction of the amorphous phase, α, the tortuosity of penetrant path, τ, and the blocking factor, B_1:

$$D = D_a \frac{\alpha n}{B_1 \tau} \qquad \ldots (2.28)$$

where, D_a is the diffusion coefficient in a hypothetical, completely amorphous polymer and n ≈ 1 is an empirical parameter, dependent on the nature of the penetrant molecule. Equation 2.28 can be used to interpret data of any multiphase system, writing B_l and τ as functions of concentration and process variables. In polymer blends, the dispersed phase can be incorporated in a wide range of volume fractions, particle sizes, and particle shapes distributed randomly or in an orderly fashion.

2.5 Nanocomposites: An Introduction

Uniform dispersion of nanoparticles can lead to an ultra large interfacial area between the constituents, per unit volume of the material. The immense interfacial area and the nanoscopic dimensions between nanoelements differentiate polymer nanocomposites (PNC's) from the traditional composites and filled plastics. Three major characteristics define and form the basis of PNC performance [15]: a confined matrix polymer, nanoscale inorganic constituents, and their arrangement.

Presence of internal filler-polymer interfaces makes the majority of polymer chains reside near an inorganic surface. Since an interface limits the number of conformations polymer molecules can adopt, the free energy of polymer molecules in this interfacial region is fundamentally different from that of those far removed from the interface (i.e, bulk). The influence of an interface is related to a fundamental length scale of the adjacent matrix, which for polymers is of the order of the radius of gyration of a chain. The restrictions in chain conformations will alter molecular mobility, relaxation behavior, free volume, and thermal transitions such as the glass transition temperature. In case of semicrystalline polymers and block copolymers the interface will alter the degree of

ordering and packing perfection and thus, crystallite and domain growth, structure and organization.

The second major characteristic of PNC's is dimension of the added elements. When the dimensions of a cluster or particle approach the fundamental length scale of a physical property (the so called confinement effect), new mechanical, optical, electrical properties arise that are not present in the macroscopic counterpart. Dispersions of nanoelements exhibiting these unique properties create bulk materials dominated by physics of the 'nano' dimension.

Finally, arrangement of the constituents critically determines the material's behavior. Spatial ordering of spherical, rod-like, or plate-like nanoelements into positional arrays with varying degrees of orientation order will result in large variety of systems. The possibilities are further expanded by varying degrees of particle-particle association, clustering, percolation (formation of an interconnected network), and heterogeneous distribution of particles. The final property of the PNC system will depend as much on the individual properties of the constituents as on the relative arrangement and subsequent synergy between the constituents.

2.6 Nanoelements

Amongst all the potential nanocomposite precursors, those based on clay and layered silicates have been more widely investigated. This is because starting clay materials are easily available and their intercalation chemistry has been studied for a long time. The various types of clay minerals are Montmorillonite, Illite, Kaolinite, and Attapulgite.

Illite is a non-swelling clay and hence, not compatible with polymeric matrix materials. Kaolinite and Attapulgite clays have low Cation Exchange Capacities (CEC) as

compared to Montmorillonite. The amount of cations that can be exchanged with organic ions is expressed in meq per 100 g of dry clay and is known as the CEC of clay. Kaolin also has a small basal spacing, and so the penetration of intercalant into the space between the individual layers is limited. On the other hand, Montmorillonite has the following advantages over other clay minerals, which make it more popular in making composites:

1. Flat plate like structures with a large aspect ratio in the range of 200-1500.
2. High CEC, in the range of 70 to 140 meq per 100 g of dry clay, as compared to other clay minerals.
3. Bentonite is the most abundantly available clay, which contains more than 50 % Montmorillonite
4. Montmorillonite is a Smectite (swelling clay) type of clay that makes it more compatible with a polymeric matrix.
5. Montmorillonite has a plate-like shape with high aspect ratio. Hence, at the same loading, it leads to a better permeation barrier when compared to Attapulgite clay, which has a needle like structure.
6. Montmorillonite develops similar increase in modulus and tensile strength at loading of 3-5% as compared to 20-60% loading of other fillers such as Kaolin and carbon black.

Hence, at the same loading, Montmorillonite leads to a better permeation barrier when compared to other clays and because of which it is used more frequently.

2.6.1 Structure of Montmorillonite

The crystal lattice of Montmorillonite, the most commonly used nanofiller, consists of two-dimensional layers. In the structure, a central octahedral sheet of alumina or magnesia is fused to two external silica tetrahedron layers by the tip. Due to this, the oxygen atoms of the octahedral sheet also belong to tetrahedral sheets. Al or Mg atoms in the octahedral sheets are coordinated with 6 oxygen atoms or hydroxyl groups located at the 6 corners of a regular octahedron.

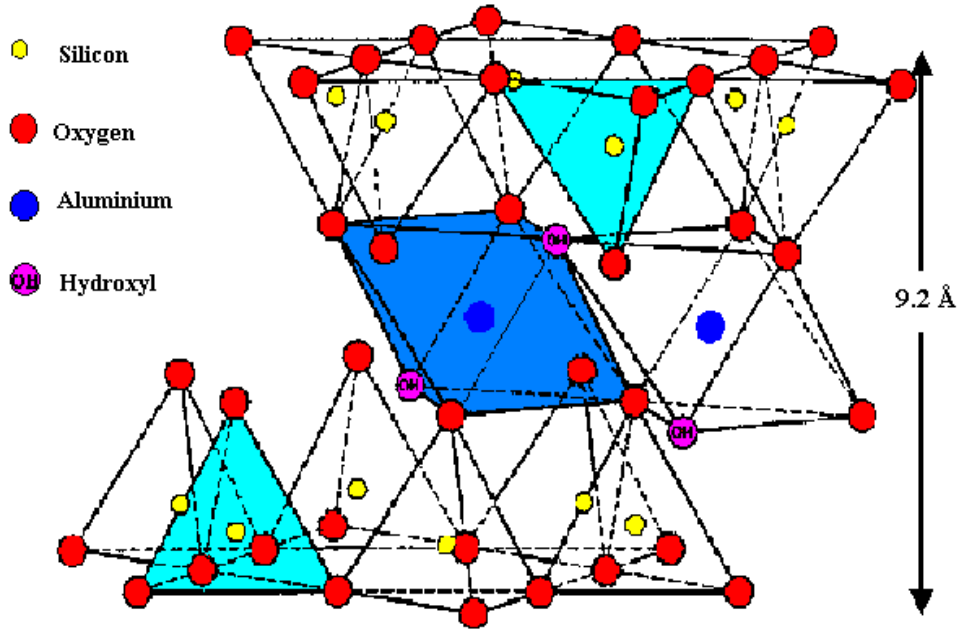

Figure 3: Structure of Montmorillonite (MMT) clay [29]

The three layers form a clay platelet or the unit cell of clay. Thickness of the platelet is around 1 nm and the lateral dimensions of the platelets organize themselves to form a stack. The stack has a van der Waals gap in between them called the interlayer or the gallery. In natural form of clay tetravalent Si atoms in the tetrahedral sheet are partly replaced by trivalent Al atoms, and/or trivalent Al atoms in the octahedral sheet are partly substituted by divalent atoms such as Fe or Mg. The lack of positive charge is

counterbalanced by alkali or alkaline ions (e.g Na^{+} or Ca^{++}) situated in the interlayer. These ions in the interlayer can be substituted with organic cations. This type of substitution makes the clay compatible with organic polymers.

2.6.2 Surface treatment

Clay by nature is hydrophilic and swells upon adsorption of moisture. To make it compatible with an organic material such as a polymer, it is given a surface treatment involving a compatibilizer. For example, organic cation molecules can be adsorbed on the surface of the clay, which changes the hydrophilic character to organophilic and improves the extent of wetting of the clay with an organic polymer. In addition to this, surface treatment serves two other purposes: (1) it reduces the layer to layer interaction, and, (2) it causes expansion of the gallery spacing to as much as 20 Å. The latter allows greater intercalation of polymer molecules between the clay platelets. Intercalation is a term given to the process by which monomer or polymer molecules enter into the gallery spacing during the preparation of a nanocomposite. This not only swells the clay by pushing the clay platelets apart, but also serves to reduce the forces of attraction between them. The individual clay particles can then be separated and dispersed into the polymer matrix. This is called exfoliation. For thermoplastic materials, exfoliation is done either during polymerization or by the application of shear forces in an extruder. For thermosetting resins, on the other hand, exfoliation is achieved by dispersing the clay in the liquid resin by the application of shear forces. Surface modification can be done by:

1.Ion Exchange method

2.Ion Dipole method

2.6.2.a Ion Exchange method

This is the simplest technique used to treat clay. Ion exchange treatment involves replacing the adsorbed cations (such as Na^{+}, Ca^{2+}) by an organic cation, typically an onium ion or an amine salt. The organic molecule replaces the cation making the clay surface organophilic. The organic molecules also enter the gallery spacing and cause the clay to swell. This technique was first developed at the Toyota Central R&D Laboratories, Japan (Lan [15], www.nanocor.com), where Montmorillonite was compatibalized with caprolactum (Nylon 6) using amino dodecanoic acid.

2.6.2.b Ion dipole method

Ion dipole surface treatment is a relatively new approach where the sodium atoms are left on the surface of clay. The induced positive charge on the sodium atoms can interact with partial negative charges on functional monomers or polymer groups. The functional groups having negative dipole moments include alcohols, carbonyls, esters, amines and ethers. Nanocor Inc., (Chicago) developed this process. (Lan [15], www.nanocor.com)

2.7 Types of nanocomposites

Based on their morphology, clay-filled nanocomposites maybe be of three types

1. Conventional composite
2. Intercalated composite
3. Delaminated or Exfoliated composite

In a conventional composite the tactoids exist in their original aggregated state with no intercalation. The basal spacing of the filler within the nanocomposite remains the same as in the pristine clay. An intercalated composite has a single, extended polymer chain intercalated between the silicate layers resulting in a well-ordered multilayer

having alternating polymer/inorganic layers. Consequently, the X-Ray Diffraction (XRD) peak would be shifted towards higher basal spacing. A delaminated composite has individual clay platelets uniformly dispersed in the matrix. A schematic representation of this is shown in Figure 4. The full potential of nanoclay is only realized in the exfoliated form. It should be noted that Montmorillonite has a high surface area, of the order of 750 m^2/g. Property enhancements are obtained due to molecular scale interactions between polymer and the clay surface. These interactions are greater in exfoliated morphology where the clay particles present the largest surface area, since they exist as individual platelets. During exfoliation clay aggregates break up into several nanometers sized individual platelets and hence, a very small clay loading can lead to significant property enhancements.

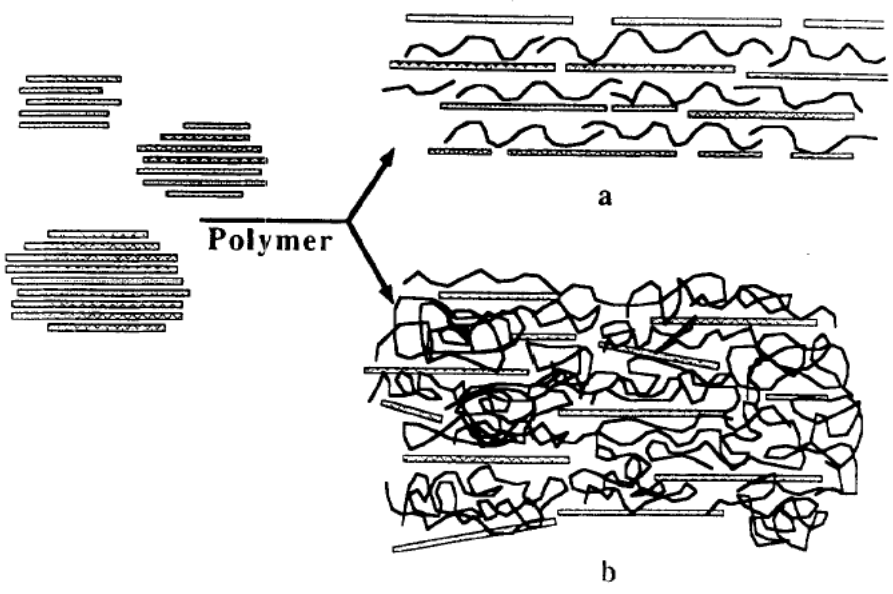

Figure 4:a) Intercalated clay composite b) Exfoliated or Delaminated composite [15]

2.8 Synthesis of nanocomposites

Interlayer distance between clay platelets increases by a significant amount on application of the compatibilizing agent. This makes it possible for monomer or the polymer molecules to enter the gallery. This then allows individual clay platelets to be dispersed. The process of clay platelets getting randomly dispersed inside the polymer is called exfoliation. Depending on the type of polymeric system involved, different methods of achieving exfoliation are being practiced.

2.8.1 In-situ polymerization

This process is conventionally used to synthesize a thermoset-clay nanocomposite. The organoclay (surface treated clay) is swollen in the monomer. The degree of exfoliation achieved in this method depends sensitively on the polarity of monomer molecules, surface treatment of the clay, swelling temperature and degree of agitation.

During the swelling phase, high surface energy of the clay attracts polar monomer molecules to diffuse between the clay platelets. Later, the polymerization reaction lowers the overall polarity of the intercalated molecules and displaces the thermodynamic equilibrium in such a way that more polar molecules are driven in between the clay layers delaminating the clay eventually.

2.8.2 Solution approach

Polar solvents can be used to synthesize nanocomposites. In this case, organoclay is swollen in the solvent. Polymer, dissolved in the same solvent, is added into the solution of swollen clay. The polymer intercalates between the clay platelets and the solvent is

then removed by evaporation under vacuum. This approach is not very practical for industrial use due to the problems associated with removing a large quantity of solvent.

2.8.3 Melt intercalation

Melt intercalation is used to synthesize nanocomposites based on thermoplastics. Molten thermoplastic is directly blended with organoclay in an extruder in order to optimize the polymer-clay interactions. The mixture is then heated and molded into any desired shape.

2.9 Theories of moisture diffusion through nanocomposites

Attempts have been made in the past to explain diffusion through heterogeneous media. Usually a heterogeneous medium consists of a phase A dispersed as small randomly shaped particles in a continuum of phase B. Maxwell [2] considered a continuum with immersed spheres so far apart that the streamline pattern about each sphere was uninfluenced by its neighbors. The following equation was proposed:

$$\frac{D_0}{D} = \frac{1+\frac{\phi}{2}}{1-\phi} \qquad \ldots (2.29)$$

Here, D_o is the diffusion coefficient without any spheres and ϕ is the loading, that is, volume fraction of the spheres.

Equation (2.29) is a mass transfer equivalent for the expression of cumulative electrical resistance derived by Maxwell for the same system. His analysis to obtain the cumulative resistance of n spheres of radius a_1 and resistance k_1, placed in a medium with resistance k_2, is presented here. Analysis [2] assumes that the spheres are at such distances apart that effect of spheres in disturbing the course of current is independent of each other.

If spheres are assumed to be placed within a shell of radius a_2, the potential at a great distance r from the center of this sphere would be of the form:

$$V = (Ar + nB\frac{1}{r^2})\cos\theta \quad \ldots (2.30)$$

where θ is the angle from the center of the sphere where the potential is being calculated, and value of B [2] can be given by:

$$B = \frac{k_1 - k_2}{2k_1 + k_2} a_1^{\,3} A \quad \ldots(2.31)$$

The ratio of the volume of n spheres to that of a sphere, which contains them, is

$$p = \frac{n a_1^{\,3}}{a_2^{\,3}} \quad \ldots(2.32)$$

The value of the potential far away from the sphere may therefore be written as:

$$V = A\left(r + p a_2^{\,3} \frac{k_1 - k_2}{2k_1 + k_2} \frac{1}{r^2} \right)\cos\theta \quad \ldots(2.33)$$

If the whole sphere of radius a_2 has been made of material of specific resistance K, the potential can be written as:

$$V = A\left(r + a_2^{\,3} \frac{K - k_2}{2K + k_2} \frac{1}{r^2} \right)\cos\theta \quad \ldots(2.34)$$

As Equation 2.33 and 2.34 are equivalent [2], we obtain:

$$K = \frac{2k_1 + k_2 + p(k_1 - k_2)}{2k_1 + k_2 - 2p(k_1 - k_2)} k_2 \quad \ldots(2.35)$$

This is the expression for cumulative resistance of n spheres in a continuum. Equation (2.29) is obtained by extending the above argument to diffusion. If D is used to represent the diffusivity of the system, and D_0 as the diffusivity of the medium without spheres, we obtain

$$D = \frac{2D_1 + D_0 + p(D_1 - D_0)}{2D_1 + D_0 - 2p(D_1 - D_0)} D_0 \qquad \ldots(2.36)$$

Here, D_1 is the diffusivity of the solute through the spheres and p is the loading. If D_1 is assumed to be zero, that is if the spheres are assumed to be impervious, then the above equation reduces to

$$D = \frac{1 - p}{1 + \frac{p}{2}} D_0 \qquad \ldots(2.37)$$

Equation (2.37) can be reduced to Equation (2.29) by replacing p by ϕ.

Note that this result is independent of the size of spheres, but varies only with their volume fraction. Also note that this is a result for a dilute suspension and is accurate only when ϕ < 0.1. If loading exceeds this value, then the assumptions involved in the derivation become redundant.

Similar results are found for other geometries as well. One such example is for a membrane containing a periodic array of infinitely long cylinders oriented parallel to the membrane surface [2]

$$\frac{D_0}{D} = \frac{1 + \phi}{1 - \phi} \qquad \ldots (2.38)$$

As before, the result is independent of the size of cylinders but only varies with their loading (ϕ). Again, this result is limited to dilute solutions.

2.9.1 Models explaining the decrease in diffusion coefficient

Barrer et al. [16] studied the permeability of a membrane having a regular array of rectangular parallelpipeds of phase A embedded in a continuum of phase B. The results that they obtained are not significantly different from the previous ones. They

emphasized that the spatial distribution of flakes and their aspect ratio play an important role in the amount of decrease in diffusivity of flake filled membranes. These issues are discuss in more detail, by models of Cussler and coworkers [18-21,24], and Nielsen [17].

2.9.1a Nielsen's model

Nielsen [17] was one of the first researchers to present models describing the diffusivity patterns of gases and liquids through flake filled polymer membranes.

In his work, the decrease in diffusion coefficient has been contended to be a result of increased tortuosity and a decrease in available area for diffusion. This decrease can be manifested as

$$\frac{P_F}{P_u} = \frac{\phi_P}{\tau} \qquad \ldots(2.39)$$

where ϕ_P is the volume fraction of the polymer and the tortuosity factor (τ) is defined as:

$$\tau = \frac{\text{distance a molecule must travel to get through the film}}{\text{film thickness}}$$

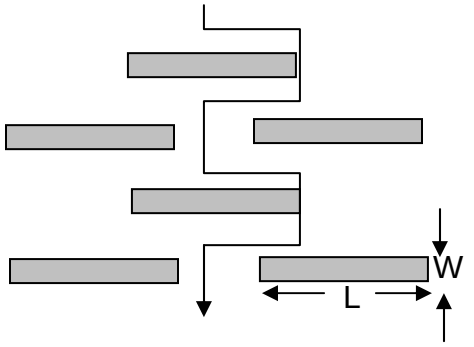

Figure 5: Figure showing the rectangular geometry used in Nielsen's model [17]

If the flakes are assumed to be rectangular plates oriented perpendicular to the direction of diffusion as shown in Figure 5, the distance a diffusing molecule has to travel is maximized. Such an arrangement gives a maximum possible tortuosity factor τ

$$\tau = 1 + \frac{L}{2W}\phi_F \qquad \ldots (2.40)$$

where L is the length of a face of the filler particle, W is the thickness of the filler plates, and ϕ_F is the loading or volume fraction of the filler particle. The permeability equation is given as

$$\frac{P_F}{P_u} = \frac{\phi_P}{1 + \frac{L}{2W}\phi_F} \qquad \ldots (2.41)$$

where P_F and P_u are the permeability values of the filled and unfilled polymer, and ϕ_P, is the polymer volume fraction.

For low flake loadings and for the case where permeation process does not have an impact on the solubility of the polymer, Equation (2.41) reduces to

$$\frac{D_0}{D} = 1 + \alpha\phi$$

where, D_0 is diffusivity of the solute through unfilled polymer, ϕ is the volume fraction of the filler, α is the aspect ratio (defined as the ratio of the length to half the width of the particle) and D, is diffusivity of the solute through flake filled polymer.

Equation (2.41) is derived on the assumption that there is an increased tortuosity when a penetrant passes through a flake filled membrane. Increased tortuosity, is a significant effect produced on the addition of nanofillers but there are several other key factors that need to be included in order to define the enhancement completely. For

example, the model does not include the effects of layer spacing. It is a very important factor that helps in determining the effectiveness of nanocomposites. For example, if the distance between the adjoining layers in a nanocomposite was increased and a corresponding decrease in the lateral spacing was made to keep the volume fraction constant, a tremendous amount of increase in the barrier property would be obtained. On the other hand, if the layer spacing was decreased and aspect ratio kept constant to maintain a constant loading level the horizontal distance between flakes would have to be increased. In this case, although, both aspect ratio and volume fraction do not change, a significantly lower decrease in diffusion coefficient is obtained. Furthermore, such an overlapping geometry is only attainable at high loading levels. This is not a practical situation, especially, for a resin system. Even though the equation is derived for high loading levels, it seems to represent practical data better for cases with low filler loading.

Nielsen also contends that permeability of liquids through filled polymers is much more complex than gas permeability. According to him, liquids often have appreciable solubility in the polymer, so that the polymer becomes swollen. In addition, a liquid may interfere with the polymer-filler interface, and the solubility or adsorption of liquid at the interface may be different from the solubility in the bulk polymer. This may be especially true if the filler has been given some treatment where a substance (different from the polymer) has been adsorbed on the surface. In the development of the Nielsen's model, an assumption is made that around each filler particle there is an interfacial layer, which has properties different from the bulk polymer saturated with liquid.

A diffusing molecule can get through the filled system by going only through the polymer, or it can diffuse along a path, which consists of both polymer and the interface. Thus, the total permeability is divided into two parts.

$$P_{FL} = P_1(\frac{\phi_{Li}}{\tau^0}) + P_2\left(\frac{\phi_P + \phi_{LP}}{\tau}\right) \quad \ldots (2.42)$$

$P_{Fl,}$ $P_{1,}$ and P_2 are the permeabilities of the liquid through: (1) filled polymer, (2) interfacial part, and (3) the saturated bulk polymer. P_2 is equal to the permeability of the liquid through the unfilled polymer, P_{PL}, unless the filler induces changes in the polymer. τ^0 is a tortuosity factor for the interfacial part; it may or may not be the same as τ. ϕ_{Li}, is volume fraction of the liquid collected in the interfacial region while, ϕ_{LP}, is volume fraction of the liquid dissolved in polymer. For whole system

$$\phi_P + \phi_F + \phi_{Li} + \phi_{LP} = 1 \quad \ldots (2.43)$$

These volume fractions are for the swollen systems. In general, ϕ_{Li} should be directly proportional to the surface area of the filler, which in turn for a given particle size is proportional to it's volume fraction.

In the interfacial region the liquid must go through both the interface and polymer to get through the film. In this region reciprocal permeabilities are additive. Therefore,

$$\frac{1}{P_1} = \frac{\theta_i}{P_i} + \frac{\theta_P}{P_{PL}} \quad \ldots (2.45)$$

or

$$P_1 = \frac{P_i P_{PL}}{P_{PL}\theta_i + P_i\theta_P} \quad \ldots (2.46)$$

where, θ_i and θ_P are the fractional lengths of diffusion path through the model for the interface and the polymer respectively.

$$\theta_i+\theta_P = 1 \qquad \ldots (2.47)$$

P_i is permeability of the liquid in the interface, which generally would be expected to be much greater than $P_{PL.}$ The desired equation is

$$P_{FL} = \frac{P_i P_{PL}}{P_{PL} + P_i\theta_P}\left(\frac{\phi_{Li}}{\tau^0}\right) + P_{PL}\left(\frac{\phi_P + \phi_{LP}}{\tau}\right) \qquad \ldots (2.48)$$

The variables in the above equation, which cannot be determined experimentally, are P_i, θ_i, and, τ^0. The only way these variables can be determined is by assuming a geometry or an arrangement of the particles inside the polymer. For instance, to determine θ_i it is necessary to calculate the thickness of polymer between the filler particles. For cubical particles the arrangement is shown in Figure 6.

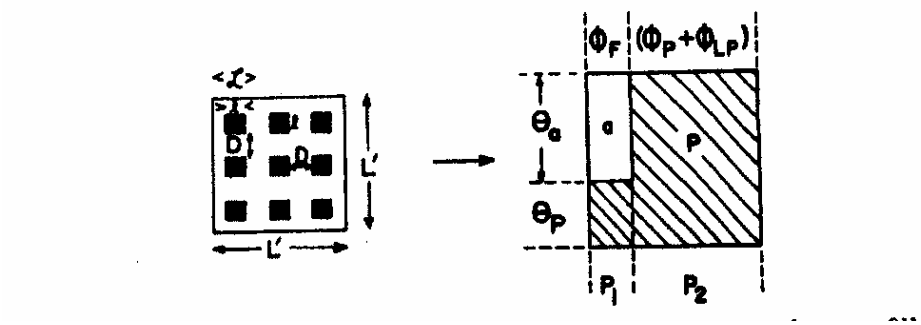

Figure 6: Model for calculating the minimum seperation of particles in a filled system (left side). On the right side is the derived model for the case where the filler particles are porous aggregates [17]

D: Minimum distance between the cube faces, i.e., thickness of polymer layer separating the particles.

l: length of cube faces of filler

L : length of "unit cell"

L' : size of specimen; L' is assumed to be 1

m: number of filler particles; if L' =1 then m is the number of filler particles per unit volume. The total volume allocated to each filler particle is

L^3 =V/m and $\phi_F = \frac{ml^3}{L'^3}$

where, V, is the total volume (L'^3).

D= L -l

$$D = \left(\frac{V}{m}\right)^{1/3} - l = \frac{L'}{m^{1/3}} - L'\left(\frac{\phi_F}{m}\right)^{1/3} = \frac{L'}{m^{1/3}}(1-\phi_F{}^{1/3}) = \frac{1-\phi_F{}^{1/3}}{m^{1/3}} \quad \ldots (2.49)$$

the total fraction of the thickness that is represented by polymer between particles is $m^{1/3}D$. Therefore

$$m^{1/3}D = (1-\phi_F{}^{1/3}) = \theta_P \quad \ldots (2.50)$$

Using a similar analysis for thin plates (L/W→∞) that are oriented parallel to the film surface, the fractional length of the thickness occupied by polymer is found to be $\phi_P or (1-\phi_F)$.

In general $\theta_i = \phi_F{}^n and \theta_P = 1-\phi_F{}^n$, where n is a constant between 0 and 1, which denotes the fractional length of the average diffusion path that is through the polymer. The constant, n, is likely to depend on particle shape, orientation and aggregation. For cubical or spherical particles, n should be roughly 1/3 while for thin plates with (L/W→∞) and it would approach 1 if the plates are oriented parallel to the plane of the sheet. For plates (L/W→∞) oriented perpendicular to the plane of sheet, n should approach zero. Diffusion of liquid through a filled sheet or film becomes

$$\frac{P_{FL}}{P_{PL}} = \frac{P_i}{P_{PL}\phi_F{}^n + P_i(1-\phi_F{}^n)}\left(\frac{\phi_{Li}}{\tau^0}\right) + \left(\frac{\phi_P + \phi_{LP}}{\tau}\right) \quad \ldots (2.51)$$

Here we discuss specific cases for the diffusion of a liquid through a filled polymer.

Case 1: Channels

One case is where the interface forms channels all the way through the film so that n = 0. For channels the above equation reduces to

$$P_{FL} = \frac{Pi\phi_{Li}}{\tau^0} + P_{PL}\left(\frac{\phi_P + \phi_{LP}}{\tau}\right) \quad \ldots (2.52)$$

this type of situation would be expected to occur where thin plates are oriented perpendicular to the surface or where the particles are not completely dispersed but form certain types of aggregates.

Case 2: Permeability when filler particles are porous aggregates

If the filler particles are not completely dispersed, they will form porous aggregates, which contain more or less free volume, and the density of the mixture will be less than expected.

If one assumes that the filler particles shown on the left side of Figure 6 are highly permeable aggregates instead of individual impermeable filler particles, a model such as shown on the right side of Figure 6 should apply. In this case $\theta_a + \theta_P = 1$, where, θ_P, and θ_a, are the fractional lengths of the diffusion path that are in polymer and aggregates, respectively. From the analysis leading to Equation (2.50), it is expected that $\theta_P = 1 - \theta_F{}^{1/3}$ & $\theta_a = \theta_F{}^{1/3}$

Also $\tau^0 = \tau = 1$, because of the void volume in the aggregates, the permeability of the liquid through them should be very high since capillary attraction and 'wicking' can occur. Thus, $P_a >> P_{PL,}$ where, Pa, is the permeability of the liquid through the aggregate. The earlier equation can be modified as follows for the case discussed above

$$\frac{P_{FL}}{P_{PL}} = \frac{P_a}{P_{PL}\phi_F^{1/3} + P_a(1-\phi_F^{1/3})} + (\phi_P + \phi_{LP}) \quad \ldots (2.53)$$

Such kind of behavior is expected to occur in systems having aggregates instead of a uniform distribution of particles. Such a system would always result in an increase in permeability instead of a decrease, which would be limited by the ratio of P_a/P_{PL} and would be maximized when P_a/P_{PL} goes to ∞.

The relevance of the above equations to our case was not determined as the part of this work. However, it is suspected that, formation of an interface might interfere with the diffusion process and in turn, with the final barrier properties of the polymer nanocomposites.

Nielsen's Work: A summary

Case A**:** If the solute does not have appreciable solubility through the polymer matrix the decrease in diffusivity is attributed to the following reasons:

1. Increase in tortuosity
2. Decrease in cross sectional area

These factors are in turn a function of flake aspect ratio and the loading. If the tortuosity is defined as

$$\tau = \frac{\text{Distance travelled}}{\text{Thickness of Film}}$$

using this,

$$\frac{D^0}{D} = (1 + \alpha\phi_F)/(1 - \phi_F) \qquad \ldots(2.53)$$

Case B: Diffusion of a liquid solute leading to considerable amount of swelling. In this case,

1. Solute interferes with the polymer-filler interface
2. Interface has a different diffusivity value than the bulk polymer.

So the diffusivity value for the filled polymer is given by a combination of two values

$$D_{FL} = D_1\left(\frac{\phi_{Li}}{\tau^0}\right) + D_2\left(\frac{\phi_P + \phi_{LP}}{\tau}\right) \qquad \ldots(2.54)$$

where, D_1, is the diffusivity for the interface and, D_2, is the diffusivity for the bulk polymer. D_1 is given by the following equation

$$D_1 = \frac{D_i D_{PL}}{D_{PL}\theta_i + D_i\theta_P} \qquad \ldots(2.55)$$

where θ_i, and, θ_P, are fractional length of diffusion path through the model for the interface and polymer, respectively. These are functions of the loading. Using the above expression

$$\frac{D_{FL}}{D_{PL}} = \frac{D_i}{D_{PL}\phi_F{}^n + D_i(1 - \phi_F{}^n)}\left(\frac{\phi_{Li}}{\tau^0}\right) + \left(\frac{\phi_P + \phi_{LP}}{\tau}\right) \qquad \ldots(2.56)$$

2.9.1 b Models By Cussler and Coworkers

Cussler and coworkers [18-21,24] studied permeation through membranes with impermeable flakes and they have discussed the possible phenomena associated with diffusion in a heterogeneous medium as is discussed below.

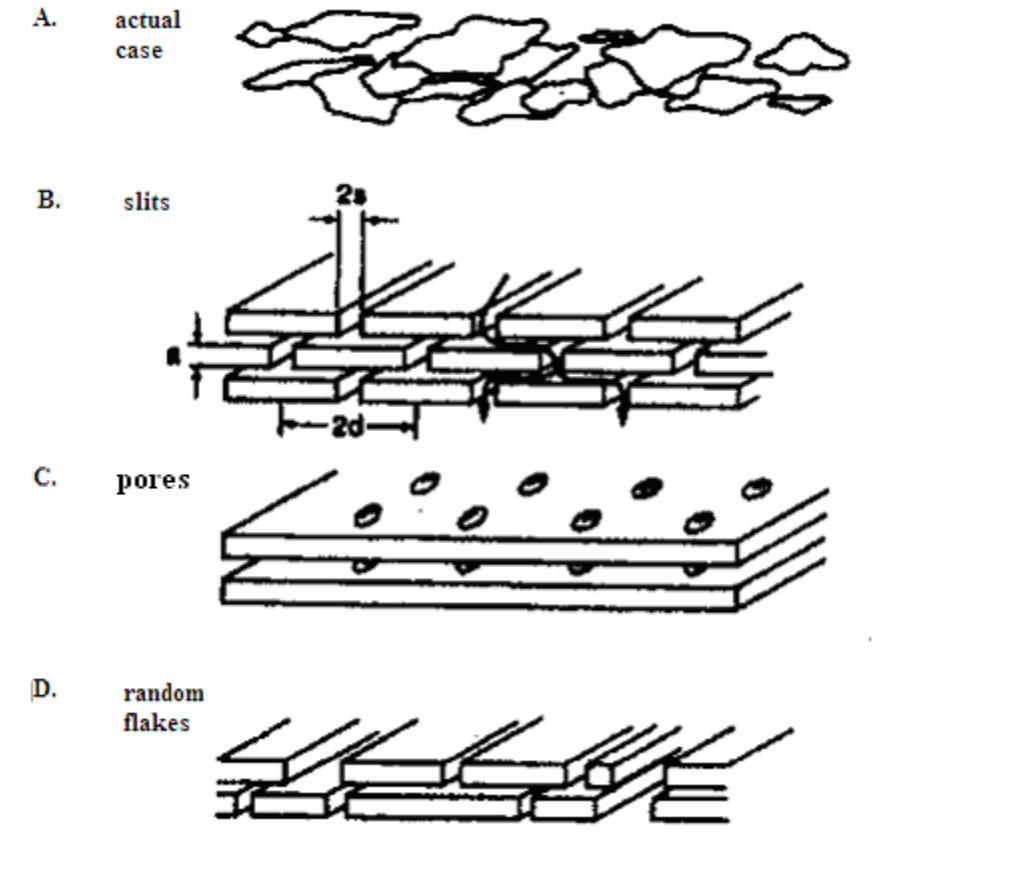

Figure 7: Models of barrier membranes containing impermeable flakes [18]

Four models of barrier membranes containing impermeable flakes aligned with the plane of the membrane are shown in Figure 7. The four models differ in the geometry assumed for the flakes. The most realistic model is shown in Figure 7(a). It has flakes that are randomly shaped and randomly distributed throughout the plane of the film. The impermeable flakes impede solute transport across the film by creating a tortuous path for diffusion. The analysis for such a model is rather impractical. Hence, an idealization is considered in two ways. First, flakes are assumed to occur periodically in a discrete number of planes within the film. Second, a particular shape and spacing for the flakes is assumed.

Three such geometries are considered. In the first case, flakes are assumed to be rectangles of uniform size but great width, regularly spaced like bricks in a wall. In such an idealization, diffusion will occur through the slits between the bricks. Alternatively, each layer of flakes can be assumed to be a flake perforated with regularly spaced pores. In this extreme idealization, diffusion is assumed to take place through pores rather than slits. The last geometry considered is probably the most realistic one, in which the flakes are randomly sized rectangles randomly located in the discrete planes.

For the three different geometries, the models relating the neat diffusion coefficient to the diffusion coefficient in the presence of flakes are discussed below.

For the slit model a unit cell of area (2dW) is considered. The total flux (J_0) through this unit cell when no flakes are present is given by

$$J_0 = D\frac{2dW}{l}\Delta c \qquad \ldots (2.57)$$

where, l, is the total thickness of the membrane and Δc is the concentration difference across the membrane. This result can be rearranged to obtain the resistance across the membrane

$$\frac{D\Delta c}{J_0} = \frac{l}{2dW} \qquad \ldots (2.58)$$

This resistance is proportional to the membrane thickness and inversely proportional to the area through which diffusion occurs.

When just one barrier is present in the membrane, the diffusing solute cannot pass through the membrane without necking down to pass through one of the periodic slits. The resistance in this case is given by

$$\frac{D\Delta c}{J_1} = \frac{l}{2dW} + \frac{b}{dW}\ln\frac{b}{2s} + \frac{a}{2sW} \qquad \ldots (2.59)$$

in which, J_1 is the flux through a unit cell of area 2dW. The first term on the right hand side in the above equation is the same as resistance without the flakes. The second term represents the constriction into and out of the slit; and the third term is the resistance of the slit itself.

This result is an approximation in the sense that part of the resistance to diffusion across the membrane is counted twice. But, as the above result is valid for the case when the permeation length is much greater than the flake length and slit size, so this is not expected to alter the results for many layers.

The resistance for a multilayer membrane is taken to be an extension of these results. The resistance for diffusion across a membrane with N flakes is

$$\frac{D\Delta c}{J_N} = \frac{l}{2dW} + \frac{b}{dw}\ln\frac{d}{2s} + \frac{Na}{2sW} + \frac{1}{2}N - 1\frac{d}{bW} \qquad \ldots (2.60)$$

As before, the first term on the right hand side is the resistance of the layer without flakes, and the second term is the resistance of the constriction into the first layer of flakes and out of the last layer flakes. These terms are the same as in the previous equation, because there is no additional constriction; once in the membrane, diffusion must follow its narrow, tortuous path. Third term is the resistance of N slits through which solute must pass to cross the membrane. This term is just N times the final term in the previous equation, as in the present case N layers are being considered instead of one. The fourth term on the right hand side reflects the tortuosity: (N-1) wiggles each, d units long. The factor of ½ in front of this term represents the reduced resistance due to the periodic array of flakes, i.e., the solute can diffuse through each slit either from the left or from the right.

The more useful form of the result is in the ratio of J_o/J_N

$$\frac{J_o}{J_N} = 1 + \frac{2b}{l}\ln\frac{d}{2s} + \frac{Nda}{ls} + \frac{N-1}{bl}d^2 \qquad \ldots (2.61)$$

If each layer is almost filled with the flakes then volume fraction or the 'loading' equals ϕ = a/(a+b). Flake aspect ratio (α) is a measure of the flake shape and point aspect ratio σ (=s/a) characterizes the pore shape.

$$\frac{J_0}{J_N} = 1 + \frac{da}{s(a+b)} + \frac{d^2}{b(a+b)} \qquad \ldots (2.62)$$

$$= 1 + \sigma\alpha\phi + \frac{\alpha^2\phi^2}{1-\phi}$$

Note that the second term on the right hand side has dropped out.

Equation (2.59) can be interpreted in two different ways. In the first case if σ/α<<1, which is the case when wiggles within the film are dominant then the above equation reduces to

$$\frac{D_0}{D} = 1 + \frac{\alpha^2\phi^2}{1-\phi} \qquad \ldots (2.63)$$

and if the diffusion is controlled by slits itself, which is the case when σ/α>>1, then Equation (2.59) reduces to

$$\frac{J_0}{J_N} = 1 + \alpha\sigma\phi \qquad \ldots(2.64)$$

Thus, in this case, the diffusion through the flakes is shown to be a function of loading flake aspect ratio and point aspect ratio.

We now look at the second geometry. This model has the same multi-layered structure as before, but the diffusion takes place through the pores instead of slits as discussed in the previous case. Diffusion from the pores in one layer to those in the next is a multidimensional process, a significant change from the previous case.

As discussed before, the resistance across a membrane containing no flakes can be written in terms of the flux, J_0.

$$\frac{D\Delta c}{J_0} = \frac{l}{4d^2} \qquad \ldots (2.65)$$

This resistance is similar to the previous case, except that the unit cell of area, 2dW, has been replaced by a unit cell of area $4d^2$. Resistance for a composite of N layers is given as

$$\frac{D\Delta c}{J_N} = \frac{l}{4d^2} + \frac{l}{2s} + \frac{Na}{\pi s^2} + (N-1)\frac{\ln\frac{d}{\sqrt{2}s}}{\pi b} \qquad \ldots (2.66)$$

As before, first term is the resistance without flakes, second term is the resistance due to the constriction into the top layer of holes and out of the bottom layer of holes. The third of these terms is the resistance of the N holes – each a units long and having an area of πs^2 through which the solute must diffuse in traversing the membrane. The fourth term on the right hand side of the equation represents (N-1) wiggles, which the solute makes. Strictly speaking, the natural logarithm in this term should be the inverse hyperbolic cosine, but this function is almost identical to the logarithm when d/s>>1, as is true here.

Again, for multilayered limit

$$\frac{J_0}{J_N} = 1 + \frac{4d^2}{a+b}\left[\frac{a}{\pi s^2} + \frac{1}{\pi b}\ln\frac{d}{\sqrt{2}s}\right]$$

$$= 1 + \frac{4}{\pi}\frac{\alpha^2}{\sigma^2}\phi + \frac{4}{\pi}\alpha^2 \ln\left(\frac{\alpha}{\sqrt{2}\sigma_2}\right)\frac{\phi^2}{1-\phi} \qquad \ldots (2.67)$$

in which α, σ, and, ϕ, are the flake aspect ratio(d/a), the pore aspect ratio, (s/a), and the loading, a/(a+b). The first term on the right hand side is the resistance of flake free membrane, the second term is the resistance of the pores, and the third term is the effect

of tortuosity. The effect of constriction has dropped out in the limit of many layers as it did in the previous case.

The third geometry consists of very thin randomly oriented flakes of the same size d, as suggested by Figure 7.

Again a membrane consisting of N layers is considered. Diffusion across this membrane will miss a flake in (N-n) layers, and hit a flake in n layers. As a result, this process can take place via (N+1) modes of probability p_n, n= 0,1…N. The probability, p_n, of hitting n flakes is

$$p_n = \frac{N}{n}\phi^n(1-\phi)^{N-n} \quad \ldots (2.68)$$

where, ϕ, is the loading in the membrane. The path for diffusion is (a+b) for each layer where a flake is missed. The path for each layer where a flake is hit is more difficult; it is increased by μd, where, μ is a geometric factor. However, the area available for this transport is proportional to, Wb, rather than, Wd. Thus, the effective path for each layer where a flake is hit is $(a+b+\mu d^2/b)$.

The average flux, J_N, across an area, d^2, of a membrane like this is

$$J_N = \sum_{n=0}^{N} p_n \left[\frac{d^2 D\Delta c}{N(a+b) + n\mu d^2 / b} \right] \quad \ldots (2.69)$$

Using the expression for probability in the above equation

$$\frac{J_N l}{D\Delta c} = \sum_{n=0}^{\infty} \left(\frac{N}{n} \right) \frac{\phi^n (1-\phi)^{N-n}}{\left[1 + \frac{n\mu d^2}{N(a+b)b} \right]} \quad \ldots (2.70)$$

in which, $l = N(a+b)$, is the total thickness of the membrane. Because N is large, this binomial distribution of probabilities is close to Gaussian; if N is very large, the only significant probability is the mean.

$$\frac{D\Delta c}{J_N l} = 1 + \mu\alpha^2 \frac{\phi^2}{1-\phi} \qquad \ldots (2.71)$$

Where, μ is a combined geometric factor characteristic of a random porous media.

All three of these geometries emphasize the simple fact that addition of flakes retards the process of diffusion by three factors: The tortuous wiggles to get around the flakes, the tight slits between the flakes, and the uncertain resistance of turning the corner to go from the wiggles into the slit. It is also important to realize that wiggles both increase the length for diffusion through the composite, and decrease the cross sectional area through which the diffusion can occur. Also, the altered diffusion depends not on the size of the impermeable material but only on its volume fraction and that the ratio, D/D_0, is independent of D_0. It does not matter if the impermeable material is put into wax or into Poly vinyl chloride; the ratio depends only on the shape and the volume fraction.

Many others have developed theoretical models for infinitely long flake geometry, which essentially substantiates the above arguments and also add other sources or resistances to the transfer of solute. One model, due to Aris [22], predicts that

$$\frac{D_0}{D} = 1 + \frac{\alpha^2\phi^2}{1-\phi} + \frac{\alpha\phi}{\sigma} + \frac{4}{\pi}\frac{\alpha\phi}{1-\phi}\ln\left[\frac{\pi\alpha^2\phi^2}{\sigma(1-\varphi)}\right] \qquad \ldots (2.72)$$

Again, the physical origin of each of the terms on the right hand side merits discussion. The first term is just unity, the limit without flakes when the loading of flakes ϕ, equals zero. The second term, involving, α^2, is the resistance to diffusion of the tortuous paths around the flakes. This path is called a 'wiggle' in this discussion. The

dependence on the square of both, α, and ϕ, reflects both the increased distance for diffusion and the reduced cross-sectional area between the flakes. This wiggling is considered to be the chief contribution to increased resistance in the flake filled barrier membranes. Its success justifies treating these systems as containing infinite flakes. The preferred path for diffusion must be predominantly around the second largest dimension, the short side, of these oriented flakes.

The third term represents the resistance to diffusion of the slits between the adjacent flakes in the same horizontal plane.

The fourth term on the right hand side represents the constriction of the solute to pass into and out of the narrow slits. Such constriction or 'necking' is easiest to imagine for a single layer of flakes pierced only by widely separated slits. Solute diffusing across such a layer would be forced to neck down to pass though the slits. This necking down would represent an additional resistance to diffusion, even when slit length is very short. This fourth term is the most controversial one. Cussler [18-21] argued that it would be significant only when entering the top layer of flakes or when leaving the bottom layer of the flakes. As a result, they argued, this resistance should be insignificant for membranes with a large number of flakes.

A modified version of the above equation is presented by Wakeham and Mason [23]

$$\frac{D_0}{D} = 1 + \frac{\alpha^2 \phi^2}{1-\phi} + \frac{\alpha\phi}{\sigma} + 2(1-\phi)\ln\frac{1-\phi}{2\phi\sigma} \qquad \ldots (2.73)$$

The difference in the above equation and one predicted by Aris is that the fourth term here does not depend on the flake aspect ratio (α).

Falla et al. [19] investigated the applicability of the above equations and also the one predicted by Cussler et al. [18], by carrying out Monte Carlo simulations, which are discussed below.

The Monte Carlo Simulation theory

A composite medium is constructed in a unit simulation volume. Monte Carlo simulations of molecular trajectories through this medium are interpreted via a mean square displacement technique based on Brownian motion. A hybrid technique was employed to cut down the simulation time. It averages the Brownian motion when far away from any flake and which follows a discrete step-by-step technique when near a flake. In particular when the solute particle is away from a solid surface, it is allowed to advance a significantly longer distance than one mean free path. This large step is then converted to the distance that would have been traveled if the molecule were following a random walk.

The simulations begin by defining a square cross section with impermeable flakes in a solvent continuum. The flakes are modeled as equal rectangles oriented so that the flake centers in one course are directly above the slits in the courses above and below. The loading, the flake aspect ratio, and the flake spacing are used to generate the structure. The trajectories are calculated from the randomly picked points near the center of the cross-section. If the location of a specific point falls outside of a flake, it is kept as an initial starting point, if it falls inside a flake, it is discarded but used to check the calculated value for loading.

The distance from this starting point to the surface of the nearest flake is then determined. If this distance is more than five times the mean free path, the particle is

allowed to advance to a random point on the circumference of an imaginary circle the radius of which is equal to the distance to the nearest flake. The time it would take a trajectory to reach this position, R, for the first time, if it were to follow a random walk, is approximated as $R^2/4D_0$. This relation is valid only if the trajectory is large compared to mean free path, and is not valid at regions close to the surface of a flake.

When the particle is within five mean free paths of the flake, it moves by taking steps equal to a mean free path. The specific mean free path is taken from an exponential distribution of mean free paths. When a step intersects a flake, the particle stops at the flake surface. After the surface is hit, the particle moves a mean free path away from the flake in a random direction. It is then advanced a mean free path in random direction until it again hits the flake or until it leaves the region around the flake. Once it leaves this region, its path is calculated as above.

Calculating the ratio of actual to effective diffusion coefficients requires estimating the mean square displacement as a function of time. The mean square displacement in the x-direction is simply the square of the x-distance from the initial starting point. The time is proportional to the total distance traveled. When the mean square displacement vs. the total distance traveled, is plotted, the slope of the plot is proportional to the diffusion coefficient.

$$\frac{D_0}{D} = \frac{2\lambda}{3(slope)} \qquad \ldots (2.74)$$

Where, λ, is the mean free path used for the calculations.

Falla et al. [19] ran the simulations with two distinct geometries, one in which the flakes are close together and, the other in which the flakes are more widely spaced. They

found that when flakes are placed close by, the variation of D_0/D with $\alpha^2\phi^2/(1-\phi)$ is consistent with the previous published results. (Cussler, [18])

When flakes were widely spaced the results from the simulations showed the dependence on resistances other than wiggling. The results from the simulations as they found for 24 geometries have been presented in Table 2. These simulations were done for a wide range of aspect ratios and slit shape factor ratios.

Table 2: A comparison of different models with Monte Carlo simulations [19]

Aspect Ratio	Slit shape σ	Loading ϕ	Aris Model	Wakeham 's	Simulations
10	0.1	0.05	9.6	14.9	20.7
		0.10	20.1	19	21.5
		0.15	32.1	24.3	24.3
		0.20	45.8	30.8	24.9
	1.0	0.05	3.6	6.0	6.5
		0.10	7.8	5.8	4.3
		0.15	13.4	6.9	5.5
		0.20	20.5	9.1	9.9
	10.0	0.05	1.6	1.2	1.8
		0.10	3.7	0.77	3.9
		0.15	6.9	1.7	7.9
		0.20	11.3	3.6	12.4
30	0.1	0.05	32.9	27	55.7
		0.10	74.3	47.9	64.0
		0.15	125	75.5	98.8
		0.20	186.4	110.8	118.4
	1.0	0.05	14.7	9.2	8.6
		0.10	37.5	16.7	20.6
		0.15	69.0	31.1	29.9
		0.20	110.4	53.1	44.8
	10.0	0.05	8.7	3.4	5.4
		0.10	25.0	9.9	22.0
		0.15	49.4	23.1	64.3
		0.20	83.0	44.0	77.4

According to them, the results are repeatable within 10 % accuracy. It can be seen from Table 2 that Aris's model predicts higher values. It is because in that equation

resistances are separated instead of combining them together. These simulations emphasize that largest reductions are obtained for small slit size and large aspect ratios, which is shown by the similarity of the results from the simulations and from the equations.

Reactive barrier films

Apart from wiggling, necking, and other resistances contributing to the decrease in diffusion coefficient, an interesting situation occurs by the incorporation of reactive groups into the membrane. Yang et al [24] studied the effect of incorporating reactive groups. They proposed that the reactive groups do not decrease the steady state value of permeability, but their effect is manifested in terms of the time taken by the groups before the permeation begins.

Theory

To see how a solute penetrates a reactive barrier, a thin barrier separating two well-stirred solutions is considered. The diffusing solute "1" is initially present in one solution, but not in the barrier or in the second solution. An immobile reagent solute "2" is present at the barrier, but not in the two adjacent solutions. At time zero, solute "1" begins to diffuse from the first solution across the barrier and into the second solution.

The mass balances within the barrier give the following relations [24]

$$\frac{\partial c_1}{\partial t} = D_1 \frac{\partial^2 c_1}{\partial z^2} - k c_1 c_2 + k' c_3 \qquad \ldots (2.75)$$

$$\frac{\partial c_2}{\partial t} = D_2 \frac{\partial^2 c_2}{\partial z^2} - k c_1 c_2 + k' c_3 \qquad \ldots (2.76)$$

$$\frac{\partial c_3}{\partial t} = D_3 \frac{\partial^2 c_3}{\partial z^2} + k c_1 c_2 - k' c_3 \qquad \ldots (2.77)$$

where, c_1 is the concentration of the solute, c_2 is the concentration of the reactive barrier in the film, c_3 is the concentration of reaction product, the D_i's are the appropriate diffusion coefficients; k and k' are the forward and reverse reaction rate constants. These mass balances are subject to the conditions

$$t = 0 \quad \text{all } z \qquad c_1 = 0 \qquad c_2 = c_{20} \qquad c_3 = 0$$

$$t > 0 \qquad z = 0 \qquad c_1 = Hc_{10}$$

$$z = l \qquad c_1 = 0$$

where, H, is the partition coefficient.

Many solutions to the above set of equations exist. The most familiar is the case for no chemical reaction, [9] for which

$$\frac{c_1}{Hc_{10}} = 1 - \frac{z}{l} - \frac{2}{\pi}\sum_{n=1}^{\infty}\frac{\sin(n\pi z/l)}{n}e^{-Dn^2\pi^2 t/l^2} \qquad \ldots (2.78)$$

The concentration in the second solution is found by other mass balance

$$V\frac{dc_1}{dt} = A\left(-D\frac{\partial c_1}{\partial z}\Big|_{z=l}\right) \qquad \ldots (2.79)$$

Subject to

$$t = 0 \qquad c_1 = 0$$

In these results, A is the barrier area and V is the volume of the second solution. The result at larger times is:

$$\frac{c_1}{c_{10}} = \left[\frac{DH}{l}\frac{A}{V}\right]\left(t - \frac{l^2}{6D}\right) \qquad \ldots (2.80)$$

When c_1 is plotted versus t, the slope gives a measure of permeability, DH. The intercept, as mentioned before, often called the 'Lag Time' allows the estimation of the diffusion coefficient, D.

The analysis from here forth assumes that the various Damkohler numbers ($k'l^2/D_3$) are much greater than one, implying that the reactions involved are instantaneous. The results for three different cases are shown below. The first two cases deal with reversible reaction and the last case deals with irreversible reactions. The three cases differ in terms of the mobility of the products formed after the reaction. If the reaction product is mobile then we have a case of facilitated diffusion where the diffusion coefficient increases.

This is manifested in terms of an increase in flux by a factor of 1+ K, where, K is the equilibrium constant. As of now the solute can either transfer in the form of species '1' or can cross the membrane in the form of species '3'. This represents the case, which makes the membrane a poor barrier and is not something that is desired.

The second special case of interest assumes the same fast reaction but assumes that the reaction products are immobile. That is, the diffusion coefficients, D_2, and, D_3, are zero. This result is similar to the one shown above but in this case, D is replaced by D/ (1+K).

The third case also involves the formation of an immobile product but in this case the amount of reagent is finite and the reaction is irreversible. An analytical solution for this case is possible as has been shown in the Table 3. One observes that the lag time is shown to be a function of c_{20} and goes to zero when c_{20} is zero. This discrepancy is a result of pseudo-steady-state approximation. The lag predicted for any significant irreversible reaction is much larger than that in the case of no reaction. Table 3 summarizes the results.

Table 3: A comparison for different reactions with lag times and diffusivities [24]

Type of Barrier	Permeance	Lag time	Key Equation

Non Reactive	$\frac{DH}{l}$	$\frac{l^2}{6D}$	$\frac{c_1}{c_{10}} = \left[\frac{DH}{l}\frac{A}{V}\right]\left(t - \frac{l^2}{6D}\right)$
Reversible reaction Yielding Mobile product	$\frac{DH}{l}(1+K)$	$\frac{l^2}{6D}$	$\frac{c_1}{c_{10}} = \left[\frac{DH}{l}(1+K)\frac{A}{V}\right]\left(t - \frac{l^2}{6D}\right)$
Reversible Reaction yielding an Immobile product	$\frac{DH}{l}$	$\frac{l^2}{6D}(1+K)$	$\frac{c_1}{c_{10}} = \left[\frac{DH}{l}\frac{A}{V}\right]\left(t - \frac{l^2}{6D}(1+K)\right)$
Irreversible Reaction Yielding an Immobile product	$\frac{DH}{l}$	$\frac{l^2}{2DH\nu}\frac{c_{20}}{c_{10}}$	$\frac{c_1}{c_{10}} = \left[\frac{DH}{l}\frac{A}{V}\right]\left(t - \frac{l^2}{2DH\nu}\frac{c_{20}}{c_{10}}\right)$

The above models relate to the following two methods, which lead to an enhancement in the barrier property of films:

1. A physical barrier to diffusion
2. Reactive species, to destroy diffusing species before they can cross the film.

The models that describe a decrease in the diffusion coefficient due to the presence of physical barrier assume that the flakes are as long as the width of the film. In reality, flakes would be randomly incorporated into the film and will be three-dimensional.

In order to estimate the effects of finite, randomly organized flakes, Moggridge et al [21] extended the simple geometric arguments described above. Hexagonal flakes were used instead of infinitely long rectangular flakes. Each of the hexagonal layers is assumed

to be in a perfect order. Now if a second layer is placed at lattice points as shown in Figure 8, there are still pathways without wiggles for diffusion across the two layers.

When a third layer of hexagons is placed as shown, these pathways are obscured. In the original theory one layer was sufficient to induce wiggles in this case two new layers have to be added. This leads to an over prediction of the effect of the flakes by a factor of two.

The picture of hexagons has a second effect as well. With the original two-dimensional model, two identical paths could be traversed after passing through the gap between the flakes to wiggle through the next slit. With hexagons, three different directions are possible, which would again lead to an over prediction by a factor of 3/2.

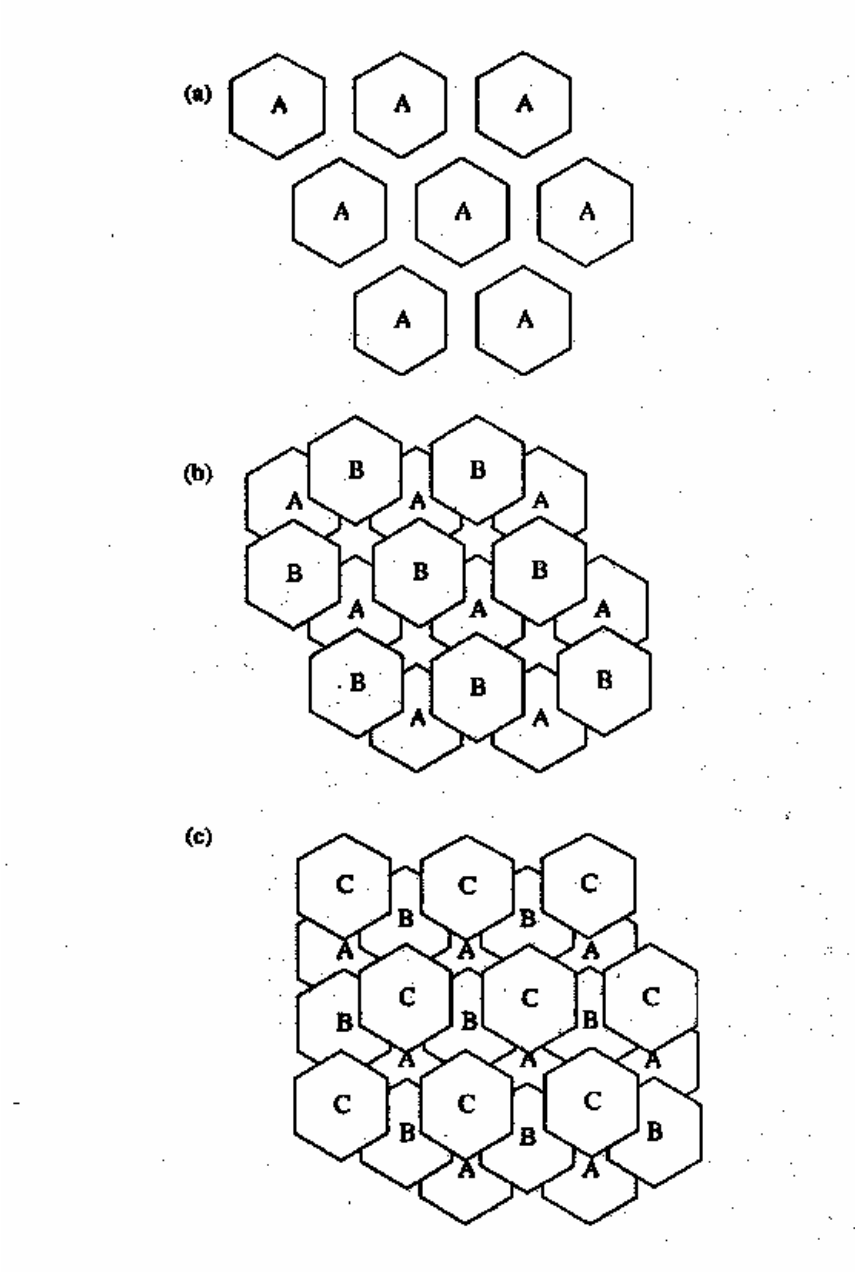

Figure 8: Cussler's hexagonal model [21]

Also, the alignment and misalignment of the layers has to be taken into account. With the ribbon-like flakes, the alignment and the misalignment were assumed to occur with equal probabilities, and a factor of ½ was added. With hexagonally shaped flakes, the results are different. Imagine that we passed through a course in position A to encounter a second course, which may be in position A, B, or C. If the flakes are in

position A, any increased tortuosity due to that course of flakes is lost. Even if that course is in position B or C a wiggle is obtained only if the third course is in position C or B, respectively. There are nine possible sequences, each with equal probability: AAA, AAB, AAC, ABA, ABB, ABC, ACA, ACB, and ACC. Only two of these ABC and ACB will force a wiggle. We therefore require a factor of 2/9 reductions on permeability to account for the random misalignment of successive layers of hexagonal flakes. For hexagonal flakes [22], a combination of these effects result in

$$\frac{D_0}{D} = 1 + \left(\frac{1}{2}\right)\left(\frac{2}{3}\right)\left(\frac{2}{9}\right)\frac{\alpha^2\phi^2}{1-\phi}$$

$$= \frac{D_0}{D} = 1 + \left(\frac{2}{27}\right)\frac{\alpha^2\phi^2}{1-\phi} \qquad \ldots (2.81)$$

Cussler's Models: A summary

Three different reasons contribute to a decrease in diffusivity.

1. Reduction in cross sectional area
2. Increased tortuosity
3. Chemical reaction between the solute and the flakes producing an immobile product.

For physical barriers**,** two limiting cases are proposed:

a) Infinitely long ribbon like flakes

b) Hexagonal flakes with layer imperfections.

For physical barriers, the path length is increased by an amount $\frac{d}{a+b}$ (Figure 7), and instead of the resistance provided by the perpendicular cross section 2dW, the resistance

is provided by the parallel cross section bW. Due to the presence of two alternate directions, a factor of 2 is added. So,

$$\frac{D_0}{D} = \left(\frac{2dW}{bW}\right)\frac{1}{2}\left(\frac{d}{a+b}\right) = \frac{d^2}{b(a+b)} = \frac{\alpha^2\phi^2}{1-\phi}$$

Now to this is added the effect misaligned layers of flakes, which is manifested in terms of a factor 1/2.

$$\frac{D_0}{D} = \frac{1}{2}\left(\frac{\alpha^2\phi^2}{1-\phi}\right) \qquad \ldots(2.82)$$

With the hexagonal structure following changes occur:

a) Three layers are required to induce wiggling (a factor of ½).

b) Three possible parallel directions (a factor of 2/3)

c) Layer imperfections (a factor of 2/9)

These factors result in the following modification in the diffusivity decrease equation

$$\frac{D_0}{D} = \frac{2}{27}\left(\frac{\alpha^2\phi^2}{1-\phi}\right) \qquad \ldots(2.83)$$

For reactive barriers following are the important considerations:

a) Reaction product should be immobile

b) Reaction should proceed fast

c) Pseudo steady state approximation is assumed.

The following equation gives the decrease in diffusivity on the addition of reactive flakes.

$$\frac{c_1}{c_{10}} = \left[\frac{DH}{l}\frac{A}{V}\right]\left(t - \frac{l^2}{2DH\nu}\frac{c_{20}}{c_{10}}\right) \qquad \ldots(2.84)$$

From above discussion, it can be inferred that, as in the case of Nielsen's model, Cussler's model also places emphasis on α and ϕ. This is true to a large extent but again,

they fail to emphasize the importance of layer spacing and the fact that such a geometry is only obtained at high filler concentrations. A change in thickness and width of the filler particle would change the aspect ratio, and if the layer spacing were also changed to keep the volume fraction at the same level, there would be no decrease in diffusivity as opposed to what is described by the equations. Let us take a look at some cases where we apply these models to data available in literature.

Table 4 shows the data obtained from the work done by Lan [26], who studied the diffusion of oxygen through polyimide-clay hybrid composites

Table 4: Permeability ratio and loading obtained from Lan's work [26]

Permeability Ratio	Volume Fraction
0.4625	0.01
0.2385	0.0246
0.2625	0.0334
0.30	0.0489
0.1	0.0756

In this case, aspect ratio of the flakes used in the experiment is not reported. Here, we present a method of analyzing the permeability data when aspect ratio is not available. This kind of analysis is mostly used to test the effectiveness of different theories for cases in which the true aspect ratio is established by other means, like a TEM analysis. It involves plotting the permeability or the diffusivity ratio as a function of loading ϕ. The functions used for Cussler's models are a) $\frac{1}{2}\left(\frac{\alpha^2\phi^2}{1-\phi}\right)$ for rectangular flakes and b)

$\frac{2}{27}\left(\frac{\alpha^2\phi^2}{1-\phi}\right)$ for hexagonal flakes. For Nielsen's model, the permeability ratio is plotted against ϕ. The aspect ratios are then obtained from the slopes of the linear fits. Table 5 shows permeability ratios and different abscissa values they are plotted against. The abscissa values correspond to different model equations. An aspect ratio value of 144 is obtained for Cussler's model with rectangular flakes. The corresponding values for Cussler's model with hexagonal flakes and for Nielsen's model are 54 and 99. Note that the value obtained for Nielsen's aspect ratio is midway between the values of the aspect ratio obtained from Cussler's upper limit and lower limit models.

Table 5:The ordinate and abscissa values used for the determination of aspect ratios [26] using different models

Permeability Ratio	Nielsen's model ϕ	Cussler's rectangular flakes model $\frac{1}{2}\left(\frac{\alpha^2\phi^2}{1-\phi}\right)$	Cussler's Hexagonal flakes model $\frac{2}{27}\left(\frac{\alpha^2\phi^2}{1-\phi}\right)$
2.16	0.01	0.000051	0.000007
4.19	0.02	0.00031	0.000046
3.81	0.03	0.000577	0.000085
3.33	0.05	0.001257	0.000186
10	0.08	0.003091	0.000458

If we now use these aspect ratios in Equations (2.42), (2.81) and (2.82), and obtain the values of permeability ratios, we find that the experimental data falls between Cussler's curves, and that Nielsen's model approximates the data with a fair degree of accuracy, as shown in Figure 9. But this is something one would expect, as the aspect ratios themselves were calculated assuming that these equations represent the data. Hence, the above analysis does not give a true indication of how well the models match up with experimental data. Such an analysis, as mentioned before, is more meaningful if the aspect ratios calculated as above were compared with true aspect ratios determined by other means.

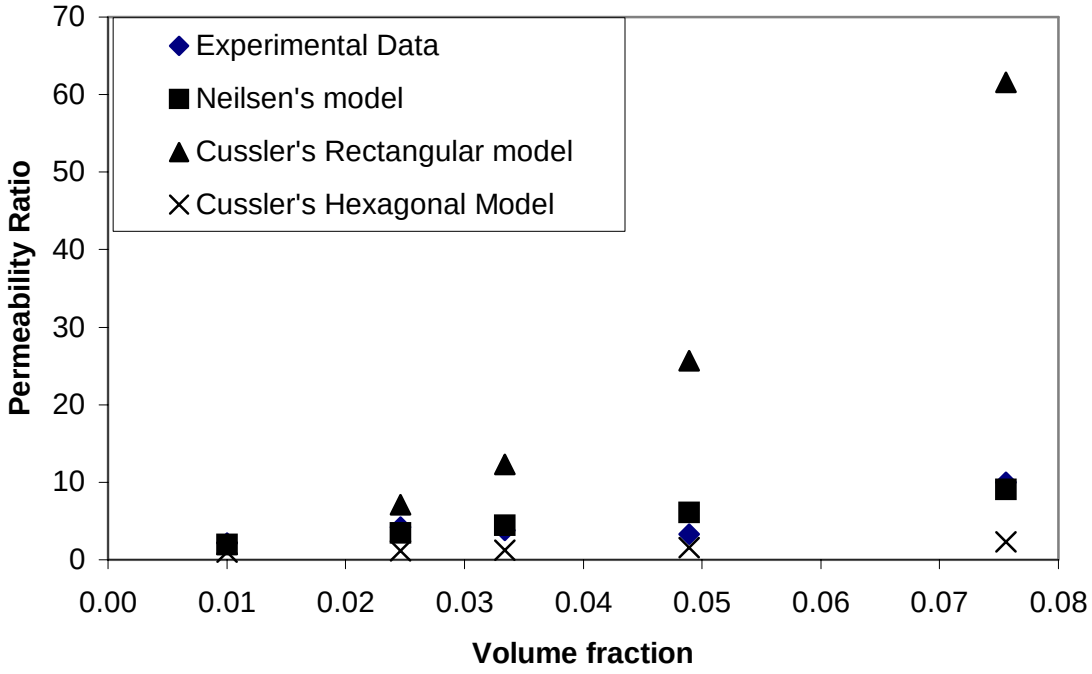

Figure 9: A comparison of different models with Lan's [26] data

Cussler and coworkers [19] first carried out Monte Carlo simulations to test the efficacy of Equation (2.68) in representing the decrease in diffusivity. Then, they applied

a similar analysis, as discussed above, to the data of HCl diffusion on PVA and PC films containing mica additives. The results obtained by them are shown in Figure10.

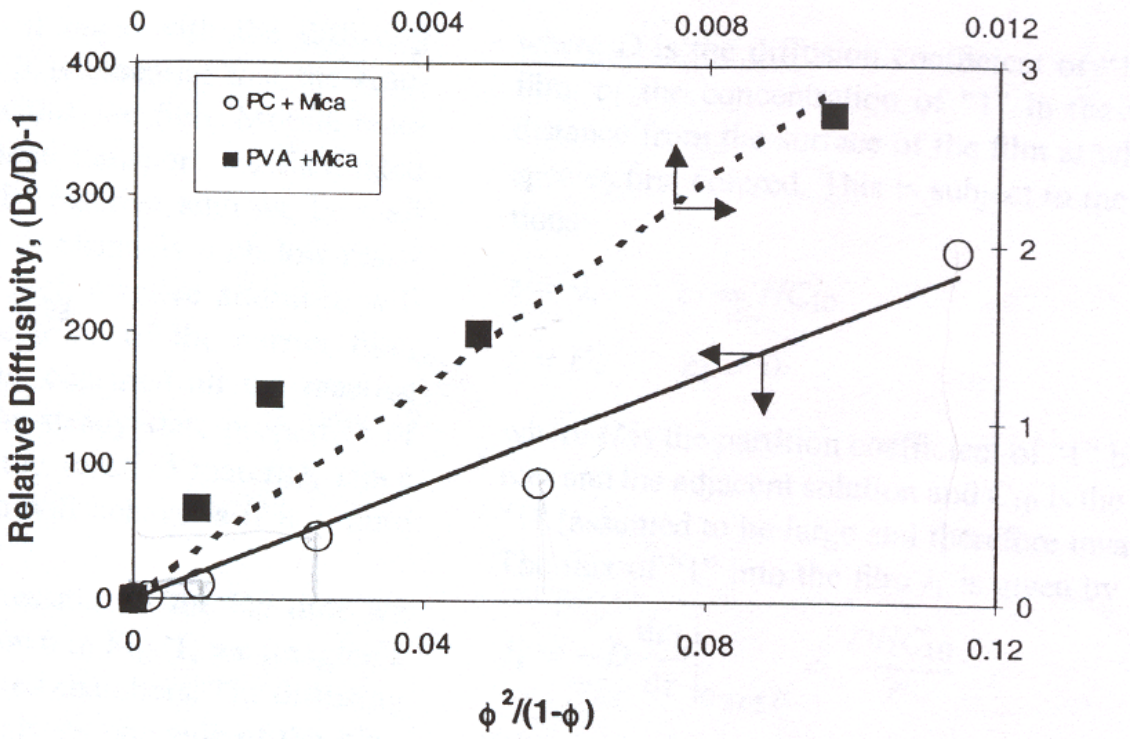

Figure 10: Diffusion vs flake loading for mica additives in PVA and PC films [21]

Table 6:Comparison of aspect ratio's measured using SEM with those obtained from Cussler's models [21]

System	Method	α	α (ribbons)	α (hexagons)
PVA+mica	SEM	20	24	63
PC+mica	SEM	100	65	170

The values of aspect ratios obtained using this analysis appear to be in good agreement with those obtained from direct measurements by Cussler and coworkers as is shown in Table 6.

Now, we present a case where the true aspect ratio was determined using microscopy [27]. Two cases are studied: oxygen diffusion and water vapor diffusion through polyimide clay hybrid composites. The aspect ratio of the flakes in this case as reported [27] is 100, as shown in Figure 11 and Table 7. Aspect ratio of the clay used in water permeation experiment is also 100 as is shown in Figure 12 and Table 8.

Table 7: Data obtained from [27] and Cussler's and Neilsen's predictions

Loading	Permeability ratio	Cussler's rectangular	Nielsen's prediction	Cussler's hexagonal	Alpha
0	1	1	1	1	100
0.005	1.58	1.13	1.51	1.02	
0.010	2.53	1.52	2.03	1.08	
0.015	4.75	2.18	2.56	1.17	
0.026	6.33	4.37	3.66	1.50	
0.042	9.50	10.06	5.39	2.34	

It can be seen that the existing models do not represent the diffusion data effectively in the above case.

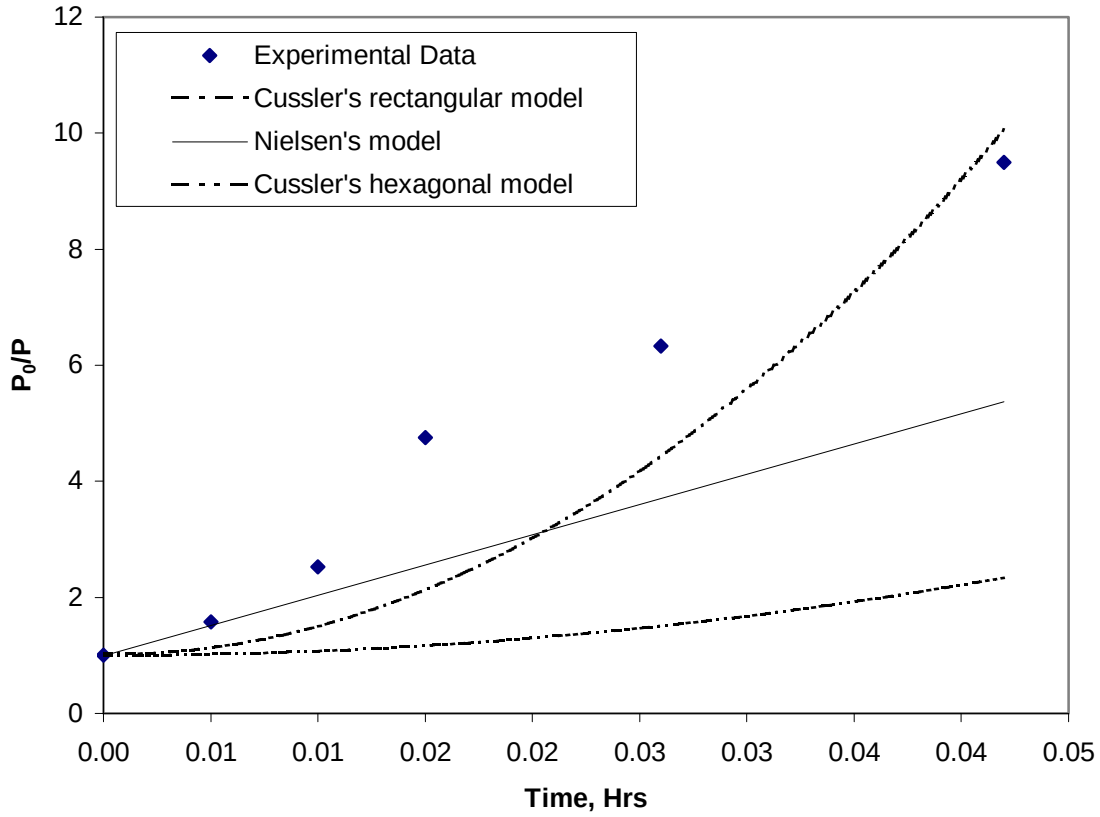

Figure 11: Comparison of oxygen diffusion data from [27] with different models

Table 8: Water diffusion data [27] and comparison with different models

Loading	Permeability ratio	Cussler's rectangular	Nielsen's prediction	Cussler's hexagonal	Alpha
0	1	1	1	1	100
0.005	1.39	1.13	1.51	1.02	
0.010	2.17	1.52	2.03	1.08	
0.015	3.13	2.18	2.56	1.17	
0.026	3.85	4.37	3.66	1.50	
0.042	6.25	10.06	5.39	2.34	

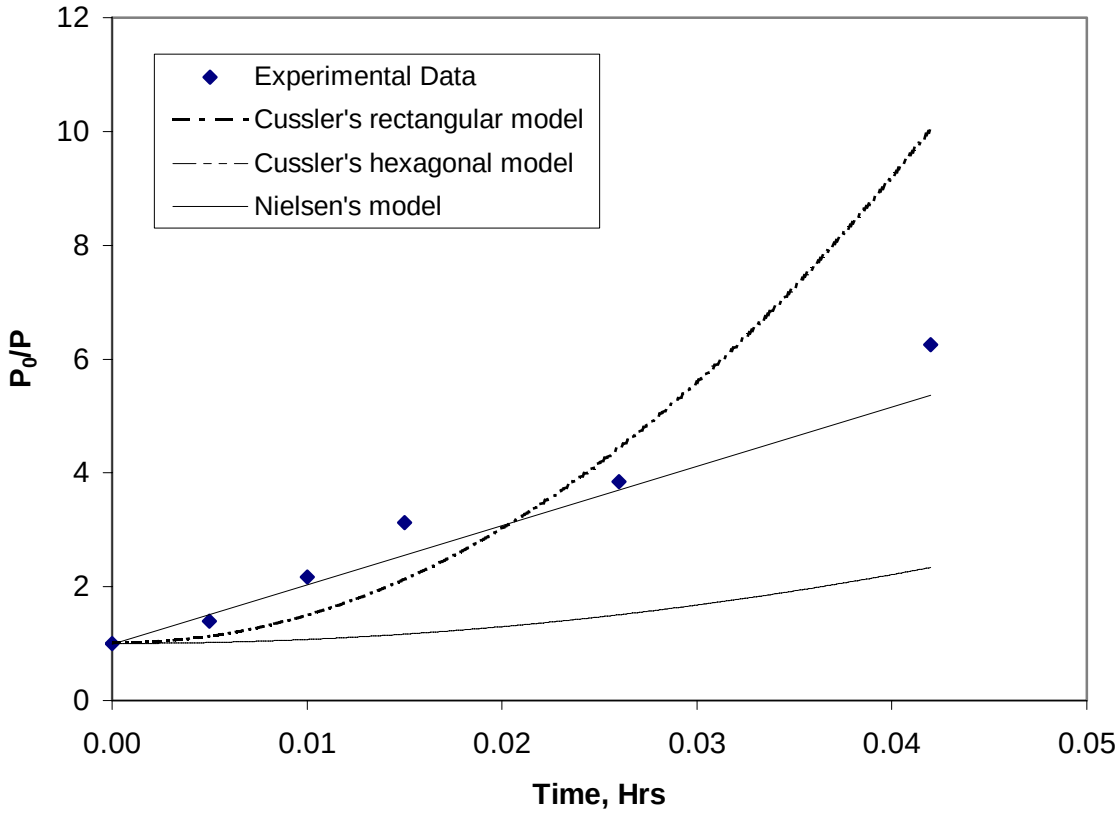

Figure 12:Comparison of water vapor diffusion data [27] with different models

Figures 11 and 12 show that, for relatively low loading values, Cussler's models do not give true limits for the decrease in permeability obtained on addition of flakes. It is also observed that Nielsen's model is closer in approximating the permeability ratio for low loading values.

Hence, it can be inferred that existing models do not always represent the data accurately. They in fact are supposed to serve as the limits within which the experimental data would lie. We think that existing models fail to take into account following things:

1. These models start with an overlapping geometry. Such geometry is not obtained unless the loading level is around 15-20 %. In most cases the flake-specific gravity is more than that of the matrix material and obtaining such high loading

levels would only be possible if about 30-35 percent by weight of fillers is added, which is highly unfeasible.

2. The effect of different layer spacing for the same aspect ratio and loading levels is not taken into account.
3. Number of particles per unit volume in the matrix with the same aspect ratio and loading level also has a bearing on the decrease in diffusivity. These models fail to take this into account.

Cussler's three-dimensional model with hexagonal flakes provides a lower limit to the decrease in diffusivity in nanocomposites, and we have found nothing contrary to this. Also, these models provide a means of obtaining rough idea of the aspect ratio of the flakes in the composites without any TEM analysis.

During the course of this work, an attempt was made to try to include the above-mentioned ideas by applying a finite difference analysis to a representative repeating unit. The basic assumption of a repeating geometry is still there, but we limit our analysis to a non-overlapping regime and address the issues mentioned above. The results obtained are encouraging.

2.9.1.c Adsorption theory

Drozdov et al [25] proposed a similar kind of model to explain the decrease in diffusion coefficient of vinyl ester samples on addition of nanoclay. In this study, adsorption of water on the surface of filler clay was assumed to be the prime reason for a decrease in permeability. Adsorption of water on the surface of filler particles was determined by a first order reaction.

The theory assumes that diffusion occurs only through the polymer matrix and not through the clay particles. This is a fairly reasonable assumption as the diffusivity for clay is several times lower than the resin. The water molecules once they reach the clay surface are immobilized on the platelet.

The rate of sorption in glassy polymers noticeably exceeds the rate of diffusion, i.e., concentration of water at surface of the sample reaches a constant value (n_1^0) as soon as the sample is exposed to a concentration gradient. So, a fraction of water molecules entering the nanocomposite are immobilized on the surface of the clay platelets increasing the concentration of water in clay, and the rest of the water molecules increase the moisture concentration in the matrix. Therefore, diffusion of water through the matrix is described by following mass balance equation:

$$\frac{\partial n}{\partial t} = -\frac{\partial J}{\partial x} - \frac{\partial n_1}{\partial t} \quad \ldots (2.83)$$

where

t : time

x: position

n: moisture concentration at time t at position x in matrix

J: mass flux of water

n_1: Concentration of water molecules immobilized at the surfaces of clay platelet

The mass flux still obeys Fick's equation:

$$J = -D\frac{\partial n}{\partial x} \quad \ldots (2.84)$$

where, D, is the diffusion coefficient.

Adsorption of water molecules on the surface of the clay platelets is determined by the following first-order, kinetic equation:

$$\frac{\partial n_1}{\partial t} = K_1 n(n_1^{\,0} - n_1) \qquad \ldots (2.85)$$

where, $n_1^{\,0}$, is the total number of sites where the molecules can be immobilized and, K_1, is the rate constant.

Equation (2.85) implies that the rate of adsorption is proportional to the concentration of water in the matrix, n, and to the current number of "unoccupied sites" on the surface of the clay platelet. Now the constant surface concentration assumption leads to the following boundary condition

$$n(t,x)_{x=\pm l} = n^0 \qquad \ldots (2.86)$$

where, n^0, is the equilibrium concentration in the matrix on the faces.

If the moisture content in a sample before the starting the transient experiment is neglected, the following can be taken as the initial conditions to solve the problem

$$n(t,x)_{t=0} = 0$$
$$n_1(t,x)_{t=0} = 0$$

This system of partial differential equation is solved numerically using the above listed boundary conditions and initial conditions for parameters D, K_1, and the ratio n_1"/n^0.

3.0 Models to quantify the decrease in diffusivity

In previous chapters, different models present in literature were discussed. These models quantify the decrease in diffusivity for nanocomposites. In Chapter 2 we also compared the predictions of the available models with experimental data present in literature. We found that at times these models were not able to provide information, which corroborates with experimental data, possibly because of the underlying assumptions involved in the derivations of these models.

One of the major assumptions underlying the present models is that the barriers, which are in the form of flakes, have one dimension that is the same as the membrane width. Besides this, the other major assumption is regarding the geometry involved, which has a configuration that could only be obtained at high loading levels and had a fixed interlayer spacing. Although we still used the same ribbon shaped flakes, we tried to answer some of the other questions raised here and before and also compared the results with the experimental data of our own.

The physical situation being considered is shown in Figure 13, where mass transfer takes place in the positive z direction through a membrane containing very large number of rectangular cross-section flakes or nanochips. Only three layers of flakes are shown although the total number of layers is very large. As seen in the front view in Figure 14, each flake has a thickness t and width w. The flakes are assumed to be extending in the y direction so that they are equal to the sample length, as shown in Figure 13. The diffusion coefficient is reduced by the presence of flakes, but the reduction is likely to be the smallest when the flakes are arranged below each other as in Figure 14, where each nanoflake completely overlaps the flake below it. The diffusion coefficient reduces

further when the chips are staggered in the x direction as shown in Figure 15; the extent of overlap in the x direction is measured via the quantity θ, which is defined as s/w (see Figure 16). Clearly, D decreases as θ decreases from its initial value of unity, but there is likely to be little additional decrease in D as the extent of stagger is increased beyond a θ value of zero, at least under some conditions. Of course, staggering the chips in the y direction can reduce the diffusion coefficient further, but this is not considered here.

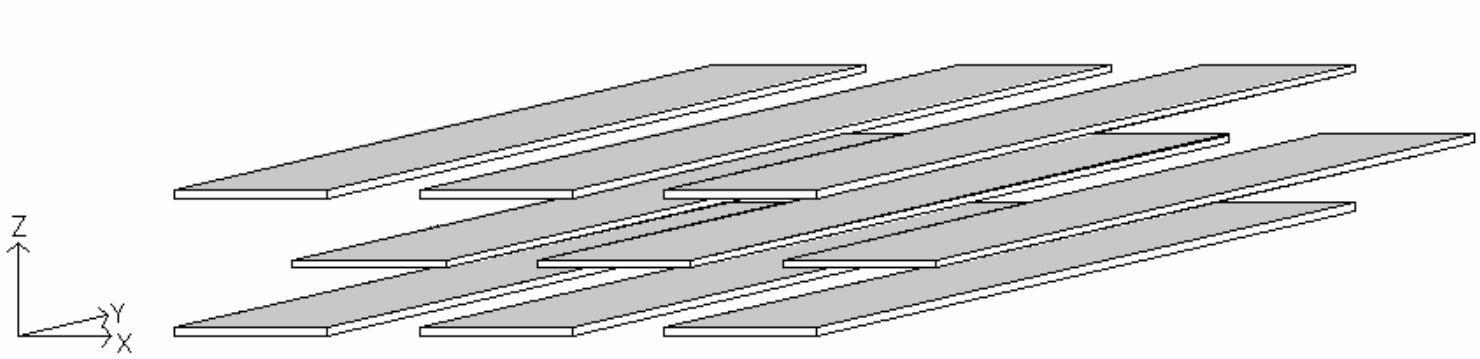

Figure 13: Nanofillers in a polymer matrix

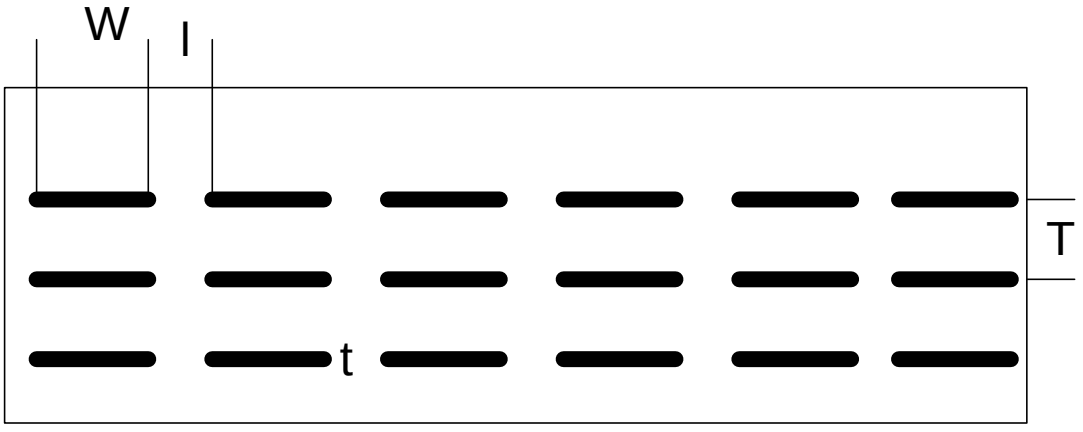

Figure 14: Nanofillers in polymer matrix (two dimensional view)

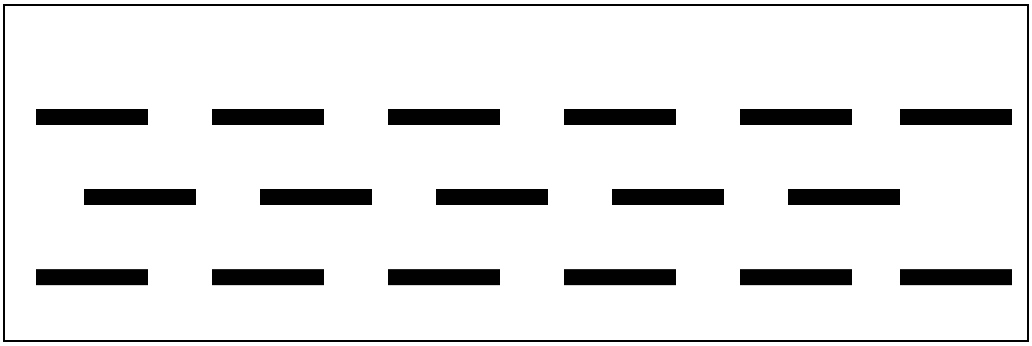

Figure 15: Staggered flakes in a polymer matrix

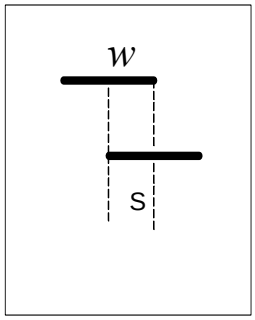

Figure 16: Definition of θ as s/w

In order to define the morphology, we also need to specify three other quantities. With reference to Figure 14, the intermediate length or the distance between neighboring flakes in the x direction is taken to be *l*, and the vertical distance between two layers is (T-t). Thus, a single chip is contained in a unit cell that is a rectangular parallelepiped of dimensions (*l* + w) in the x direction, to the thickness of the polymer sample in the y direction and T in the z direction. As a consequence, the volume fraction of filler ϕ is (wt)/[(*l* + w)T]. Note that for small values of *l*, it is possible for a chip to cross the boundary of a neighboring cell as θ is decreased or as the stagger is increased.

From an analytical standpoint, therefore, we seek to obtain the value of the nano-composite diffusivity D for specified values of α, ϕ, θ, l, t and T.

3.1 Solution Procedure

Since we have repetitions after 2 layers, we divide the region of interest into cells that repeat themselves in three dimensions. One such representative cell is shown in Figure 17.

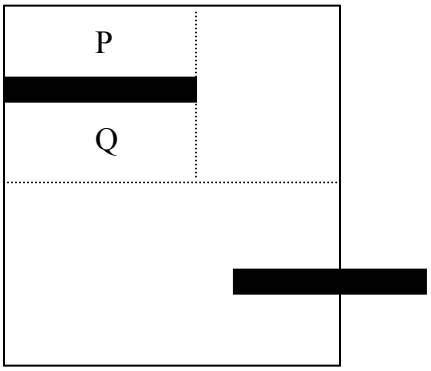

Figure 17: A representative cell

The resistance to mass transfer, defined as the ratio of the concentration driving force to the mass transfer rate, for any of the cells described above, can be calculated using the series parallel method. With reference to Figure 18, the resistance R_p of the block P will be

$$R_P = \frac{L_p}{D_{pol} A_P} \tag{4.1}$$

in which D_{pol} is the diffusion coefficient for the neat polymer.

Similarly, the resistance of the chip will be

$$R_{chip} = \frac{t}{D_{clay} A_P} \tag{4.2}$$

where D_{clay} is the diffusion coefficient for clay, and its value is taken to be very close to zero.

Again, the resistance of the block Q will be

$$R_Q = \frac{L_Q}{D_{pol} A_P} \tag{4.3}$$

and the resistance of the left block (R_{PQ}) will be ($R_P + R_Q + R_{chip}$) as the blocks P and Q and the chip are in series. The resistance of the block R (R_R) can be calculated in a similar manner and the effective resistance of the whole block will be $(\frac{1}{R_{PQ}} + \frac{1}{R_R})^{-1}$.

Using this strategy, the resistances of the other layer of the repeating cell shown in Figure 17 can also be calculated.

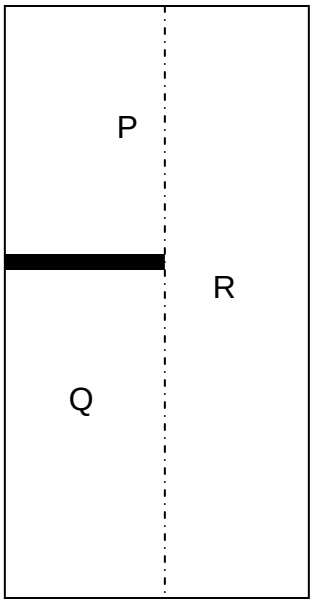

Figure 18: Sample block with imbedded nanochip in the polymer matrix

and the effective diffusivity *D* can be calculated as

$$D = \frac{Thickness\ of\ 2\ layers}{(Total\ Area)(R_{total})} \tag{4.4}$$

from which the ratio of the two diffusivities $(\frac{D_0}{D})$ can be easily calculated. This procedure is used when there is complete overlap. When there is only partial overlap between the chips in the top layer and the bottom layer, the mass transfer path is the one shown in Figure 19. The path length now is larger than before, while the area for diffusion is smaller than before; this is the reason why the diffusivity decreases with increasing stagger. As the amount of stagger is increased, at small values of *l*, the diffusivity will go through a minimum since further increases in stagger will bring one back to the starting configuration. At very large values of *l*, on the other hand, the diffusivity will decrease initially but then remain unchanged.

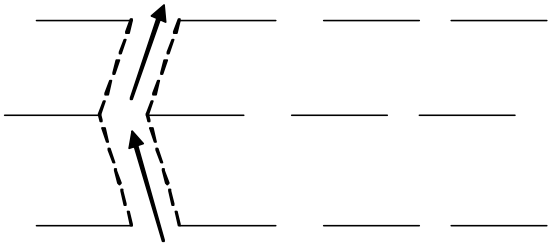

Figure 19: Path of diffusant

We believe that this very simple approach of ours captures the essential physics of the problem, and the computational results allow us to reach useful conclusions.

The computational results are presented in dimensionless form in Tables 9-11. Since we are interested in polymer nanocomposites, it is helpful to think in terms of a flake thickness of 1 nm. If the width w is taken to be 20 nm, the aspect ratio α becomes 10. If we take the distance *l* to be 0.1 nm, the flakes are very close to each other, and the dimensionless intermediate length σ, defined as the ratio of the intermediate length *l* to

the flake thickness, has the value 0.1. Then, at a low loading level ϕ of 0.05, the corresponding value of T is 19.9 nm. The effect of keeping the upper layer of flakes undisturbed (fixed α and σ) while staggering the lower layer (by changing θ at fixed T) or changing the layer spacing (by changing ϕ at fixed l) is explored in Table 9. Since the gap between neighboring flakes is very small, the resistance to mass transfer is large, and even when the flakes are situated below each other (θ = 0.9999), the ratio D_0/D is 201. Upon decreasing θ even slightly, the gap between the flakes is completely covered by the layer of flakes above and below a given layer. This results in a progressive increase in the path length and a progressive decrease in the mass transfer area for the diffusing molecules with a concomitant increase in D_0/D. As a consequence, D_0/D increases until a given flake is directly below the gap in the upper layer of flakes; when θ equals 0.5, D_0/D has a value of 251.75, which is close to the maximum value for this quantity. Further reductions in θ then lead to decreases in D_0/D. When the loading level ϕ is increased, keeping the other quantities unchanged, the layer spacing (T-t) decreases. Thus, at a ϕ value of 0.1, T is 9.95 nm, while when ϕ equals 0.2, T is 4.975 nm. Consequently, at a fixed value of θ, increasing ϕ makes the diffusion path more and more tortuous, *except when θ is unity*. As a result, D_0/D is independent of ϕ (at fixed σ) when θ equals 1.0, but it increases and then decreases in an essentially symmetrical manner as θ is reduced. The maximum value of D_0/D, however, depends sensitively on the loading level ϕ. In other words, the parameters α and ϕ are, by themselves, not enough to theoretically determine D_0/D as suggested by Equations (2.41) and (2.63).

Table 9: Values of diffusivity ratio for α= 10

ϕ	θ	$\frac{D_0}{D}$ $(\sigma = 0.1)$	$\frac{D_0}{D}$ $(\sigma = 1.0)$	$\frac{D_0}{D}$ $(\sigma = 10)$
0.05	0.0001	201.00	21.05	4.68
	0.25	214.201	23.31	6.79
	0.5	251.75	26.79	4.68
	0.75	213.68	222.45	3.42
	0.9999	201	21.00	3.00
0.2	0.0001	201.0	21.93	30.00
	0.25	412.21	54.34	63.75
	0.5	1013.1	113.61	30.0
	0.75	404.01	44.75	9.75
	0.9999	201.00	21.00	3.0

Table 10: Values of diffusivity ratio for α= 30

ϕ	θ	$\frac{D_0}{D}$ $(\sigma = 0.1)$	$\frac{D_0}{D}$ $(\sigma = 1.0)$	$\frac{D_0}{D}$ $(\sigma = 10)$
0.05	0.0001	601.0	61.16	9.38
	0.25	944.72	101.35	21.88
	0.5	1957.8	202.86	28.43
	0.75	940.19	96.48	12.36
	0.9999	601.00	61.0	7.00
0.2	0.0001	601.00	63.55	45.16
	0.25	6100	706.6	245.2
	0.5	22309	2330.8	350.0
	0.75	6028	628.45	92.75
	0.9999	601.0	61.00	7.00

Table 11: Values of diffusivity ratio for α= 50 and σ = 0.1

ϕ	θ	$\frac{D_0}{D}$
0.05	0.0001	1001
	0.25	2580
	0.5	7269.8
	0.75	2568.2
	0.9999	1001
0.2	0.0001	1001
	0.25	2627
	0.5	10130
	0.75	26706
	0.9999	1001

Table 9 also examines the effect of increasing the intermediate length *l*, using a σ value of 1.0. Now, the gap between the flakes is ten times larger than the value employed previously. This results in a sharp and essentially proportionate reduction in D_0/D; when θ is close to unity, the value of D_0/D is 21. Changes in θ and ϕ lead to qualitatively and proportionately similar variations in D_0/D as those seen earlier. When the horizontal distance *l* between neighboring flakes is taken to be half the flake width, D_0/D further reduces to 3 when all the flakes are arranged below each other. As θ tends to zero, the flakes in a given layer are again able to cover the gaps between the flakes in the layers above and below. As a consequence, D_0/D increases and then decreases with decreasing θ. If *l* were to be increased by a further order of magnitude, no amount of stagger would completely cover the gap, and the very large variation of D_0/D with θ would no longer be observed. In this case, D_0/D at $\theta = 1$ would still give the smallest value of D_0/D, and it would become maximum at $\theta = 0$, but remain unchanged thereafter. Furthermore, when θ has reached the value zero, changing the aspect ratio (or having a distribution of flake widths) at constant flake thickness will not affect the results. Clearly, the computations of Table 9 suggest that experimental results for D_0/D, at constant values of α and ϕ, can lie in a fairly wide range. Practically speaking, this reflects the influence of the extent of dispersion, and it happens because of reasonable variations in the values of *l* and T corresponding to the same values of α and ϕ. *This fact does not seem to have been recognized in the literature, and it is a key message of the present work.*

Table 10 examines the effect of changing the aspect ratio α from 10 to 30. If we assume that α decreases from 30 to 10 because of a decrease in the chip width w, due to

attrition, then a comparison of Tables 9 and 10 shows that, at the same values of σ and ϕ, D_0/D is very significantly smaller. This comes about because the fractional area available for mass transfer gets increased when w is decreased without decreasing *l*. On the other hand, we may assume that α is reduced from 30 to 10 because three chips having w = 60 nm and t = 1 nm have got stuck together. In this case, if *l* is taken to be unchanged at 1 nm, say, the numbers in Table 10 should be compared with those in Table 9 at a value of σ that is 1/3 that in Table 10. One now finds that decreasing the aspect ratio tends to reduce D_0/D because of the aspect ratio effect just considered, but the reduction is less than expected because it is partly offset by a decrease in the dimensionless gap between neighboring chips. Thus, at a fixed value of ϕ, changes in aspect ratio, brought about by a decrease in w, are not equivalent to those resulting from an increase in t.

Table 10 also looks at the effect of changing the extent of stagger at different fixed values of nanofiller loading. The trends are similar to those seen earlier in Table 9, but the values of D_0/D are now much larger, demonstrating the strong effect of aspect ratio in the presence of overlap of one layer of chips by another layer of chips. This is further reinforced by the calculations presented in Table 11 where the aspect ratio has been increased further to 50. Clearly, if the goal is to reduce diffusivity by a few orders of magnitude, this can be accomplished at fairly low loading levels simply by employing flakes of large aspect ratio, by reducing the gap between neighboring flakes in any given layer and by staggering the flakes so as to cover the (small) gaps in the layer above and the layer below.

3.2 Finite Difference Calculations

Having examined the situation where the flakes are very close to each other, we now turn to the situation where the flakes are far apart. This is a more likely scenario for polymer nano-composites containing a few weight percent of nano-fillers. For this purpose, a finite difference scheme was used to compute the steady-state concentration profiles by solving Laplace's equation over the region shown in Figure 20; this unit cell repeats itself in two dimensions. Continuity of concentration and flux was assumed at the interface between the two phases. As before, the barrier cross-section is a rectangle of dimensions W and T resulting in an aspect ratio α of w/2t. The volume fraction of filler ϕ is clearly 2wt/WT.

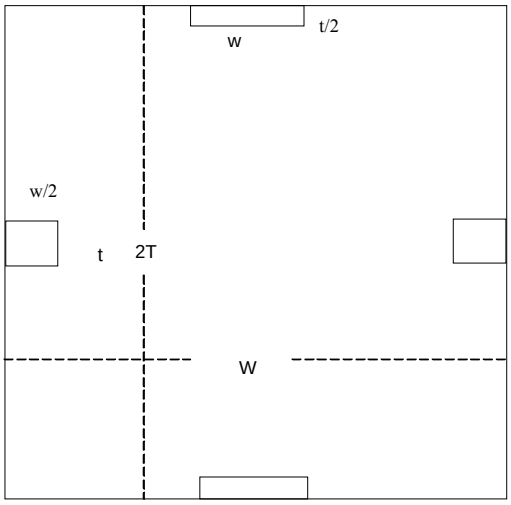

Figure 20: Representative element used for finite difference analysis

3.2.1 Method of Solution

Finite difference scheme is used to solve the steady-state Laplace differential equation

$$\frac{\partial^2 c}{\partial x^2} + \frac{\partial^2 c}{\partial y^2} = 0 \qquad \ldots(4.5)$$

subjected to the following boundary conditions ($\frac{\partial c}{\partial y} = 0 \,\&\, \frac{\partial c}{\partial x} = 0$, at the nodes where nano-chips are present). For the nodes inside the chips, the use of no flux boundary condition reduces to a zero concentration boundary condition. So $C_{nanochip}$=0 boundary condition is applied to obtain the concentration profile in the polymer block with nanochips. We divide the barrier cross-section into nodes as shown in Figure 21.

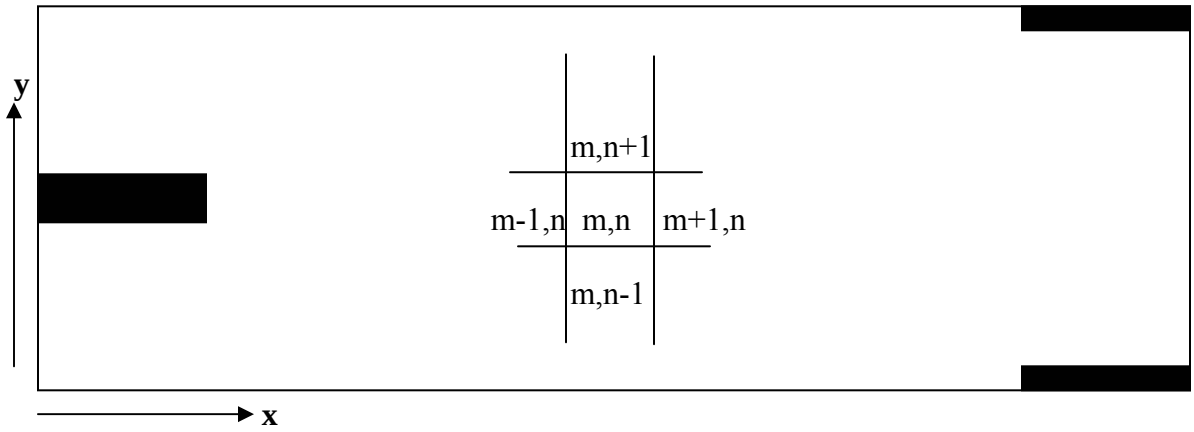

Figure 21: A figure showing half of the repeating unit divided into different nodes

Figure 21 shows, half of the actual element shown in Figure 20. The concentration profile for the other half would just be a mirror image of the concentration profile obtained for element shown above.

Each of the rectangular blocks represents a node and forms the volume element to be used in the explicit finite differences method to solve the steady state PDE. The nodes that fall on the chips have zero flux boundary condition, as the chips are considered to be impervious.

Let M be the number of nodes in x direction & N be the number of nodes in y direction.

$$\Delta x : \frac{W}{M}$$
$$\Delta y : \frac{L}{N} \qquad \ldots(4.6)$$

The thickness in the z direction is assumed to be the same for the polymer unit and the chips. The areas A_x and A_y will be $\Delta y \times 1$ and $\Delta x \times 1$. For an internal node (m,n) applying mass balance at steady state

Mass in from left + Mass in from the right + Mass in from the top + mass in from the bottom = Accumulation

$$D\frac{c(m-1,n)-c(m,n)}{\Delta x}\times A_x + D\frac{c(m,n+1)-c(m,n)}{\Delta y}\times A_y + D\frac{c(m+1,n)-c(m,n)}{\Delta x}\times A_x$$
$$+D\frac{c(m,n-1)-c(m,n)}{\Delta y}\times A_y = 0 \qquad \ldots(4.7)$$

Dividing by A_xA_y we have the following equation for an internal node

$$\frac{c(m+1,n)+c(m-1,n)-2\cdot c(m,n)}{\Delta x^2}+\frac{c(m,n-1)+c(m,n+1)-2\cdot c(m,n)}{\Delta y^2}=0 \qquad \ldots(4.8)$$

For a node on the boundary on the left and not lying inside the flake

$$\frac{c(m+1,n)-c(m,n)}{\Delta x^2}+\frac{c(m,n-1)+c(m,n+1)-2\cdot c(m,n)}{\Delta y^2}=0 \qquad \ldots(4.9)$$

Symmetry is also used for every node, which is a mirror image of the node on the left.

With dimensions of (W = 800, w= 100, t=1, and T = 5, typical ratios of the dimensions in the x and y directions) we obtain the concentration profile, and an average concentrations in the x direction were determined as a function of y to determine an

average value for $\frac{\partial c}{\partial y}$. The values for W, w, T, and t shown above represent the true size ratios that would exist in an actual polymer sample.

If c_m and c_n were two adjacent nodes in the element next to the boundary, the flux would be given by

$$Flux = \frac{\sum D_0 \frac{c_m - c_n}{\Delta y}.\Delta x}{T} \qquad ...(4.10)$$

and the ratio D_E/D_0 can be obtained from

$$D_E \left(\frac{\partial c}{\partial y} \right)_{ave} = Flux \qquad ...(4.11)$$

4.0 Experimental Details

The permeation experiments were carried out using MOCON PERMATRAN W3/33, details for which are provided later in the chapter. The experiments for studying the mechanical and dynamic mechanical properties of the nanocomposites, as a function of clay, were also carried out.

4.1 Materials

The resin used in the study is HETRON™ epoxy vinyl ester resin obtained from the ASHLAND chemical company. The resin contained 45 % dissolved styrene. The resin was cured at room temperature as recommended by the company. 1 wt % of methyl ethyl ketone peroxide (9% active oxygen) was used as an initiator and 0.03 wt% of 6% cobalt naphthenate was used as catalyst. Both chemicals were obtained from Sigma Aldrich Company.

4.1.1 Nano-Fillers Used:

Nano-Composites were made using following fillers:

(i) Nano-Clay

Cloisite 10A®, a surface treated montmorillonite, obtained from Southern Clay Products; it is in the form of platelets that are 1 nm thick and about 180 nm in lateral dimensions.

(ii) Kevlar Fibers:

Kevlar® pulp obtained from the DuPont Company. This material has a specific gravity of 1.44 and is made up of 2 mm long, 12 μm diameter fibers that are surrounded by smaller attached fibrils. Kevlar® pulp is generally used in adhesives and sealants and also in FRPs.

(iii) Carbon Nano Wires. One hundred to two hundred nm diameter carbon nanofibers, Pyrograf 3, grade PR-19 obtained from ASI, Inc.

(iv) Glass Fibers: Bi-directional glass fiber fabric of density 0.543 kg/m^2 obtained from Vectorply Inc.

4.2 Sample Preparation

Samples for permeation experiments were made using Resin Transfer Molding (RTM). Typical dimension of the samples used for permeation experiments were 10 cm x 10 cm. Sample thickness was around 1 mm. Polymer was allowed to cure at room temperature for 24 hours. Post curing of the samples was carried out in an oven at 185° F for 2 hours. Nano-composite samples were prepared by mixing different weight percentages of Cloisite 10A® in the resin. To ensure the uniform distribution of clay, mixing was carried out for 24 hours using a stirrer. To reduce the amount of voids in the sample the RTM process was done under vacuum. The samples containing Kevlar and carbon nano fibers were made using hand molding because Kevlar and carbon fibers increase the matrix viscosity enormously which makes the resin unsuitable for use in the RTM machine.

4.3 Overview of the RTM Experiment

Following steps were performed in preparation of a sample using resin transfer molding.

Step 1: Re-circulation: This step involves circulating the resin or resin/clay mixture, back and forth from the resin tank to the injection sprue. It is a critical step because it helps in removing air bubbles from the system.

Step 2: Mold Preparation: This involves application of silicon mold releasing spray and placement of glass fiber (if a fiber glass sample is being made) in the mold.

Step 3: The prepared mold is kept under vacuum for 15 minutes before injection. This is done to evacuate as much air as possible from the mold.

Step 4: Injection: The next step involves injection of resin inside the mold. It is done in three steps. Each time 100 cm^3 of resin (resin + 1.5 wt% catalyst) is pumped into the mold.

Step 5: Finally, the whole system is flushed with acetone and the mold is kept untouched to set for 24 hours.

Step 6:The sample is taken out after 24 hours and post cured at 185 F for two hours using a compression-molding machine.

Step 7: The post-cured sample is then cut using a tile-saw to a 10cm by 10cm size.

A typical RTM apparatus is shown in Figure 22. The injection pressure required for injecting the resin inside the mold is obtained from the laboratory air supply line, which provides air at a pressure of 80 psi.

Figure 22: A typical RTM set up

4.4 Injection Machine

The machine used for resin transfer molding process is Megaject RTM-Sprint, which is a pneumatically-powered, medium-output machine designed for accurate mixing and injection of a wide range of resin systems. The precision fluid pumps achieve mix output as low 150 g/min up to 6 kg/min. Standard features include a variable catalyst ratio, solvent flush and both resin and catalyst re-circulation at the mix-head. The Megaject RTM-Sprint incorporates Mould Pressure Guard (MPG) designed to protect the mold from excessive injection pressures and optimize mold fill performance

4.4.1 Parts of the Injection Machine

Various parts of the injection machine are enumerated below.

a) Mold Pressure Guard

The mold pressure guard is a control system, which allows the Megaject to maximize it's output by automatic proportional speed control guarding excessive mold pressure.

b) Pre-Determining Counter (PDC)

Pre-determining stroke counter (count rate every 100 cc) allows for programming the predetermined volume of resin. When the pre-determined count is reached the machine stops automatically.

c) Flow Meter (FM-001)

The FM-001 Flow Meter is a LED read-out and provides a real time indication of the flow rate in liters per minute.

d) Autosprue

An automatic injection sprue is a semi-permanent mold fixture, which controls the flow of mixed resin into the mold cavity. Opened by a control signal from the injection machine, the Autosprue allows material to flow until a predetermined volume has been injected. Upon completion of the injection the Autosprue closes, isolating the mold, and is then flushed through automatically, ready for the next injection cycle.

e) SP-2 Solvent Pump System

Non-pressurized solvent tank incorporates a submersible pump, which provides a pre-set variable solvent flush volume between 30cc and 180cc.

f) Molds

Two types of molds are used:

Aluminium mold: It has a provision of evacuation of air from four vents strategically placed in each of the four top corners of the upper mold half.

Steel Mold: This mold is smaller in size and was made here in WVU. Silicon Spray obtained from Fischer Scientific is used as a releasing agent.

g) Vacuum Pump

The injection in the mold is done after degasifying the sample. Degasifying is done by keeping the sample under vacuum, using vacuum bags and a pump, which sucks the air out. This is done to reduce the number of voids in the sample.

4.5 Overview of the Permeation Experiment

The equipment used for carrying out permeation experiments is a PERMATRAN W 3/33 module purchased from MOCON. It measures the water vapor transmission rate across barrier materials. The sample to be tested is placed in the test cells, which are divided into two chambers separated by the sample material. The inner chamber is filled with nitrogen and the outer chamber with water vapor. The rate of permeation experiment is calculated at equilibrium.

The basic process of testing consists of the following steps:

1. Setting the nitrogen gas flow
2. Conditioning the sample
3. Achieving a baseline zero (Re-zero)
4. Calibrating the system
5. Testing
6. Bypass.

Setting the Nitrogen Gas Flow

Maintaining a proper flow rate of nitrogen is a critical factor. For films having low permeation rates, increased sensitivity is required which is obtained by lower flow rates. The flow rate should be at the same value at which calibration of the standard NIST film was done.

Conditioning the Sample

This refers to the period of time that a sample requires to acclimatize to the environment of the test cell and reach equilibrium.

Rezero

It refers to the baseline value that needs to be subtracted from the flux value before the final values are shown on the screen.

Calibrating the system

The system is calibrated with a standard reference film or available NIST traceable certified film.

Testing

The following steps are involved in the testing process.

First step: Clay-vinyl ester samples obtained using RTM or hand molding, are placed inside the test cells.

Second Step: Degasification: For the use of Time Lag method, (used to obtain the value of diffusivity) it is absolutely critical to remove as much water from the samples, as possible. This is done by keeping the samples at elevated temperatures, (150 F, below Tg), before putting them inside the test cells. Dry nitrogen (supplied from compressed

Nitrogen gas cylinder) is then run on both sides of the samples until low transmission rate values are obtained.

Third Step: If the experiment is being carried out at a relative humidity (RH) value of less than 90%, the required humidity is obtained by adding water to the water-well, where the required humidity is generated by two-pressure method (described later in the chapter). If the experiment is being carried at 100% RH the desired relative humidity is obtained by adding water to the sponges as shown in Figure 23.

Fourth Step: When steady state is reached, data is saved and diffusivity calculated using Time Lag method.

Bypass state

To preserve a low baseline, the cell value is automatically placed in the bypass state.

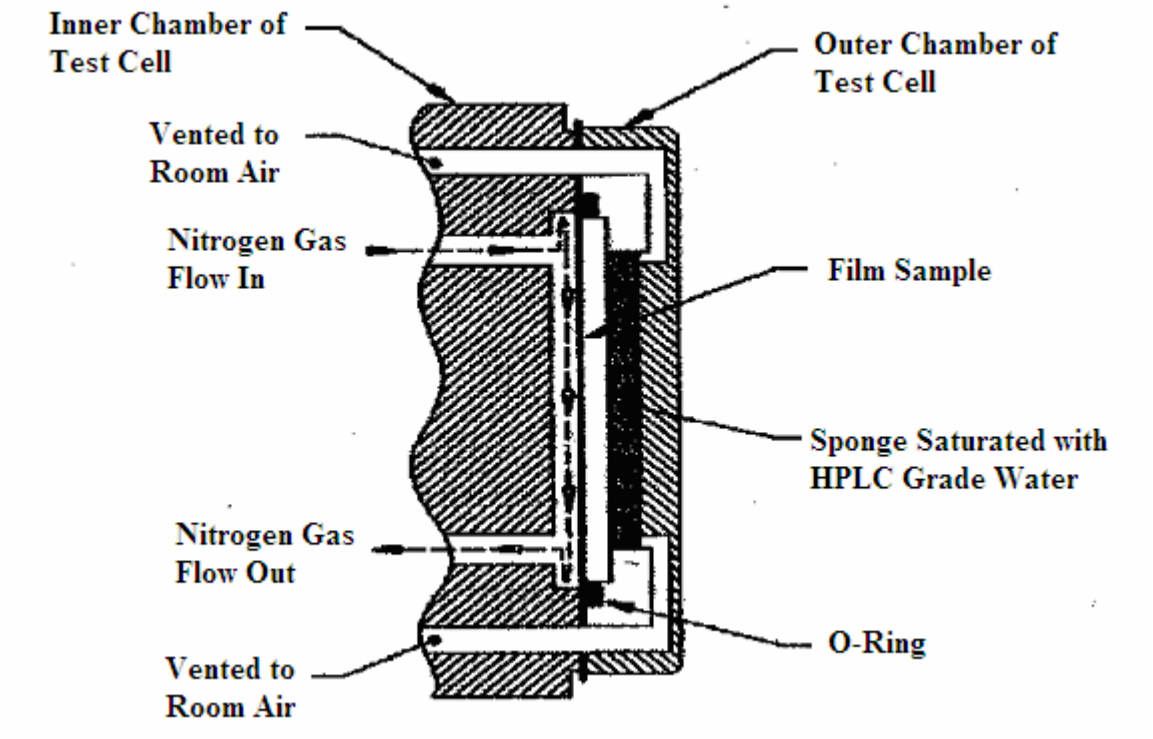

Figure 23: Set up for permeation experiment at 100 % RH (MOCON Permatran User's Manual)

4.6 Factors that Affect Water Vapor Transmission

1. Test Temperature

2. Relative Humidity

3. Flow

4.6.1 Relative Humidity

Relative Humidity is defined by the following ratio:

$$\frac{\text{Amount of water vapor present in the air}}{\text{Maximum amount of water vapor air can hold at given temperature and pressure}}$$

The maximum amount of water that a given amount of air can hold is affected by the temperature and barometric pressure. A given volume of warm air can hold more water than the same volume of cold air, if the pressure is held constant.

In terms of partial pressures relative humidity is expressed as

$$\text{Relative Humidity} = \frac{P_w}{P_s} \times 100$$

where

P_w= the pressure of water vapor present in the air

P_s = the pressure of the maximum amount of water vapor that air can hold

4.6.2 The Relative Humidity Sensor

The PERMATRAN-W 3/33 uses a solid state CMOS semi-conductor device. The sensor consists of an integrated circuit mounted on an eight-pin transistor header and enclosed within a protective stainless steel cover. It is plugged into a standard transistor socket. The sensor package is about 0.370” in diameter and 0.375” high.

4.6.3 Infrared Sensor Theory

When a test film is installed in the test cell, it is exposed to a continuous flow of dry nitrogen gas across the inside and diffusing gas (water vapor) on the outside. The gas leaving the test cell, via the exhaust port, consists of a mixture of nitrogen and water vapor in a ratio determined by the nitrogen flow rate through the test cell and the rate of resulting water vapor transmission through the film barrier. With the nitrogen flow rate, set to a constant value, the resulting water vapor density in the exhaust line of the cell will be determined by the water vapor transmission rate of the film barrier.

The exhaust of the test cell is sent to a pressure-modulated, infrared detection system. The detection system consists of a bellows pump, a sensing chamber, an infrared source, a 2.6-micrometer infrared filter, a lead sulfide photo detector and an amplifier.

The pump varies the pressure and the density of the gas mixture in the sensing chamber. As pressure and density of the gas mixture varies, the absorption rate of infrared energy by water vapor also varies. The infrared photo detector senses the change in infrared energy reaching it and produces a low-level electrical signal, which is transmitted to an amplifier.

The amplifier amplifies, filters, and rectifies the signal from the detector, producing a DC output, which is directly proportional to the water vapor in the exhaust of the test cell, and thus proportional to the water vapor transmission rate of the barrier material. The DC output is converted to a digital value and transmitted to the computer.

4.6.4 Calibration Theory

The PERMATRAN-W 3/33 is a relative (not absolute) water vapor transmission rate (WVTR) measurement system. When using a known transmitter as a reference, the

system determines the relationship between the moisture content of the carrier gas (nitrogen) after it exits the test cell and the moisture content of the carrier gas (nitrogen) after it exits the reference cell.

A reference film at any arbitrarily constant test flow will produce an arbitrary constant amount of water vapor in the carrier gas. The infrared sensor/amplifier produces a DC output proportional to the amount of water vapor. The DC output is converted to a value and transmitted to the computer. The computer subtracts the Re-zero value from the DC output value. The result is converted to the units of water vapor transmission rate (WVTR) using a scaling factor determined by the nitrogen gas flow rate

4.6.5 The Two Pressure Method of Generating RH

The two-pressure method is based on the principle that if pure water and a pressurized gas are confined in a chamber, the gas will reach relative humidity equilibrium of 100%. If that gas is released to an area (or another chamber) at a different (lower) pressure, the percent relative humidity in the new area will be reduced. The amount of reduction will be a ratio of the first and the second pressures.

$$RH = 100 - \frac{[psi_{GAUGE} \times 100]}{psi_{GAUGE} + 14.7}$$

where psi = pounds per square inch

4.7 Flow

The rate at which nitrogen sweeps the moisture in the test cell also have an impact on permeability values obtained from Permatran. For better barriers, Nitrogen flow rate should be slow, so that enough time is available for the equilibrium to set in.

5.0 Results

The results presented in this section have been obtained by analysis of the data obtained from Permatran W3/33. This analysis was first applied to 0.001 cm thick polypropylene film to make sure that the method employed is correct. The value of permeability for polypropylene at 25°C was found to be 27.7 barrers, which is within the range enlisted in literature (15-50 barrers) [3]. The time lag value is 3.32 minutes in this case.

5.1 Results for vinyl ester clay composites

Vinyl ester samples made using resin transfer molding were tested for diffusivity by carrying out permeation experiments. The analysis aimed at finding the dependence of diffusivity on concentration difference and temperature. As mentioned before, the sample thickness was (1 ± 0.15) mm. The first important step involved in the analysis was to determine the dependence of diffusivity of water vapor though vinyl ester composites on concentration. That is to determine whether the diffusion of water vapor through vinyl ester clay composites followed Fick's law. Figures 24 and 25 show results for diffusivity of water vapor through neat vinyl ester and 1 % clay composite samples. The figures have time as abscissa and cumulative amount of water vapor diffusing in time (t) as the ordinate. The experiments were conducted at three different concentrations or relative humidity values of water vapor at the high-pressure side, with zero RH at the lower pressure side. Time lag values were determined at three different values of concentration difference for both neat vinyl ester and composite samples. It is found that the time lag does not vary for experiments carried out at different concentration differences, as is shown in the figures. These experiments were carried at 37.8 °C, which is an ASTM

standard for permeation tests. The results obtained show that the samples with vinyl ester and clay follow Fick's law. From Figures 24 and 25 it can be seen that cumulative amount of water vapor passing through the samples is larger for experiments where higher difference in concentration was used. This concurs with Fick's law, which suggests that flux through a membrane is proportional to the concentration gradient with diffusivity being the constant of proportionality. The diffusivity values for vinyl ester composites containing different amounts of clay are shown in Table 12. In all cases, for different partial pressure values of water vapor, time lag values were found to be same. Thickness of the samples used in the experiments shown in Figure 24 and 25 are 1.1mm and 1.06 mm respectively.

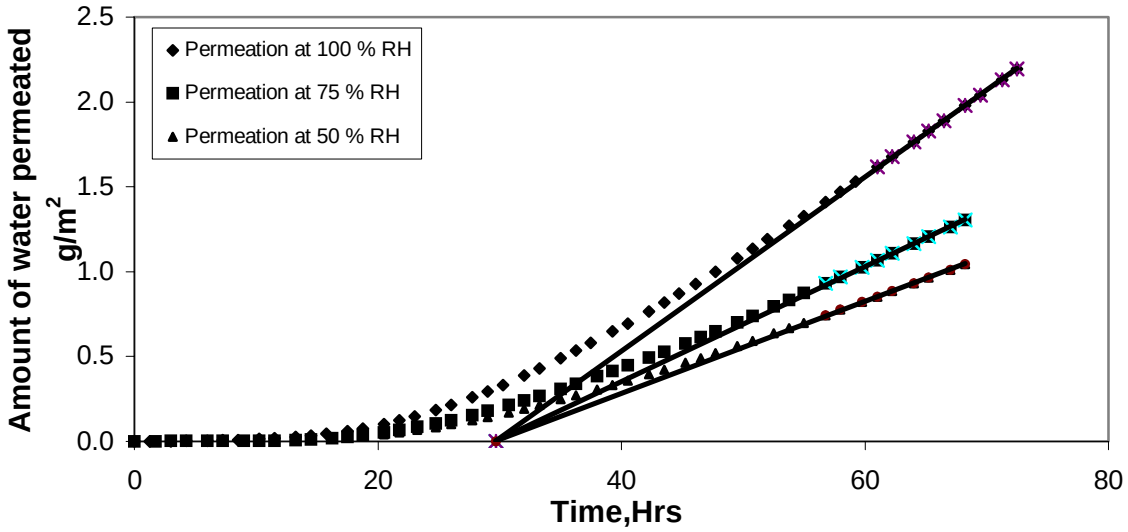

Figure 24 Time lag curve for neat vinyl ester for three different RH values

These figures capture the essential physics of the problem. For films that follow Fick's Law and for which diffusivity is a function of the type of matrix material used and temperature at which it is measured, the improvement can be brought about only by increasing the lag time.

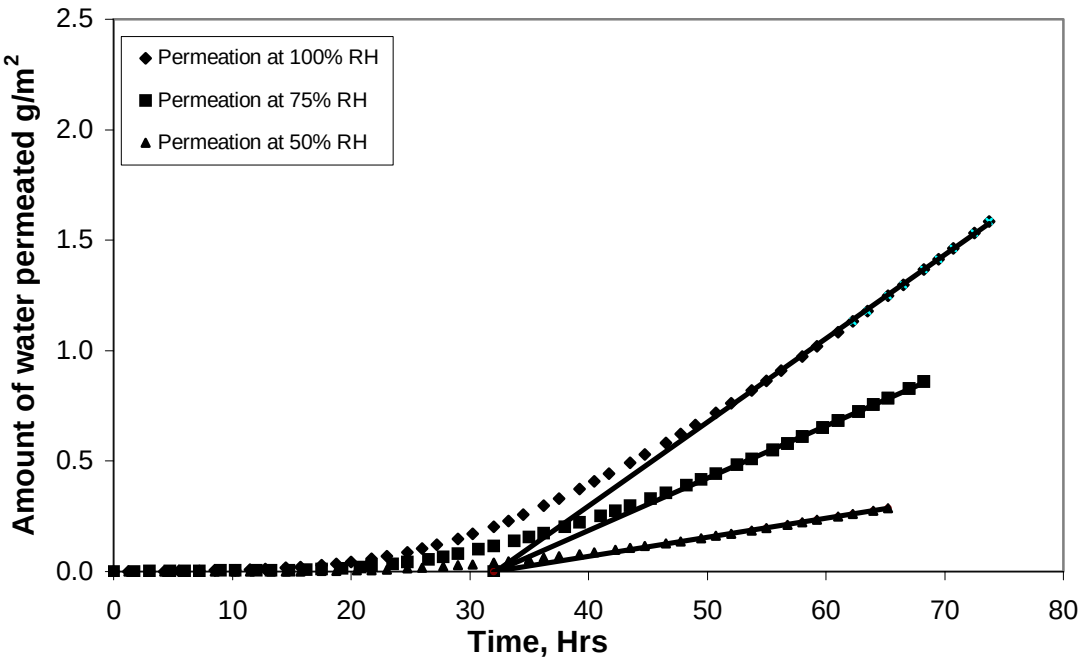

Figure 25: Time lag curve for 1% clay vinyl ester sample at three different RH values

Table 12: Diffusivity values for vinyl ester samples at 37.8 °C

Weight % Clay/VE	Diffusivity x 10^8 cm^2/sec
0	**1.56**
1	**1.43**
2	**1.25**
3	**1.13**
4	**1.07**
5	**0.99**

The diffusivity value reported for diffusion of water vapor through vinyl ester in literature [29] is 1.40 x 10^{-8} cm2/sec at 37.8 °C.

An attempt was also made to study the effect of temperature on vinyl ester clay composites. There are two effects to be studied:

1) Arrhenius law dependence
2) Behavior of clay in reducing the diffusivity at different temperatures

Permeation experiments were conducted at three different temperatures: 37.8 °C, 25 °C, and 15 °C. According to Arrhenius' law, a plot of diffusivity values for a penetrant with the reciprocal of temperature, on a log-log scale, is a straight line. We tried to determine whether this was true in the case of vinyl ester composites. Figures 26 and 27 show the cumulative water vapor permeation curves for neat vinyl ester and for 5 % clay vinyl ester composite at three different temperatures. Three different time lag values are obtained and diffusivity values determined. The sample thickness of the sample used for carrying out experiments with neat vinyl ester is 1.12 mm and for clay composite is 1.05 mm.

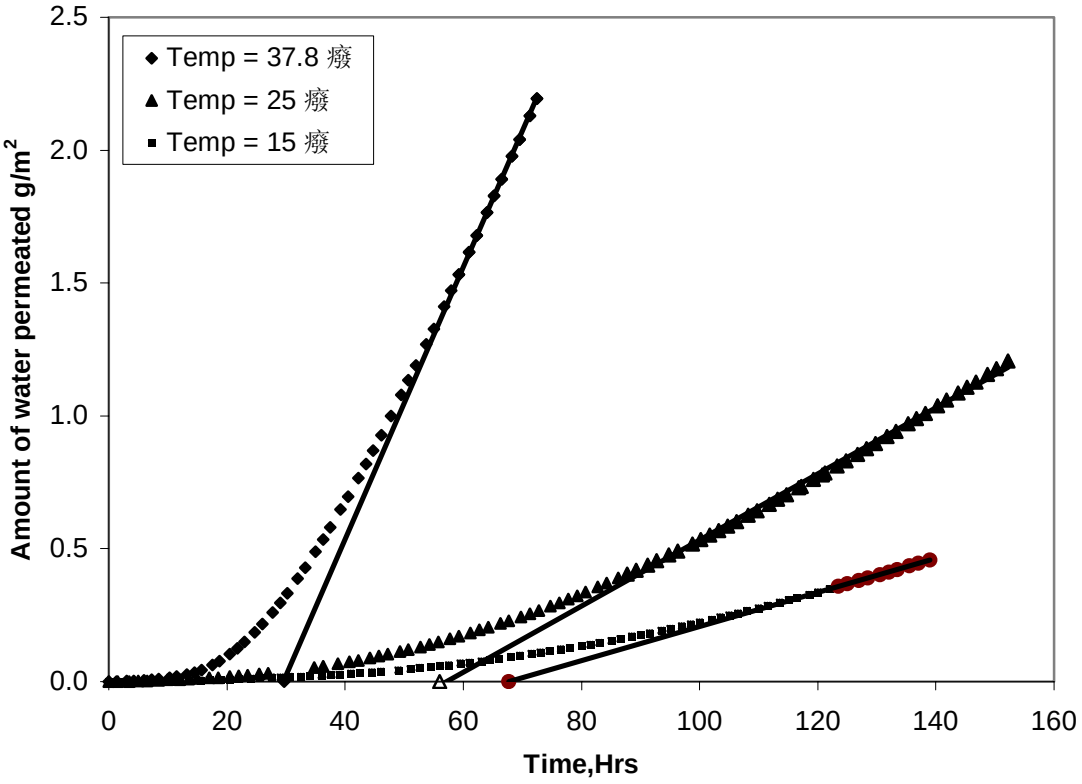

Figure 26:Three different time lag values for three different temperatures at 100 percent RH for neat vinyl ester

It can be seen that although the concentration difference across the samples was kept same, a lower flux is obtained at lower temperatures. Lower diffusivity values are obtained at lower temperatures. This is because the percentage of molecules having sufficient energy to cross the activation energy barrier is lower at lower temperatures.

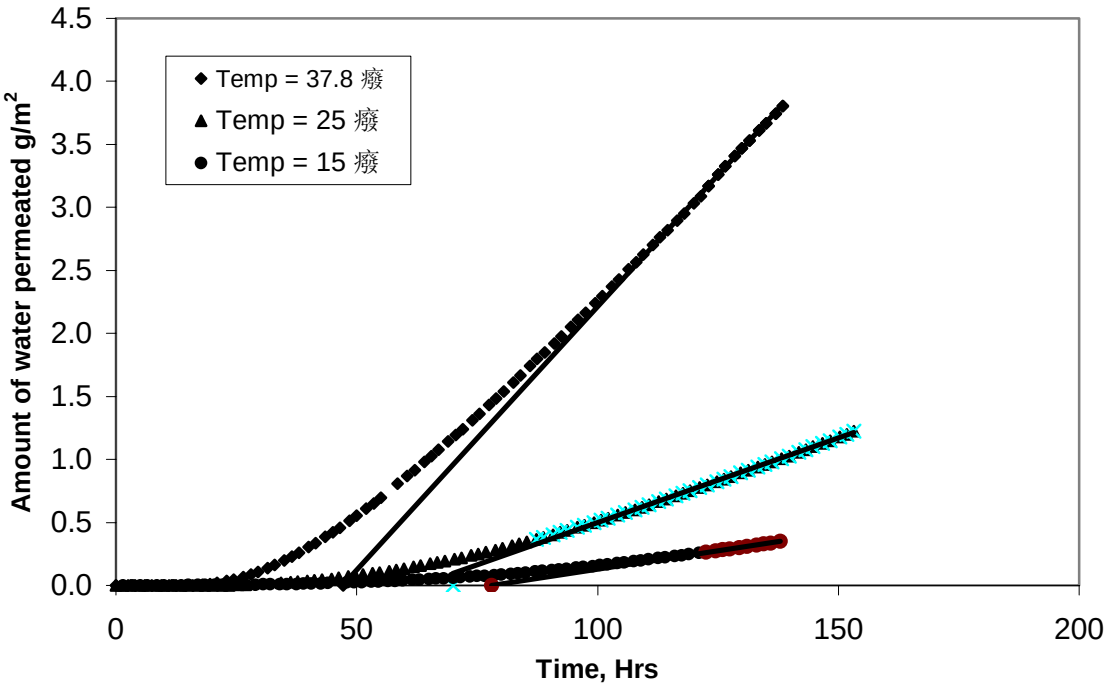

Figure 27: Three different time lag values for three different temperatures for 5 % clay sample

Figures 28 and 29 show the plot of diffusivity values for neat vinyl ester and 5 % clay composite against the inverse of temperature. The diffusivity values tend to fall on a straight line. Congruence with Arrhenius's law further demonstrates that the permeation experiments obey Fick's law. From such an analysis, one can infer that determination of activation energies from intercepts and their comparison can provide valuable insights in determining the differences in morphology for neat vinyl ester and composite samples. Such an analysis, however, was not done during the course of this work and is open to further exploration.

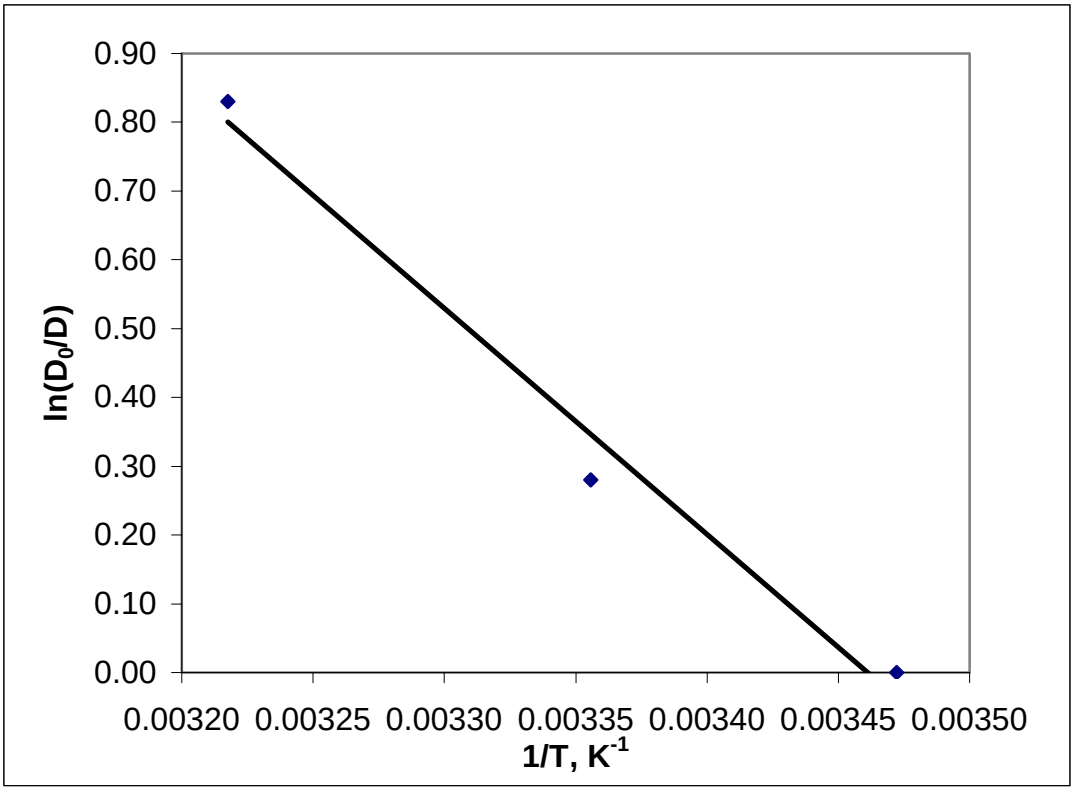

Figure 28: ln(D_0/D) vs 1/T plot for neat vinyl ester samples at 100 % RH

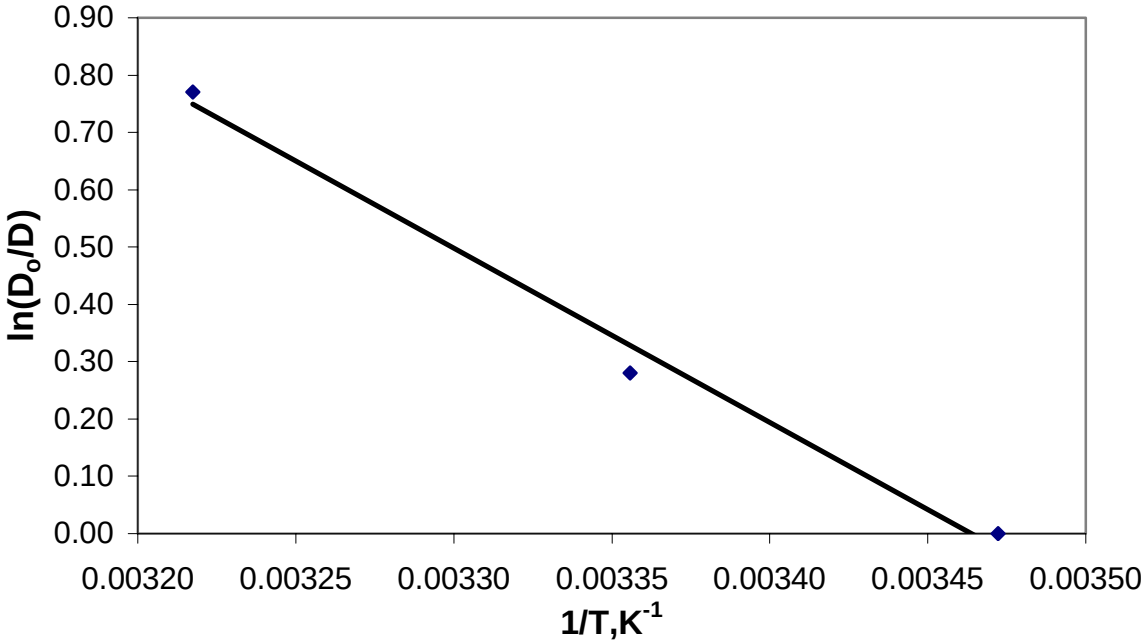

Figure 29: ln(D_0/D) vs 1/T plot for 5 % clay VE samples at RH 100

The second important aspect, as far as temperature is concerned, is determining whether there is a difference in the amount of decrease obtained in diffusivity on the use of physical barriers (clay) in vinyl ester at different temperatures. Table 13 shows the diffusivity values for 5 % clay composite and neat vinyl ester at three different temperatures. Table 13 shows the diffusivity values for neat vinyl ester and vinyl ester clay composites at three different temperatures. It can be observed that the ratio of diffusivity for the neat resin and clay composite at different temperatures lies in a very a narrow range suggesting that it is a constant. This is a very important result as it states that the effect of adding physical barriers is independent of temperature and that the decrease is a result of increased tortuosity and a decrease in the available area of diffusion.

Table 13: Diffusivity for neat and 5% clay VE samples at 3 different temperatures

Temperature °C	Diffusivity Value through neat vinyl ester $cm^2/sec \times 10^8$	Diffusivity Value through 5% clay composite $cm^2/sec \times 10^8$	Ratio of Diffusivities for Neat VE and clay composite
37.8	1.56	0.99	1.57
25	0.90	0.64	1.40
15	0.68	0.45	1.51

Computational results are presented in Figure 30, and it is seen that for fixed values of w, t, α, and ϕ, the reduction in diffusivity also depends on the spacing between two adjacent barrier layers. In other words, as one adjusts W and layer spacing, T, to keep

the product WT constant, D_0/D changes significantly. As explained earlier, this is understandable. For small values of T, W is so large that there is one-dimensional mass transfer and $D = D_0(1-2w/W)$. Here, w is, as defined before, the thickness of the flake and W is the thickness of the computing cell. At the other extreme, for large values of T, W is so small that it approaches the minimum value of 2w and mass transfer effectively ceases. The significance of this result is that it is difficult to predict the observed diffusivity reduction, especially at low filler contents, since the layer spacing is not known et al. Indeed, at nanofiller volume fractions of less than 0.05, the volume fraction is so small that one platelet is unlikely to overlap with another platelet. Consequently, the reduction in diffusivity is likely to be quite modest. Under these circumstances, an increase or decrease in aspect ratio brought about by increasing or decreasing w, while keeping t and ϕ constant, will not affect D_0/D; this happens because a decrease in the number of filler particles compensates for the increase in aspect ratio, and this is contrary to the predictions of the equations developed by Nielsen, and Cussler and coworkers. If, however, the aspect ratio is increased by decreasing the thickness of the flakes while holding w and ϕ unchanged, the diffusivity must decrease.

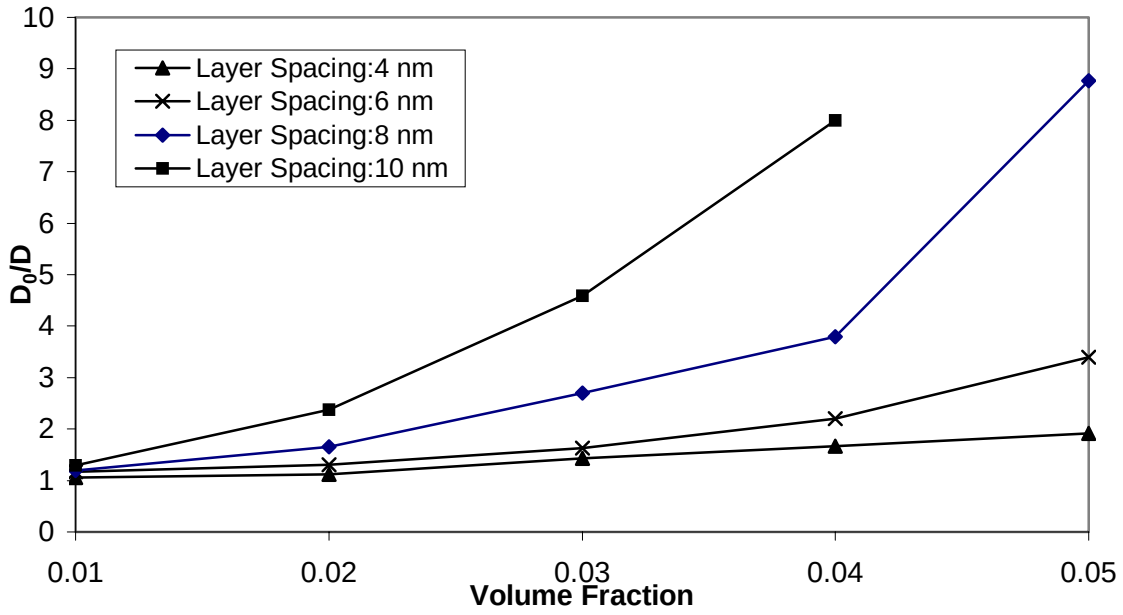

Figure 30: Variation of decrease in diffusivity for a sample with different layer spacing and loading levels

Figure 31 shows a comparison of the available theoretical models, with the diffusion data obtained from vinyl ester clay composites and with our finite differences model. The lowermost curve (curve titled Cussler's model with rectangular flakes) provides the lower limit, as is suggested by Cussler and co-workers, and is not close to the experimental data. Cussler's rectangular model approximates the experimental data at low volume fraction and then diverges. Nielsen's model over predicts the decrease for all loading levels. The finite differences model and the one-dimensional model are more effective in following the trend for experimental data. This suggests that in order to predict the decrease in diffusion for nano-composites a finite differences scheme might be more effective. Although the finite differences scheme was employed on a sample with low loading levels (such that overlapping of flakes was not considered), it would be a good approach for predictions as it is not practical to have high filler loading levels.

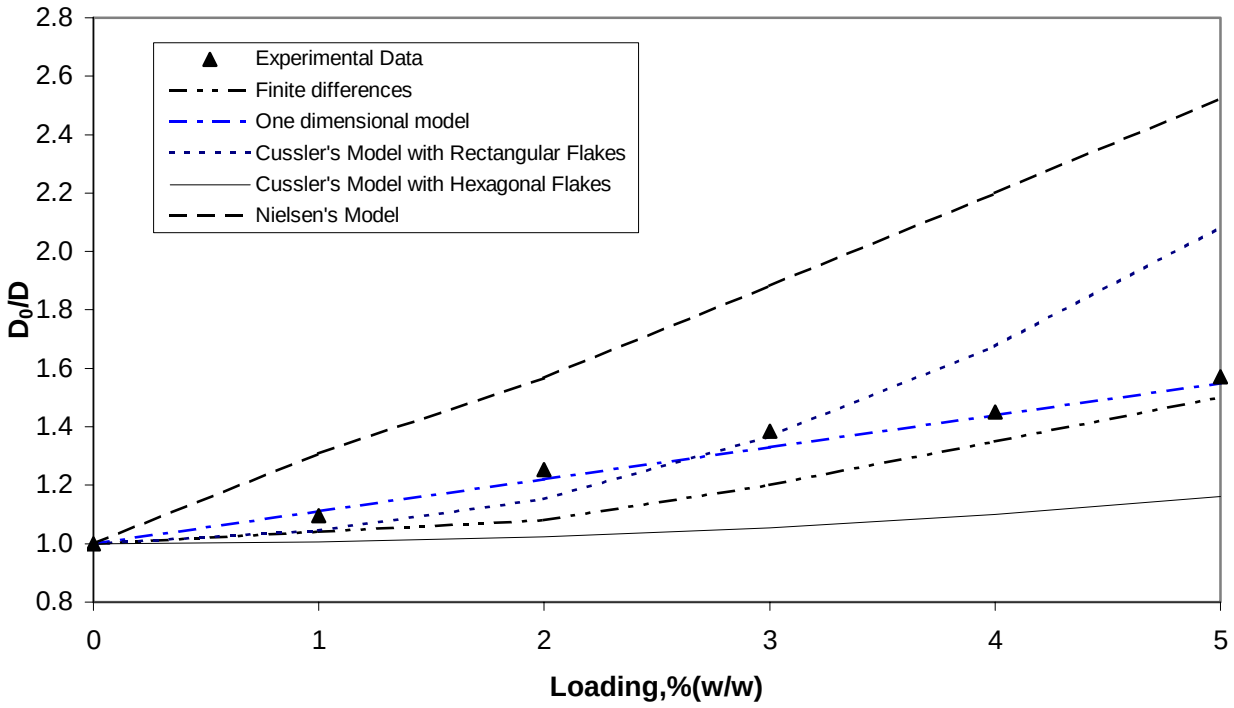

Figure 31: Comparison of different models with the experimental data obtained from clay/vinyl ester composites

5.2 Results for vinyl ester carbon nanofiber composites

Similar permeation experiments were carried out on vinyl ester carbon nanofiber composites. Figure 32 shows the time lag curves for three different amounts of carbon fibers in the composite. It was determined that the diffusion of water vapor through carbon nanofiber composites also follows Fick's Law. Diffusivity values for carbon nanofiber samples are shown in Table 14. It was also determined that the decrease in diffusivity obtained on the adding carbon fibers is consistent at different temperatures as is shown in Table 15. The results obtained for carbon nanofiber composites are better than those obtained on the use of clay composites. A comparison with existing models is also presented in Figure 33.

Table 14: Table showing the diffusivity values of carbon nano-fibers vinyl ester composites at 37.8 °C

Percent carbon fibers in VE (w/w)	Diffusivity value $cm^2/sec \times 10^8$
1	1.03
2	0.93
3	0.84

Carbon nano fiber composites have a color different than that of neat vinyl ester. For transportation structures and bridges, this should not be an issue. Improvements in mechanical properties for carbon nanofiber composites are also significant. All these results are rather unexpected owing to the cylindrical shapes. A cost comparison with clay composites is required to determine the extent of their use in glass fiber reinforced composites. The thickness of the samples used for these experiments are: for 1 % composite – 1.0 mm, for 2 % composite – 1.08 mm and for 3% composite – 1.1 mm.

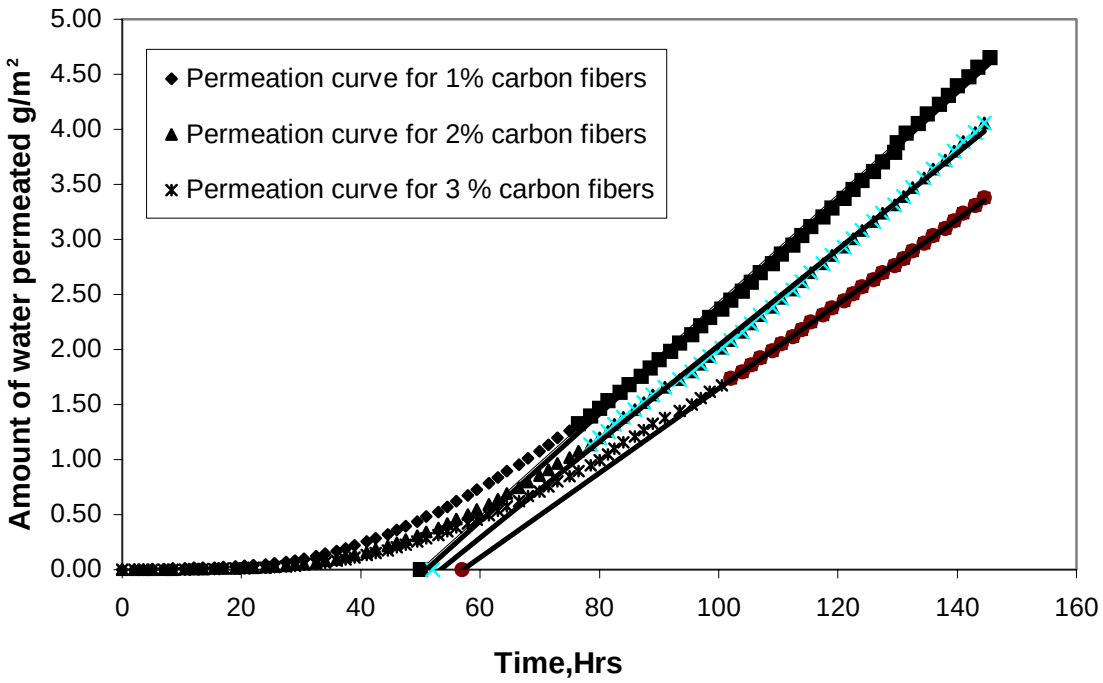

Figure 32: Time lag curves for samples containing carbon fibers at 37.8 °C

Table 15: Diffusivity values for 2 % carbon nano-fiber (CNF) composites at three different temperatures

Temperature °C	Diffusivity Value through neat vinyl ester $cm^2/sec \times 10^8$	Diffusivity Value through CNF composite $cm^2/sec \times 10^8$	Ratio of Diffusivities for neat VE and CNF composite
37.8	1.56	0.93	1.68
25	0.90	0.478	1.90
15	0.68	0.390	1.74

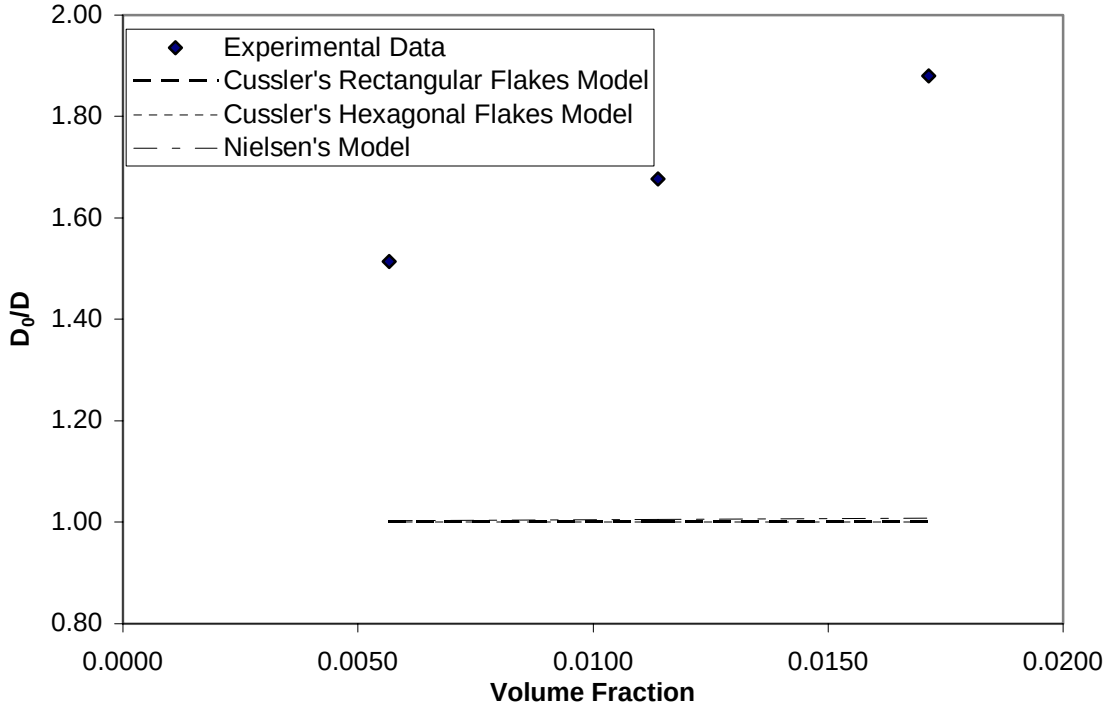

Figure 33: Comparison of experimental diffusion data for carbon nanofiber composites with the existing models

Figure 33 shows a comparison of experimental results obtained for carbon nanofiber composites with the prediction of existing models. It is seen that Cussler's and Nielsen's models are not good in predicting results for cylindrical fillers. These results are important, as in this case macro-sized fillers are more efficient in reducing the diffusion coefficient. The results presented in this section emphasize the need for looking at the picture of composites in entirety, as assuming nano-size fillers extend along the length of the sample results in over estimation.

5.3 Results for vinyl ester Kevlar composites

Experimental results for diffusion through composites made out of Kevlar and vinyl ester are shown in Table 16. It can be seen that the lag time for just 1 % Kevlar composite is greater than 5 % clay composite. Time lag curves for Kevlar composites are shown in

Figure 34. The thickness of the samples used here is 1.0 mm for 1% Kevlar composite and 1.05 mm for 2% Kevlar composite. As seen before, the cumulative amount of water vapor that crosses through 1% Kevlar composite is more than that crosses through 2% Kevlar composite for the time for which experiment was run. Kevlar composites would be more effective in use for construction purposes as they provide enhanced mechanical properties in addition to barrier properties.

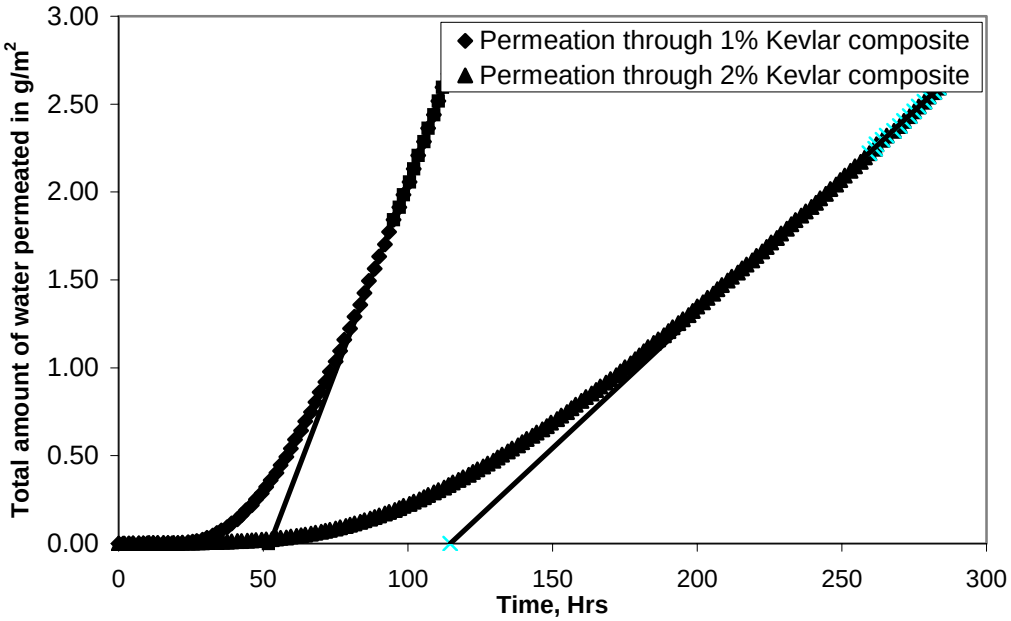

Figure 34: Time lag curve for 1 and 2% Kevlar vinyl ester composite

Table 16: Diffusivity value for Kevlar vinyl ester nanocomposite at 37.8 °C

Weight percent of Kevlar in VE	Diffusivity $cm^2/sec \times 10^8$
1	0.86
2	0.58

An important observation can be made from the above data: The diffusion process through vinyl ester composites shows consistent trends. It follows Fick's Law, and the

impact of fillers, both 'micro' and 'nano', in decreasing the diffusivity is same at different temperatures. Figure 35 shows the effect of temperature on diffusivity of water vapor through 1 % Kevlar composite. Sample used here is 1.0 mm thick.

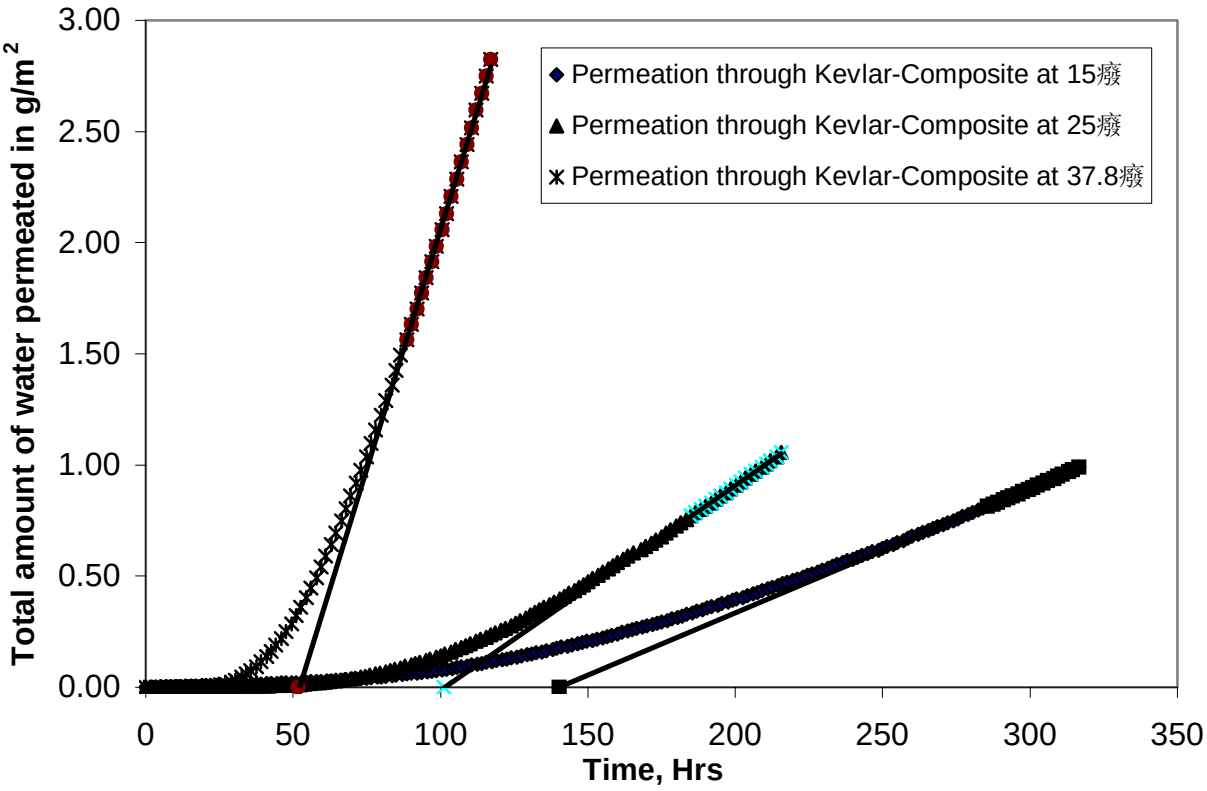

Figure 35: Time lag curves for permeation through 1% Kevlar composite at 100 % Relative Humidity and 3 different temperatures

Table 17 shows the diffusivity values, for water vapor, at three different temperatures through 1 % Kevlar composite. From Tables 13,15, and 17, it can be observed that the effect of adding physical barriers on the barrier property of vinyl ester composite is independent of temperature. This is manifested in terms of consistency in the ratios of diffusivities as shown in the tables. The reduction in the diffusivity remains a constant with varying temperatures. This is an important result because this proves that the

apparent reduction in diffusivity is mainly because of the increase in path length and reduction in the available area for diffusion.

Table 17: Diffusivity values for 1 % Kevlar composite at three different temperatures

Temperature °C	Diffusivity Value through neat vinyl ester $cm^2/sec \times 10^8$	Diffusivity Value through Kevlar composite $Cm^2/sec \times 10^8$	Ratio of Diffusivities for Neat VE and Kevlar composite
37.8	1.56	0.86	1.85
25	0.90	0.46	1.98
15	0.68	0.36	2.00

5.4 Results for vinyl ester POLYMOS composites

It has been contended that a membrane containing reactive additives or fillers that react with the diffusant and produce immobile products produce a reduction in diffusivity. We tried using partial hydrolysate of polymethyl silane, POLYMOS, as a reactive barrier, to bring about a reduction in the diffusivity of vinyl ester composites. The results obtained on carrying out permeation experiments on POLYMOS composites are presented in this section. Table 18 contains the diffusivity values for POLYMOS composites. It can be seen that the diffusivity for POLYMOS composites was less than that of neat vinyl ester.

It has also been contended that a combination of reactive and physical barriers can bring about an even greater decrease in diffusivity. For the case of POLYMOS and clay, the

results (Table 19) show that the diffusivity does not change on using different amounts of clay for a POLYMOS composite. This is something we did not expect and is open to further investigation.

Table 18: Table showing the diffusivity values of POLYMOS vinyl ester composites at 37.8 °C

% POLYMOS in VE (w/w)	Diffusivity value $cm^2/sec \times 10^8$	Diffusivity Ratio
1	1.42	1.10
3	1.24	1.26
5	1.11	1.42

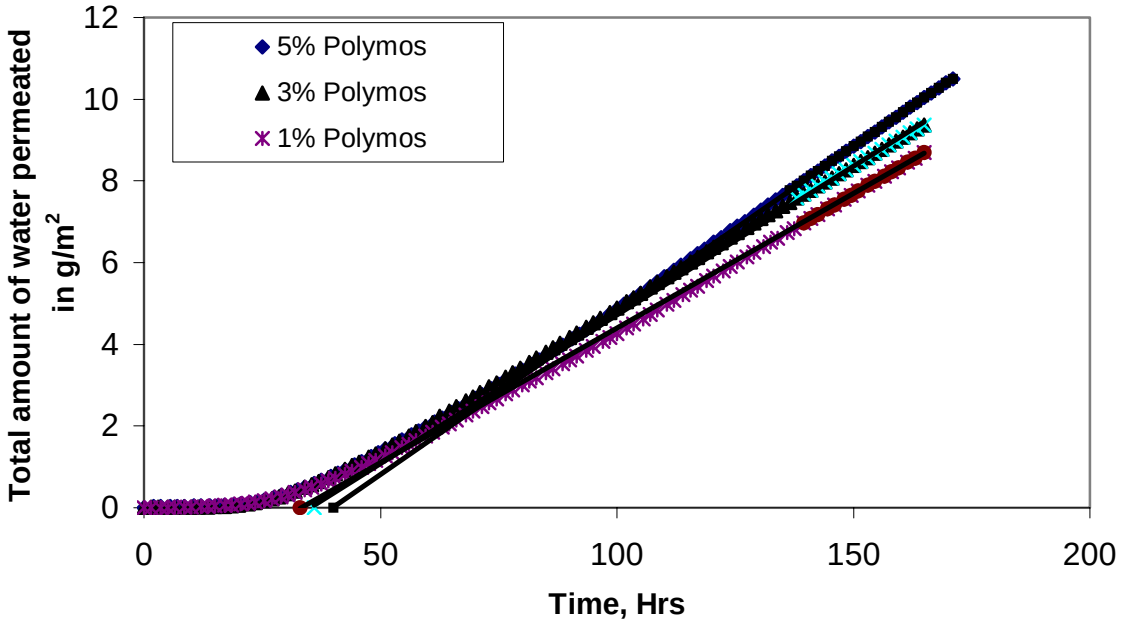

Figure 36: Figure showing the cumulative water permeation curves for POLYMOS composites

Figure 36 shows the water permeation curves for POLYMOS vinyl ester composites. These experiments were carried out at 37.8 °C. The thickness of the samples used in the these experiments were 0.95 mm for 1% composite, and 1.05 mms for both 3 % and 5% composite.

Table 19: Table showing the diffusivity values of 3%POLYMOS clay vinyl ester composites at 37.8 °C

% Clay in POLYMOS/VE (w/w)	Diffusivity value $cm^2/sec \times 10^8$
0	1.24
3	1.23
5	1.27

5.5 Results for vinyl ester glass fiber composites

Results for glass fiber composites are shown in Table 20. The decrease obtained in diffusivity for glass fiber clay composites was about the same as obtained without glassfiber. This is a significant result and again verifies the mechanism of decrease through vinyl ester nanocomposite on the use of fillers.

Table 20: Table showing the diffusivity values of glass fibers vinyl ester composites at 37.8 °C

% Clay in VE (w/w)	Diffusivity value $cm^2/sec \times 10^8$
1	1.45
3	1.12
5	1.01

6.0 Conclusions

The use of surface-treated, montmorillonite clay, carbon nanofibers, and Kevlar fibers resulted in the formation of composites having enhanced barrier properties. Permeation tests conducted by exposing the nanocomposites to water vapor using MOCON Permatran 3/33, showed that the fillers were effective in reducing the diffusion coefficient of water through vinyl ester. Surprisingly, the reduction in the diffusion coefficient was the best for Kevlar composites, which is not a nano-scale filler.

It was found that the diffusion through the composites obeys Fick's law of diffusion. It was also found that the increase in the barrier property obtained on the addition of fillers was independent of the temperature at which the experiment was carried out. This is an important result as it substantiates the reasons provided for the apparent decrease in the diffusivity of water vapor through nanocomposites, which are an increase in the path length that a solute has to travel and a decrease in the available area for diffusion. That is, the reduction in diffusivity is because of the presence of a physical barrier and, hence, has to be independent of temperature.

A comparison of data available in the literature showed that the available models had their limitations in predicting the decrease effectively. A finite differences analysis, and a diffusive resistance model, developed during the course of this work, suggested that the decrease is dependent on more factors than just the aspect ratio and loading level. Extent of overlapping of flakes, layer spacing, and orientation are other important factors, which come into play in correctly assessing the enhancement in the barrier property.

A combination of reactive and physical barriers should provide synergistic effects and provide a significant increase in the barrier property. The experiments conducted using clay and POLYMOS do not provide the kind of results that were expected. Considering the inability of the physical barriers to provide a significant enhancement in barrier property, a combination of physical and reactive barrier could help in the development of better barrier matrices.

Acknowledgements

This research was supported, in part, by the U.S. Department of Transportation, Federal Highway Administration, under the Center of Excellence Project (contract no DTFH61-01-R00002).

References

1. Mallick P.K, “Fiber Reinforced Composites: Materials Manufacturing and Design” 2nd ed, Marcel Dekker, Inc., New York, 41-64, 1993.

2. Maxwell J.C, “Treatise on Electricity and Magnetism”, Vol. I. Clarendon Press, London, 1881.

3. Koros J.W and M.C Zimmerman, “Transport and Barrier Properties”, American Chemical Society Desk Reference, 2003.

4. Kumar A and R. K.Gupta, “Fundamentals of Polymer Engineering”, 2nd ed, Marcel Dekker, Inc., New York, 2003.

5. Michaels A.S, and H. J.Bixler, “Solubility of gases in Polyethylene” J. Polym. Sci. 50, 393-396, 1961.

6. Michaels A.S, Vieth and J.A Barrie “Diffusion of gases in Poly (ethylene terepthalate)” J. Appl. Phys. 34, 13-15, 1963.

7. Crank J. “Mathematics of Diffusion.” Oxford University, London 1956.

8. Frisch H.L and J. M. Hammersley, "Percolation processes and related topics," J. Soc. Ind. Appl. Math. 11, 894–918, 1963.

9. Crank J. and G.S. Park, “Diffusion in Polymers”, Academic Press: London, 1968.

10. Barrer R.M and G.Skirrow “Transport and Equilibrium Phenomena in Gas-Elastomer Systems.” J. Pol. Sc., 3, 564-575, 1948.

11. Taylor R.L., D. B. Hermann, and A. R. Kemp “Fickian diffusion: an unsolved problem” Ind. Engg. Chem., 28, 1255-1263, 1936.

12. Barrer R.M. “Diffusion in and through Solids”, Cambridge University Press, London, 1941.

13. Stannett V. and H.Yasuda, "In testing of Polymers", Interscience, New York, 1, 393-498, 1965.

14. Sivadjian J. and D. Ribeiro, J.Appl.Polym.Sci., 8, 1403-1407, 1964.

15. Lan T, Y. Liang, G.W. Beall and K. Kamena, "Advances in Nanomer Additives for Clay/Polymer Nanocomposites", Nanocor, Inc, Chicago, USA, 2001.

16. Barrer R.M., and J.H.Petropoulos, "Diffusion in heterogeneous media: lattices of parallelpipeds in a continuous phase."Brit .J. Appl .Phys., 12, 691-697, 1961.

17. Nielsen.E.L, "Models for the permeability of filled polymer systems." J. Macromol. Sci, A1(5), 929-942, 1967.

18. Cussler E.L, S.E. Hughes and R.Aris, " Barrier Membranes" J.Memb.Sci., 38, 161-174, 1988.

19. Falla .W.R, M.Mulski and E.L.Cussler, " Estimation Diffusion through Flake Filled Membranes" J.Memb.Sci., 119, 129-136, 1996.

20. Eitzman D.M, R.R.Melkote, and E.L.Cussler, " Barrier Membrane with Tipped Impermeable Flakes" AIChE –J, 42, 2-7, 1996.

21. Moggridge G.D., Nancy K Lape, Chuanfang Yang and E.L.Cussler, "Barrier Films Using Flakes and Reactive Additives," Progress in Organic Coatings, 46, 231-240,2003.

22. Aris R, "On a Problem on Hindred Diffusion" J.Memb.Sc., 48, 35-42, 1995.

23. Wakeham.W.A and E.A.Mason, "Diffusion through Multiperforate Laminae", Ind. Engg. Chem. Fundam., 18, 4-7, 1979.

24.Yang C, Eric E. Nuxoll, and E.L.Cussler. "Reactive Barrier Films" AIChE. J., 47, 2-10, 2001.

25. Drozdov A.D, Apoorva Shah, Rakesh.K.Gupta, and J.Christiansen. “Models for Anomalous diffusion through a Polymer-Clay nanocomposites.” J.Poly.Sci Part B Polym Phys., 41, 476-492, 2003

26. Lan, Padmananda, D Kaviratna, and Pinnavaia “Manufacture of Polyimide-Clay Hybrid Films” J.Chem. Mater., 6, 573-575, 1994.

27. Yano.K, A. Usuki, and A.Okada, “ Diffusion Properties of Polyimide-Clay Hybrid Films” J.Polym Sci., Part A, 31, 2493-2502, 1993.

28. Chin J.W., Nguyen T., Aouadi K., “Sorption and Diffusion of water, salt water and concrete pore solution in composite matrices”, J Appl. Polym Sci., 71, 483 – 492, 1999.

29. Kornmann X., Berglund L. A., Sterte J., Giannelis E. P., “Nanocomposites Based on Montmorillonite and Unsaturated Polyester”, Polym. Eng. Sci., 38, 1351 – 1358, 1998.

APPENDICES

APPENDIX 1

List of programs used to carry out simulation

A.1.1 Driver file for the finite differences routine

```
clear
l=5e-07
w=4e-05
chiplenth=2e-05
chpln2=0.5*chiplenth
% number of nodes
nx=20         %number of columns
ny=6           %number of rows
%%%%%%%%%%%%%%%%%%%%%%%%%%%%%%%%%%%%%%%%%%%%%%%%%%%%%%%%%%%%%%%%%%%%%%%%%%%%%%%

for i=1:nx
    for j=1:ny
    cini(j,i)=100
end
    cini(ny,i)=0
end

    %for j=2:ny-1
 %   for i=1:nx
  %      cini(j,i)=100-100/(ny-(j-1))
  % end
  %end
%options=optimset('Display','off')
[c,fn]=fsolve(@nanofunM2,cini)
```

A.1.2 Finite Differences Routine to obtain the concentration profile through a representative repeating unit

```
function fn = nanofun(c)
% This program divides the region into nodes and calculate the
compositions
% at various nodes in a typical section of a polymer with nanochips
% imbedded.
l=5e-07
w=4e-05
chiplenth=2e-05
chpln2=0.5*chiplenth
chpln2=50
% number of nodes
nx=20            %number of columns
ny=6             %number of rows
%%%%%%%%%%%%%%%%%%%%%%%%%%%%%%%%%%%%%%%%%%%%%%%%%%%%%%%%%%%%%%%%%%%%%%
delx=w/nx
dely=l/ny
%%%%%%%%%%%%%%%%%%%%%%%%%%%%%%%%%%%%%%%%%%%%%%%%%%%%%%%%%%%%%%%%%%%%
delx=10
dely=1
dely1=0.75
% CHANGE MADE ABOVE NOTE THIS THING%


%for i=1:nx
 %   for j=1:ny
  %      c(i,j)=0
  % end
  %end
 nyby2=6
 nyby2p1=nyby2+1
 nyby2p2=nyby2+2
 nyby2m1=nyby2-1
 nyby2m2=nyby2-2
 nyby2p2=nyby2+2
nchpnode=5
 for i=3:4
    for j=2:nx-1
        fn(i,j)=(c(i,j-1)+c(i,j+1)-2*c(i,j))/delx^2 +(c(i-
1,j)+c(i+1,j)-2*c(i,j))/dely^2
    end
end

i=5
 for j = 5:nx-1

        fn(i,j)=(c(i,j-1)+c(i,j+1)-2*c(i,j))/delx^2 +(c(i-1,j)-
c(i,j))/dely1^2+(c(i+1,j)-c(i,j))/dely^2
    end
i=2
    for j = 2:15
```

```
           fn(i,j)=(c(i,j-1)+c(i,j+1)-2*c(i,j))/delx^2 +(c(i-1,j)-
c(i,j))/dely1^2+(c(i+1,j)-c(i,j))/dely^2
    end

for i = 2:4
    fn(i,1)=(c(i,2)-c(i,1))/delx^2 + (c(i+1,1)+c(i-1,1)-
2*c(i,1))/dely^2
end
for i= 3:5
fn(i,nx)=(c(i,nx-1)-c(i,nx))/delx^2 + (c(i+1,nx)+c(i-1,nx)-
2*c(i,nx))/dely^2
end
for i=2:4
    fn(5,i)=(c(5,i+1)+c(5,i-1)-2*c(5,i))/delx^2 + (c(4,i)-
c(5,i))/dely^2
end
fn(5,1)=(c(5,2)-c(5,1))/delx^2 + (c(4,1)-c(5,1))/dely^2
for i=16:19
    fn(2,i)=(c(2,i+1)+c(2,i-1)-2*c(2,i))/delx^2 + (c(3,i)-
c(2,i))/dely^2
end
fn(2,nx)=(c(2,nx-1)-c(2,nx))/delx^2+(c(3,nx)-c(2,nx))/dely^2

%nchpnode=2
for i=1:15
    fn(1,i)=c(1,i)-100
end
for i=16:20
    fn(1,i)=c(1,i)-0
end

% CHANGE MADE BELOW ... NOTE I
%%%%%%%%%%%%%%%%%%%%%%%%%%%%%%%%%%%%%%%%%%%%%%%%%%%%%%%%%%%%%%%%%%%
for i=6:15

    fn(ny,i)=c(ny,i)-50
end
fn(6,16)=c(6,16)-50
fn(6,17)=c(6,17)-50
fn(6,18)=c(6,18)-50
fn(6,19)=c(6,19)-50
fn(6,20)=c(6,20)-50
for i = 1:nchpnode
    fn(i,nyby2)=c(i,nyby2)-0
end
%c2=fsolve(fn,c)
```

A.1.3 The resistance calculator program

```
% This program is to calculate the diffusivity of a unit where there
are
% displaced nanochips. First we calculate the resistance of seven
sample
% cells and then assemble the unit using these cells.
%
% Cell 1 has chip in the center and no displacement..
% Cell 2 has no chip. and length depends only on distance between the
chips
% Cell 3 is same as cell 1
% cell 4 is same as cell 1 but may have a displaced chip that is going
out
% of the cell
% cell 5 is same as cell 2 but may have an entering chip
% cell 6 is same as cell 1 but may have an exiting chip and an entering
% chip.
% cell 7 has an enterng chip only
% Based on cells 4 5 and 6  we define a left unit a right unit and a
mid unit
% cells 1 2 and 3 form an undisplaced unit and the combined unit we
call
% the toplayer
%%%%%%%%%%%%%%%%%%%%%%%%%%%%%%%%%%%%%%%%%%%%%%%%%%%%%%%%%%%%%%%%%%%%%%%%
%%%%%%%
clear;
fid=fopen('dataunit3.m','r');
frewind(fid)
dpol=fscanf(fid,'%f',1);
dclay=fscanf(fid,'%f',1);
alfa=fscanf(fid,'%f',1);
sigma=fscanf(fid,'%f',1);
chipthk=fscanf(fid,'%f',1);
phi=fscanf(fid,'%f',1);
frac=fscanf(fid,'%f',1);
nunit=fscanf(fid,'%f',1);
fclose(fid)
%%%%%%%%%%%%%%%%%%%%%%%%%%%%%%%%%%%%%%%%%%%%%%%%%%%%%%%%%%%%%%%%%%%%%%%%
%                    chip dimensions
%%%%%%%%%%%%%%%%%%%%%%%%%%%%%%%%%%%%%%%%%%%%%%%%%%%%%%%%%%%%%%%%%%%%%%%%
chiplenth=alfa*chipthk*2
chipbreth=chiplenth
chipvol=chiplenth*chipbreth*chipthk
%%%%%%%%%%%%%%%%%%%%%%%%%%%%%%%%%%%%%%%%%%%%%%%%%%%%%%%%%%%%%%%%%%%%%%%%
%                         unit dimensions
%%%%%%%%%%%%%%%%%%%%%%%%%%%%%%%%%%%%%%%%%%%%%%%%%%%%%%%%%%%%%%%%%%%%%%%%
interlenth=sigma*chipthk
interlenthbase=interlenth
unitlenth=chiplenth+interlenth
unitbreth=chipbreth
unitareab=unitlenth*unitbreth
unitvol=chipvol/phi
unitthk=unitvol/(unitlenth*unitbreth)
unitthkbase=unitthk
celthkb=unitthk
```

```
%%%%%%%%%%%%%%%%%%%%%%%%%%%%%%%%%%%%%%%%%%%%%%%%%%%%%%%%%%%%%%%%%%%%%%%%%%%%
%%%%              inter dimensions
%%%%%%%%%%%%%%%%%%%%%%%%%%%%%%%%%%%%%%%%%%%%%%%%%%%%%%%%%%%%%%%%%%%%%%%%%%%%
%%%%%%%%%%%%%%%%%%%%%%%%%%%%%%%%%%%%%%%%%%%%%%%%%%%%%%%%%%%%%%%%%%%%%%%%%%%%
%%%%%%%%%%  Symmetry condition %%%%%%%%%%%%%%%%%
sym1=chipthk*sigma
sym2 = (1-frac)*chiplenth
sym3=frac*chiplenth
sym4=0.5*sigma*chipthk
sym5=chiplenth/2
sym6=sym3+sym4
fracbas=frac
if frac < 0.5
if sym1 <  sym2
if sym6 < sym5
   frac=1-fracbas
end
end
end
if alfa==sigma
    if fracbas < 0.001
        frac=0.5
    end
end
%%%%%%%%%%%%%%%%%%%%%%%%%%%%%%%%%%%%%%%%%%%%%%%%%%%%%%%%%%%%%%%%%%%%%%%%%%%%
%%%%% end of symmetry %%%%%%%%%%%%%%%%%%%%%%%%
%%%%%%%%%%%%%%%%%%%%%%%%%%%%%%%%%%%%%%%%%%%%%%%%%%%%%%%%%%%%%%%%%%%%%%%%%%%%


unitthkbase=unitthk
unithor=(sigma*chipthk)+(frac*chiplenth)
interbreth=unitbreth
intareabase=interlenthbase*interbreth
chpfrc=(1-frac)*chiplenth
polfrc=(sigma*chipthk)+(0.5*chiplenth)

if chpfrc >= polfrc
    unitthk=sqrt((unitthkbase^2)+(unithor^2))
    interlenth=(sigma*chipthk)*unitthkbase/unitthk
    celthk=unitthk
end
if chpfrc < polfrc
uni2=unitthkbase^2
fr1=(1-frac)*chiplenth
fr2=fr1^2
  unitthk=sqrt(uni2+fr2)
  interlenth=(sigma*chipthk)*unitthkbase/unitthk
  celthk=unitthk
end
factor=unitthkbase/unitthk
facsq=factor*factor
intarea=interlenth*interbreth
interarea=intarea
interlenthn=interlenth
interlenthb=interlenthbase
%interlenth=interlenthbase
interthk=(unitthk)
```

```
unitarea=unitlenth*unitbreth
celthk=(unitthk)
celthkn=unitthk
%celthk=celthkb
chiparea=chiplenth*chipbreth
difthk=celthkb-chipthk
celtopthk=(celthkb-chipthk)/2
celbotthk=(celthkb-chipthk)/2
%%%%%%%%%%%%%%%%%%%%%%%%%%%%%%%%%%%%%%%%%%%%%%%%%%%%%%
%                     Cell 1
%%%%%%%%%%%%%%%%%%%%%%%%%%%%%%%%%%%%%%%%%%%%%%%%%%%%%%%
%celthk=celthkb
%%%%%%%%%%%%%%%%%%%%%%%%%%%%%%%%%%%%%%%%%%%%%%%%%%%%%%%
% resistance of polymer above and below chip..
% %%%%%%%%%%%%%%%%%%%%%%%%%%%%%%%%%%%%%%%%%%%%%%%%%%%%
restoppol=celtopthk/(dpol*chiparea)
resbotpol=celbotthk/(dpol*chiparea)
reschip=chipthk/(dclay*chiparea)
rescellone=restoppol+resbotpol+reschip
ressoneinv=1/rescellone
%%%%%%%%%%%%%%%%%%%%%%%%%%%%%%%%%%%%%%%%%%%%%%%%%%%%%%%%%%%%%
%                   Cell 2
%%%%%%%%%%%%%%%%%%%%%%%%%%%%%%%%%%%%%%%%%%%%%%%%%%%%%%%%%%%%%
%interarea=interlenth*interbreth
rescelltwo=interthk/(dpol*intarea)
rescell2inv=1/rescelltwo
%%%%%%%%%%%%%%%%%%%%%%%%%%%%%%%%%%%%%%%%%%%%%%%%%%%%%%%%%%%%%%
%                   Cell 3
%%%%%%%%%%%%%%%%%%%%%%%%%%%%%%%%%%%%%%%%%%%%%%%%%%%%%%%%%%%%%
rescell3=rescellone
rescell3inv=1/rescell3
%%%%%%%%%%%%%%%%%%%%%%%%%%%%%%%%%%%%%%%%%%%%%%%%%%%%%%%%%%%%%%
% total resistance of top layer
%%%%%%%%%%%%%%%%%%%%%%%%%%%%%%%%%%%%%%%%%%%%%%%%%%%%%%%%%%%%%%%
reslayer1=(ressoneinv+rescell2inv+rescell3inv)^(-1)
reslayer1inv=1/reslayer1
rsmdtopinv=reslayer1inv+(rescell2inv)
rsmdtop=1/rsmdtopinv
%%%%%%%%%%%%%%%%%%%%%%%%%%%%%%%%%%%%%%%%%%%%%%%%%%%%%%%%%%%%%%%
%                   Cell 4
%%%%%%%%%%%%%%%%%%%%%%%%%%%%%%%%%%%%%%%%%%%%%%%%%%%%%%%%%%%%%%%%%
%%%  cells 4 5 6  and 7 have fractions of the chip in them
%%%%%%%%%%%%%%%%%%%%%%%%%%%%%%%%%%%%%%%%%%%%%%%%%%%%%%%%%%%%%%%%%
%%%%%%%%%%%%%%%%%%%%%%%%%%%%%%%%%%%%%%%%%%%%%%%%%%%%%%%%%%%%%%%%%
%%%%  increase in cell thickness due to stagger %%%%%%%%%%
%%%%%%%%%%%%%%%%%%%%%%%%%%%%%%%%%%%%%%%%%%%%%%%%%%%%%%%%%%%%%
%if chpfrc < polfrc
%uni2=unitthkbase^2
%fr1=(1-frac)*chiplenth
%fr2=fr1^2
 % unitthk=sqrt(uni2+fr2)
 % interlenth=(sigma*chipthk)*unitthkbase/unitthk
 % celthk=unitthk
 %end
%%%%%%%%%%%%%%%%%%%%%%%%%%%%%%%%%%%%%%%%%%%%%%%%%%%%%%%%%%%%%%%%%%%%%%
frac4=frac
fracchiparea=frac4*chiparea
```

```
fracpolarea=(1-frac4)*chiparea
rsfree4=(celthkn)/(dpol*fracpolarea*factor)
rschip4=(chipthk)/(dclay*fracchiparea)
rsrem4=(celthkb-chipthk)/(dpol*fracchiparea)
rsremtot4=rsrem4+rschip4
rscell4inv=(1/rsfree4)+(1/rsremtot4)
rescell4=1/rscell4inv
%%%%%%%%%%%%%%%%%%%%%%%%%%%%%%%%%%%%%%%%%%%%%%%%%%%%%%%%%%%%%%%%%%%%%%%%
%%%%%%%%%%%%  cell 5 %%%%%%%%%%%%%%%%%%%%%%%%%%%%%%%%%%%%%%%%
%%%%%%%%%%%%%%%%%%%%%%%%%%%%%%%%%%%%%%%%%%%%%%%%%%%%%%%%%%%%%%%%%%%%
%celthk=celthkn
frac5=1-frac
fraclenth=frac5*chiplenth
fracarea=frac5*chiparea
if interlenthb > fraclenth
rschp5=chipthk/(dclay*fracarea)
rsrem5=(celthkb-chipthk)/(dpol*fracarea*facsq)
rsremtot5=rschp5+rsrem5
delarea=(intareabase-fracarea)
rsfree5=celthkb/(dpol*delarea*facsq)
rescell5=((1/rsremtot5) + (1/rsfree5))^(-1)
end
if interlenthb<= fraclenth
    rschp5=chipthk/(dclay*intarea)
    rsrem5=(celthkb-chipthk)/(dpol*intarea*factor)
    rescell5=rschp5+rsrem5
end
%celthk=celthkb
%%%%%%%%%%%%%%%%%%%%%%%%%%%%%%%%%%%%%%%%%%%%%%%%%%%%%%%%%%%%%%%%%%%%%%%%
%%%%%%%%%%%%%%%%
%%%%%%%%%%%%%%%%%%%%%%%%%%%%%%%%%%%%%%%%%%%%%%%%%%%%%%%%%%%%%%%%%%%%%%%%
%%%%%%%%%%%%%%%
%%%%%%%%%%%%%%%%%% cell 6 %%%%%%%%%%%%%%%%%%%%%%%%%%%%%%%%%%%%%%%%%%%%%%%
%%%%%%%%%%%%%%%%%%%%%%%%%%%%%%%%%%%%%%%%%%%%%%%%%%%%%%%%%%%%%%%%%%%%%%%%
%%%%%
if interlenthb >= fraclenth
    rescell6=rescell4
end
if interlenthb< fraclenth
    enterchiplenth=fraclenth-interlenthb
    exitchiplenth=(frac)*chiplenth
    freepollenth=(chiplenth-enterchiplenth-exitchiplenth)*factor
    entarea=chipbreth*enterchiplenth
    exitarea=chipbreth*exitchiplenth
    polarea=freepollenth*chipbreth

rsent6=(chipthk)/(dclay*entarea*factor)+(difthk)/(dpol*entarea*facsq)

rsexit6=(chipthk)/(dclay*exitarea*factor)+(difthk)/(dpol*exitarea*facsq
)
    rsfree6=celthkn/(dpol*polarea)
    rescell6=((1/rsent6)+(1/rsexit6)+(1/rsfree6))^(-1)
end
%%%%%%%%%%%%%%%%%%%%%%%%%%%%%%%%%%%%%%%%%%%%%%%%%%%%%%%%%%%%%%%%%%%%%%%%
%%%%%%%%%%%%%%%%%%%
                       %%%%%%%%%%%%%%%% cell 7 %%%%%%%%%%%%%%%
```

```
%%%%%%%%%%%%%%%%%%%%%%%%%%%%%%%%%%%%%%%%%%%%%%%%%%%%%%%%%%%%%%%%%%%%%%%%
%%%%%%%%%%%%%%%%%%%
if interlenthb >= fraclenth
    rescell7 = celthkn/(dpol*chiparea)
end
if interlenthb < fraclenth
    enterchiplenth=fraclenth-interlenth
    freepollenth=(chiplenth-enterchiplenth)*factor
    entarea=chipbreth*enterchiplenth
    polarea=freepollenth*chipbreth
    rsent7=(chipthk)/(dclay*entarea)+(difthk)/(dpol*entarea*facsq)
    rsfree7=celthkn/(dpol*polarea)
    rescell7=((1/rsent7)+(1/rsfree7))^(-1)
end
%%%%%%%%%%%%%%%%%%%%%%%%%%%%%%%%%%%%%%%%%%%%%%%%%%%%%%%%%%%%%%%%%%%%%%%%
%%%%%%%%%%%%%%%%%%%%%%%%%%
rslft4=rescell4
rslft5=rescell5
rslft6=rescell6
rsrt4=rescell6
rsrt5=rescell5
rsrt6=rescell7
rsmd4=rescell6
rsmd5=rescell5
rsmd6=rescell6
reslftbotinv=(1/rslft4)+(1/rslft5)+(1/rslft6)
reslftbot=1/reslftbotinv
resrtbotinv=(1/rsrt4)+(1/rsrt5)+(1/rsrt6)
resrtbot=1/resrtbotinv
resmdbotinv=(1/rsmd4)+(2/rsmd5)+(1/rsmd6)
resmdbot=1/resmdbotinv
%rslft=reslayer1+reslftbot
%rslftinv=1/rslft
%rsmid=rsmdtop+resmdbot
%rsmidinv=1/rsmid
%rsrt=reslayer1+resrtbot
%rsrtinv=1/rsrt
nmid=nunit-2
rstopinv=reslayer1inv+reslayer1inv+(nmid*rsmdtopinv)+rescell2inv
if nmid==0
    rstopinv=reslayer1inv+reslayer1inv+rescell2inv
end
rstop=1/rstopinv
rsbotinv=reslftbotinv+resrtbotinv+(nmid*resmdbotinv)+(1/rsmd5)
if nmid==0
    rsbotinv=reslftbotinv+resrtbotinv+(1/rsmd5)
end
rsbot=1/rsbotinv
%rsmdtotinv=nmid*rsmidinv
%rstotinv=rslftinv+rsrtinv+rsmdtotinv
rstot=rstop+rsbot
%chipareadebug=chiparea
%intareadebug=intarea
%areatot=nunit*(unitarea+chiparea) + (nmid*2*intarea)
areatot=nunit*(unitareab+chiparea) + ((nmid+1)*intareabase)
if nmid==0
    areatot=nunit*(unitarea+chiparea) + (intarea)
```

```
end
if nunit==1
rsbot=resrtbot
rstop=reslayer1
rstot=rstop+rsbot
areatot=unitarea+chiparea
areatot=unitarea+chiparea
end

diffefec=2*unitthkbase/(areatot*rstot)
drat=dpol/diffefec
dratinv=1/drat
```

APPENDIX 2

A.2 Sample Calculation for 3% clay and 3% POLYMOS sample

The following table provides a sample calculation used for finding out diffusivity. A brief treatment of the raw data obtained from the machine provides column 1 and 2. It is assumed that during the test interval permeation occurs at a constant flux value, which is equal to the final value obtained at the end of that particular interval. Flux when multiplied by the time interval gives the amount permeated per unit area during that interval. This amount when added cumulatively provides the total amount of water permeated during the test. This is shown in the last column. A plot between time and cumulative amount of water permeated provides the lag time, which in turn provides the diffusivity value.

Time	Flux $g/m^2/day$	Amount Permeated $g*hr/m^2/day$	Cumulative Permeation	Cumulative amount of water permeated g/m^2
0	0.000	0.000	0.000	0.000
1.5	0.012	0.018	0.018	0.001
3.5	0.033	0.066	0.083	0.003
5	0.046	0.069	0.152	0.006
7	0.054	0.107	0.259	0.011
8.5	0.072	0.108	0.367	0.015
10	0.094	0.141	0.508	0.021
12	0.155	0.310	0.818	0.034
13.5	0.217	0.326	1.144	0.048
15.5	0.313	0.626	1.769	0.074
17	0.405	0.607	2.376	0.099
18.5	0.492	0.739	3.115	0.130
20.5	0.591	1.182	4.296	0.179
22	0.678	1.017	5.314	0.221
24	0.745	1.491	6.805	0.284
25.5	0.796	1.194	7.999	0.333
27	0.850	1.275	9.273	0.386

29	0.955	1.909	11.183	0.466
30.5	1.004	1.505	12.688	0.529
32.5	1.058	2.117	14.805	0.617
34	1.086	1.630	16.434	0.685
35.5	1.133	1.700	18.134	0.756
37.5	1.203	2.405	20.539	0.856
39	1.241	1.861	22.401	0.933
41	1.248	2.497	24.898	1.037
42.5	1.277	1.916	26.813	1.117
44	1.302	1.954	28.767	1.199
46	1.331	2.661	31.428	1.310
47.5	1.306	1.959	33.387	1.391
49.5	1.359	2.719	36.106	1.504
51	1.383	2.075	38.182	1.591
52.5	1.401	2.101	40.283	1.678
54.5	1.421	2.843	43.125	1.797
56	1.445	2.167	45.293	1.887
58	1.467	2.935	48.227	2.009
59.5	1.457	2.186	50.413	2.101
61	1.471	2.206	52.620	2.192
63	1.486	2.971	55.591	2.316
64.5	1.525	2.288	57.879	2.412
66.5	1.496	2.992	60.871	2.536
68	1.510	2.265	63.136	2.631
69.5	1.519	2.279	65.415	2.726
71.5	1.489	2.978	68.393	2.850
73	1.458	2.187	70.580	2.941
75	1.489	2.979	73.559	3.065
76.5	1.493	2.239	75.798	3.158
78	1.510	2.265	78.063	3.253
80	1.515	3.030	81.094	3.379
81.5	1.542	2.313	83.406	3.475
83.5	1.550	3.099	86.505	3.604
85	1.578	2.367	88.872	3.703
86.5	1.606	2.410	91.282	3.803
88.5	1.597	3.193	94.475	3.936
90	1.591	2.387	96.862	4.036
92	1.585	3.170	100.032	4.168
93.5	1.592	2.388	102.420	4.268
95	1.603	2.404	104.825	4.368
97	1.574	3.148	107.972	4.499
98.5	1.554	2.331	110.303	4.596
100.5	1.586	3.172	113.475	4.728
102	1.577	2.365	115.841	4.827
103.5	1.586	2.378	118.219	4.926
105.5	1.584	3.168	121.387	5.058
107	1.596	2.393	123.780	5.158
109	1.593	3.186	126.966	5.290

110.5	1.596	2.393	129.360	5.390
112	1.605	2.407	131.767	5.490
114	1.601	3.202	134.969	5.624
115.5	1.605	2.408	137.377	5.724
117.5	1.588	3.176	140.553	5.856
119	1.640	2.459	143.012	5.959
120.5	1.623	2.435	145.447	6.060
122.5	1.640	3.281	148.728	6.197
124	1.649	2.474	151.202	6.300
126	1.661	3.322	154.524	6.438
127.5	1.670	2.504	157.028	6.543
129	1.671	2.506	159.534	6.647
131	1.661	3.322	162.856	6.786
132.5	1.680	2.521	165.377	6.891
134.5	1.666	3.333	168.710	7.030
136	1.677	2.515	171.225	7.134
137.5	1.696	2.544	173.769	7.240
139.5	1.689	3.379	177.147	7.381
141	1.682	2.523	179.670	7.486
143	1.677	3.354	183.025	7.626
144.5	1.651	2.477	185.502	7.729
146	1.625	2.437	187.939	7.831
148	1.629	3.259	191.198	7.967
149.5	1.640	2.461	193.658	8.069
151.5	1.642	3.284	196.942	8.206
153	1.661	2.492	199.434	8.310
154.5	1.639	2.459	201.893	8.412
156.5	1.665	3.331	205.224	8.551
158	1.676	2.513	207.738	8.656
160	1.668	3.337	211.074	8.795
161.5	1.683	2.524	213.599	8.900
163	1.688	2.531	216.130	9.005
165	1.677	3.355	219.485	9.145
166.5	1.681	2.521	222.006	9.250
168.5	1.636	3.272	225.279	9.387
170	1.618	2.427	227.705	9.488
171.5	1.637	2.455	230.161	9.590
173.5	1.627	3.254	233.415	9.726
175	1.635	2.452	235.867	9.828
177	1.628	3.256	239.123	9.963
178.5	1.623	2.435	241.558	10.065
180	1.637	2.456	244.013	10.167
182	1.649	3.297	247.310	10.305
183.5	1.672	2.508	249.819	10.409
185.5	1.654	3.307	253.126	10.547
187	1.636	2.454	255.580	10.649
188.5	1.651	2.476	258.057	10.752
190.5	1.666	3.332	261.389	10.891

192	1.613	2.419	263.808	10.992
194	1.626	3.251	267.059	11.127
195.5	1.615	2.423	269.482	11.228
197	1.619	2.429	271.910	11.330
199	1.595	3.189	275.100	11.462
200.5	1.594	2.392	277.492	11.562
202.5	1.589	3.178	280.669	11.695
204	1.614	2.422	283.091	11.795
205.5	1.637	2.456	285.546	11.898
207.5	1.637	3.274	288.820	12.034
209	1.654	2.480	291.300	12.138
211	1.636	3.271	294.571	12.274
212.5	1.656	2.484	297.055	12.377
214	1.656	2.484	299.539	12.481
216	1.615	3.230	302.769	12.615
217.5	1.590	2.385	305.154	12.715
219.5	1.634	3.267	308.421	12.851
221	1.670	2.505	310.926	12.955
223.5	1.681	4.201	315.127	13.130
225.5	1.701	3.401	318.528	13.272
227	1.713	2.570	321.098	13.379
229	1.702	3.403	324.502	13.521
230.5	1.710	2.565	327.066	13.628
232	1.743	2.615	329.681	13.737
234	1.715	3.429	333.110	13.880
235.5	1.726	2.588	335.699	13.987
237.5	1.716	3.432	339.130	14.130
239	1.709	2.564	341.695	14.237
240.5	1.762	2.643	344.338	14.347
242.5	1.692	3.383	347.721	14.488
244	1.587	2.381	350.103	14.588

APPENDIX 3

A.3 Chemistry of POLYMOS

POLYMOS is a partial hyrdolyzate of tetramethoxysilane and, as such, is very reactive with water. Since it is a polar molecule, it is soluble in polar polymers. The POLYMOS used in the study was supplied by OSI Specialties, Inc. The POLYMOS reacts differently with water in solution and when incorporated in the polymer nano-composites. This has been discussed in the following sections.

A.3.1 Reaction of Poly-MOS with water

POLYMOS, due to its polar nature, undergoes hydrolysis when exposed to moisture. As is shown in Figure 37, the bond existing between silicon and oxygen is partially polar, with a positive dipole existing within the proximity of the silicon backbone of the polymer chain. When it is exposed to water, the lone pair of electrons on a water molecule attacks the silicon oxygen bond. The hydrophilic attack causes the water to donate a proton to the leaving methoxide group, and methanol is formed as is shown in Figure 38.

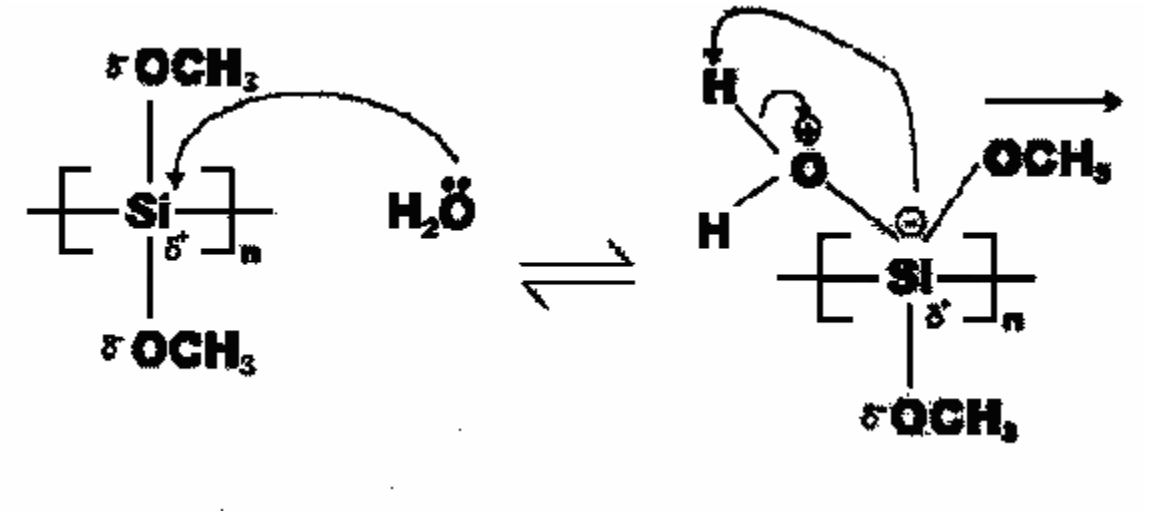

Figure 37: Reaction of water with POLYMOS

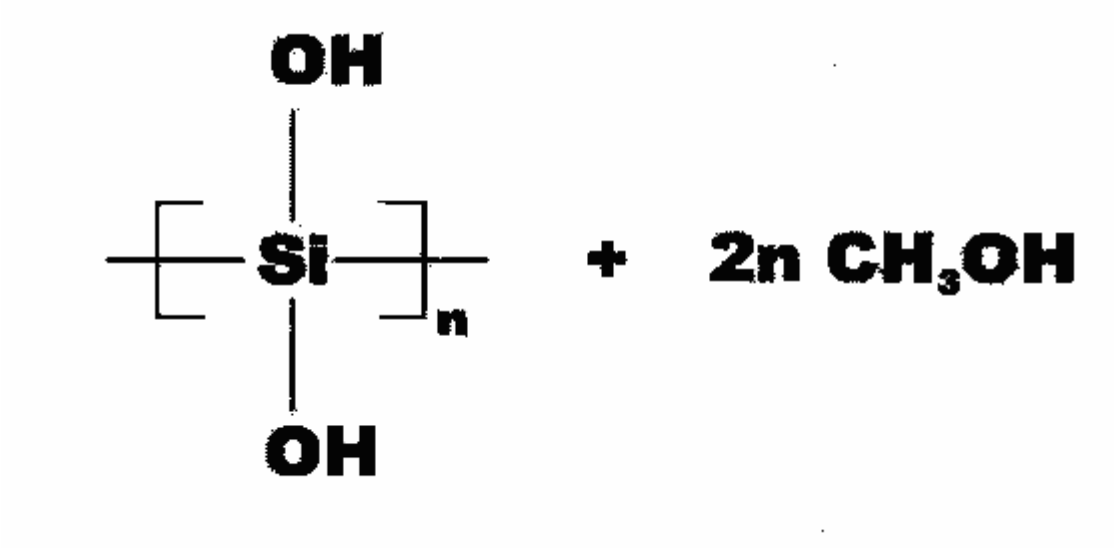

Figure 38: Products of the reaction of POLYMOS with water

If the reaction takes place in solution, the chains of the hydrated polymer are rather mobile, and, as pairs of the hydrated silicon monomers interact in solution, they condense to form silica like material, liberating one mole of water as is shown in Figure 39. If the additive is incorporated into a densely cross-linked resin, however the process of silicate condensation should be much slower, since the polymer chains are not as mobile.

Figure 39: Reaction products for the reaction of water with POLYMOS in solution